Spectroscopic and Kinetic Studies of Metal-Containing Proteins

By

Kelly Natalia Chacón

A DISSERTATION

Presented to the Institute of Environmental Health
and the Oregon Health & Science University
School of Medicine
in partial fulfillment of
the requirements for the degree of

Doctor of Philosophy

May 2015

Institute of Environmental Health
Division of Environmental & Molecular Biology
School of Medicine
Oregon Health and Science University

CERTIFICATE OF APPROVAL

This is to certify that the Ph.D. dissertation of
Kelly Natalia Chacón
has been approved

_____
Dr. Ninian J. Blackburn, Thesis Advisor
Professor

_____
Dr. Pierre Moënne-Loccoz
Associate Professor

_____
Dr. Bradley Tebo
Professor

_____
Dr. Martina Ralle
Assistant Professor, OHSU Molecular & Medical Genetics

TABLE OF CONTENTS

LIST OF TABLES

LIST OF FIGURES

ABSTRACT

Spectroscopic and Kinetic Studies of Metal-Containing Proteins

Kelly Natalia Chacón, B.S.

Doctor of Philosophy

Division of Environmental and Biomolecular Systems within

The Institute of Environmental Health

And the Oregon Health and Science University

School of Medicine

May, 2015

Thesis Advisor: Ninian J. Blackburn

The overarching goal of our research is to better understand the mechanisms by which metalloproteins obtain and transport their target metal ions. We have characterized the maturation of a copper-containing subunit of cytochrome c oxidase (CuA) in *T. thermophilus*, as well as the metal ion transport mechanism of a tripartite Cu/Ag ion efflux pump and metallochaperone in *E. coli* (CusF(CBA)) **These characterizations are vital to understanding the basic and applied biochemistry of metal ion homeostasis in living cells, and will inform future research of detrimental mutations and metal ion related diseases in humans as well as possible antimicrobial targets.**

Cytochrome c oxidase (CcO) is a large terminal respiratory enzyme, belonging to the heme copper oxidase superfamily, and is present in all eukaryotes, and some aerobic prokaryotic organisms. The CuA protein is(~14kD) located in subunit 2 of the

ba_3–type cytochrome oxidase from *Thermus thermophilus*, and contains a unique, binuclear Cu center which is able to delocalize a single electron between the two Cu atoms. The assembly of this site within the periplasmic membrane is believed to be mediated by the copper chaperones Sco and/or PCuAC, but the biological mechanisms are still poorly understood. Furthermore, because the CuA center has an electron-delocalized $Cu^{1.5}$– $Cu^{1.5}$ center, both Cu(II) and Cu(I) states are implicated in the metallation process. We studied the formation of mixed-valence CuA by stopped-flow UV−vis, EPR, and XAS at both Cu and Se edges, while the formation of fully reduced di-Cu(I) CuA was studied by XAS alone. Our results establish important differences between the metallation reactions of Tt and purple CuA azurin and allow us to extend mechanistic inferences to formation of the di-Cu(I) state which, may be more relevant to biological CuA assembly.

We also investigated the periplasmic efflux pump CusCBA and its metallochaperone CusF, which are vital to the detoxification of copper and silver ions in the periplasm of *Escherichia coli*. We used selenomethionine (SeM) active site labels in a series of biological X-ray absorption studies at the selenium, copper, and silver edges to establish a "switch" role for the membrane fusion protein CusB. We determine that metal-bound CusB is required for activation of cuprous ion transfer from CusF directly to a site in the CusA antiporter, showing for the first time (to our knowledge) the in vitro activation of the Cus efflux pump. This metal-binding site of CusA is unlike that observed in the crystal structures of the CusA protein and is composed of one oxygen and two sulfur ligands. Our results suggest that metal transfer occurs between CusF and apo-CusB, and that, when metal-loaded, CusB plays a role in the regulation of metal ion transfer from CusF to CusA in the periplasm.

ACKNOWLEDGEMENTS

A thankful heart is not only the greatest virtue, but the parent of all other virtues.
– Cicero

I would like to first acknowledge my tireless and brilliant instructors, professors and the members of my committee. From entering the Clatsop Community College GED tutoring room long ago, to now completing my doctorate, it truly was the time investment made in me by these educators that allowed me to achieve anything at all. I thank the Stanford Synchrotron Radiation Lightsource, the National Science Foundation, Vertex Pharmaceuticals, and the National Institute of Health for funding.

A warm acknowledgement to my mentor, Dr. Ninian J. Blackburn – thank you for letting me learn to do science on my own terms, so that I could navigate the independent and creative process of research. I am so grateful that you will be my lifelong mentor and colleague. Above all, thank you for sharing with me your joy in the beamline – making your tea was the least I could do in return.

A hearty thank you to Dr. Pierre Moënne-Loccoz, for letting me break things and helping me to fix them, for allowing me to take up your precious time with scientific conversations, and for frank constructive criticism when it was needed. You have made me a better critic of my own work and I am indebted always.

Thank you to my friends and family, for forgiving me all of the things I missed out on and yet providing me with so many wonderful moments. I love you. Thank you to my lab mates past and present, for always being there no matter what.

Finally, I thank my husband Niles. Mere words of thanks seem empty, my love.

CHAPTER 1

AN INTRODUCTION TO METAL ION HOMEOSTASIS

1.1 General principles of metal ion homeostasis:

Metal ions have extremely diverse chemistries that make them invaluable in the living cell. As a result, organisms have evolved over millennia to employ many types of metal ions for otherwise unattainable levels of energy needed not just to survive, but also to thrive. Today, biologically relevant metal ions such as Ca, Na, K, and Mg are crucial to the proper function of nerves, tissue, and nucleic acids, while transition metals such as Fe, Cu, Zn, Ni, Mn and others serve a wide variety of biological needs. Paradoxically, at times the acquisition of these metal ions can be a highly difficult task, while at others, these metals can be found dangerously in excess. Living organisms must therefore be ready to contend with both of these scenarios, and have evolved to do so in a process that is broadly termed *metal ion homeostasis*.

1.2 Eukaryotic and Prokaryotic metal ion transport and flux:

To obtain more scarce metals, or in times of metal-limited conditions, organisms must scavenge trace amounts of metal ions while concurrently defending against organisms competing for the same bionutrients. This competition can often develop into what is known as a "host-pathogen" relationship, in which a host sequesters metal away from an invading pathogen, while the pathogen attempts to breach the host's defenses in order to obtain the metal ions.

Broadly speaking, all metal ions must be brought into the cell by passing through the lipid bilayer, which can only occur by proteins and molecules (ionophores) imbedded within the bilayer that can mediate metal ion transport. Proteins that are responsible for this kind of transport fall into three well-established categories: carriers, pumps, and channels (**Figure 1.1**) . Organisms employ all of these types of transporters, in both highly specific *and* deliberately non-specific ways, in order to maintain the proper balance of the correct metal ions in the cell.

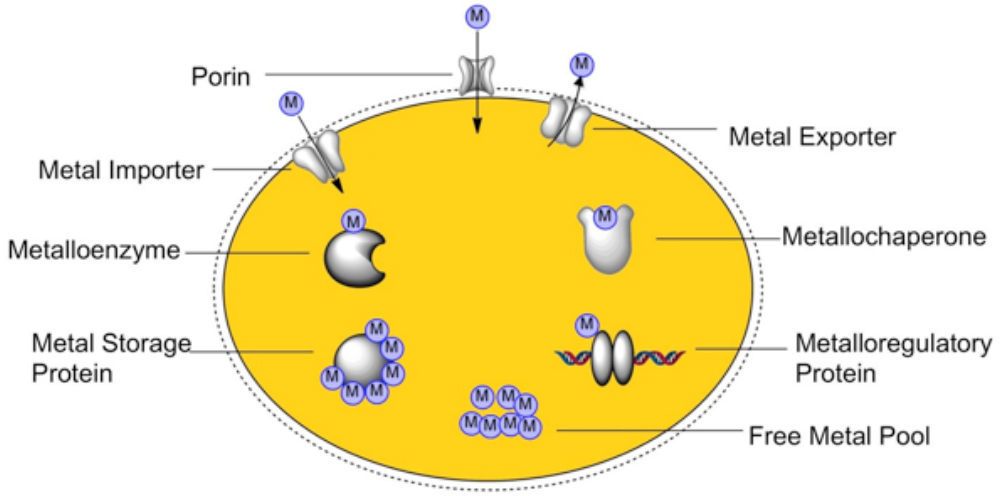

Fig 1.1 Schematic of metal-ion handling in the cell

In humans, the balancing act of maintaining metal homeostasis can be further complicated by diseases of metal ion trafficking and uptake, as well as malnutrition due to lack of available bionutrients in the environment. Diseases of metal ion trafficking and uptake such as hemochromatosis, enteropathica, acrodermatitis, and Menkes disease are often due to mutations in the proteins in pathways responsible for those tasks. Therefore, understanding the mechanisms that underlie the uptake,

trafficking and utilization of metal ions is of great importance to human health, as well as critical to understanding the basic biochemistry of metals.

Metal-ion homeostasis is extremely complex and filled with delicate interplay between multiple systems, frustrating our understanding of how homeostasis truly works. It is well understood that prokaryotes and eukaryotes both use carriers, pumps, and channels to obtain and move metals in the cell, but the particular machinery and strategies for homeostasis can vary greatly between the organisms.

Bacillus subtilis has long served as a model organism to explore how bacteria maintain metal ion homeostasis. As a result, much is now known regarding bacterial management of Fe, Zn, Mn, Cu, and even rare "toxic" metals like Cd, Se, and As. Broadly speaking, bacterial metal homeostasis is governed by a series of highly metal-selective uptake and efflux regulators which can act directly (binding metal and acting as a gene or operon repressor or de-repressor) or indirectly (binding metal and initiating a signal cascade that will eventually act to repress or de-repress a gene or operon).

It has been established that metal-sensing, gene-repressing machinery are responsible for Fe, Zn, and Mn homeostasis in *B. Subtilis*. The best understood families responsible for the overarching management of these metals are Fur, and DtxR, which in turn effect gene-regulating proteins such as Fur, Zur, and MntR. Cu *efflux* is mostly attributed to the Mer and ArsS families which are responsible for Cd, Ag, and As efflux, but much less is currently known about Cu *uptake* mechanisms in *B*. *subtilis*. However, recent work (Hirooka *et al.* 2012) indicates the involvement of a

newly discovered 9-transmembered-domain membrane protein YcnJ, which may be mediated by a *ycnKJI* operon which responds to low intracellular Cu.

Eukaryotic metal ion homeostasis is markedly more difficult to fully understand, but studies in *saccharomyces cereviciae* have illuminated how metal-ion homeostasis of all vital metals may be carried out in these organisms, which includes humans. Similar to the case in prokaryotes, homeostasis is managed by families of metal-responsive transcription factors: Fe, Zn, Cu levels are regulated by Aft, Zap and Ace, respectively (Rutherford and Bird 2004). These factors are responsible for the transcription of hundreds (at least as of now) of varied machinery such as transporters, metallothionines, chaperones, and stress response proteins. It does seem that a key distinction between prokaryotic and eukaryotic metal regulation is that eukaryotes employ multiple layers of regulatory control over the process of homeostasis – an important safeguard, should a damaging mutation affect one or more mechanisms of control of metal regulation.

1.3 The chemistry of metal ions in the cell:

In a strictly chemical context, metal ions are necessary in the cell to act as charge neutralizers, as linkers in compounds, and as the heart of a complex, where it may or may not act as a redox agent. While the key prerequisite of being used in a cell is a metal's availability during evolution, the next important attribute of a metal is that it is able to form chemically useful interactions with a non-metal such as S, H, C, N, O, or P. This has led to the common use of the hard soft acid base (HSAB) treatment of metals in biology as "hard" (light, small atomic radii, higher affinity toward O and N ligands over S) and others as "soft" (heavy, larger atomic radii, and

higher affinity toward S than N or O). With these designations, it may come as no surprise that Nature has, with some key exceptions, chosen metals that classify as "borderline" according to HSAB theory – but all are still classified as Lewis acids. This borderline behavior may contribute to the relative flexibility of possible ligand sets available in the cell for a given metal, while the hard and soft exceptions (Fe(III), Cu(I), respectively) may impart a necessary stringency for a fixed ligand set.

Just as metals are classified, biological ligands fall into the category of hard, borderline, and soft – but all are considered to be Lewis bases. Generally speaking, hard metals prefer hard bases, soft metals prefer soft bases, and so on. Most biological ligands are either part of an amino acid side chain, the bases of nucleic acids, small nonproteinaceous ligands, or organic cofactors. In a protein, the most common amino acid ligands are the thiolate of cysteine, the methyl thioether of methionine, the imidazole of histidine, the carboxylates of aspartate and glutamate, and the phenolate of tyrosine. Finally, the unique folding of any given protein may allow for any combination of these ligands and can also allow reactive chemistry to take place that would be difficult or impossible to carry out synthetically.

1.4 Biochemical and inorganic chemical basis for metal ion recognition:

Central to the understanding of transport mechanisms is the question of what governs the overall affinity of the protein for its target metal. In essence, a protein acts as a multidentate ligand – that is to say, a scaffold upon which one or more amino acids are poised to interact with a metal. Unlike the case in which overall metal ion–ligand affinities are dictated by the conditional stability constant **K'**, which takes into account any competing equilibrium from all possible species in solution, for proteins

the overall formation constant $\mathbf{K_m}$ can be used. In the formation of a metal complex such that :

$$\mathbf{M_F + L_F \leftrightarrow ML}$$

$\mathbf{K_m}$ is defined as:

(1) $$K_m = \frac{\mathbf{[ML]}}{\mathbf{[M_F][L_F]}}$$

Where **ML** is the concentration of metal ligand complex, and $\mathbf{M_f}$ and $\mathbf{L_f}$ are the concentrations of free metal and free ligand, respectively. K_m can be used to find the degree of formation of the protein–metal complex so long as the amount of free metal can be determined. This can be accomplished by adding a competing metal chelator that is easily quantifiable once complexed with metal. However, it has become increasingly more common to calculating the degree of formation by measuring the heat change produced by metal binding to proteins via isothermal calorimetry (ITC).

A major complication to the concept of protein–metal ion interaction is the fact that within the living cell, there are in theory multiple types of metals available for binding to a given protein, particularly nascent proteins. If only the Irving Williams series is considered (which states that affinities for essential metals in the +2 state tend to follow a universal order of preference [Mg^{2+} and $Ca^{2+} < Mn^{2+} < Fe^{2+} < Co^{2+} < Ni^{2+} < Cu^{2+} > Zn^{2+}$)]) then a protein would always simply bind Cu^{2+}. However we know that this must not be what occurs *in vivo*, and therefore the cell must have many strategies in place for ensuring that the correct metal goes to the proper protein, and that by the same token, strategies must exist that ensure that a metallochaperone has an absolute method for recognizing and delivering the correct metal to its target. An important global strategy employed by bacteria to ensure fidelity is to confine the

majority of certain types of metal ions to the periplasm (such as Cu(I)) and others mainly to the cytoplasm, as well as limiting metal contact by compartmentalizing where a nascent protein is actually being folded. But it is also becoming clearer that the cell creates a heavy competition for the overall amount of a given metal ion available to a pool of various metalloproteins. By allowing these proteins to compete for that metal only on the basis of degree of formation, metal to protein specificity is largely maintained.

1.5 The nature of metalloprotein-metalloprotein recognition and transfer, using spectroscopic investigations of the Atx1/Ccc2 pair as a case study:

How is a protein bound-metal ion "recognized" by another metal transport partner? Much work has been done to study the nature of metal-mediated protein-protein interaction, in particular within the realm of copper loading and transfer, which serves as an excellent resource for case studies. One set of experiments, which used electrospray ionization mass spectrometry (ESI-MS) to investigate copper binding affinity of representative proteins in conditions that mimic the cell, indicate that copper is drawn to the enzymes that require it by passing from one copper protein site to another, therefore exploiting gradients of increasing copper-binding affinity and suggesting an overall thermodynamically favored mechanism (Banci *et al.* 2010). This does simplify the question of how transfer might occur between proteins that have different affinities for the same metal. However, this theory does not address known scenarios in which two proteins have nearly *identical* affinities for a given metal, and yet transfer is directional.

One example of proteins that are nearly identical, yet exhibit directional metal

ion transfer is the metal-mediated transfer between the yeast protein Atx1 (known as HAH1 in humans) and the metal binding domains (MBDs) of its partners, the P(1B)-type ATPases. In humans, these ATPases are known as the Menkes (ATP7A) and Wilson (ATP7B) proteins, while in yeast, the same role is played by the protein Ccc2 – but all are copper transporters located in the Golgi apparatus that, once given Cu(I) by Atx1, pumps Cu into the lumenal side of the trans Golgi network (TGN). At this point the lumenal, metal binding domain of the ATPase will unload its cargo into secreted apoproteins, and the now-mature metalloproteins can be shipped to their cellular destinations.

Atx1 and its ATPase partners are all structurally well characterized. Atx1 adopts a ferredoxin-type fold with a highly conserved MxCxxC motif that selectively binds Cu(I) in addition to other heavy metals, such as Hg(II) and Cd(II) (Arnesano *et al.* 2001b; Klomp *et al.* 1997). The N-terminal MBDs of Ccc2 are in fact homologous to Atx1, and also have the MxCxxC domain (Banci *et al.* 2001). The Atx1 and Ccc2 structures are superimposable, and the metal binding affinities of each are identical(Xiao *et al.* 2011), which led to deep speculation as to the mechanism for directional metal ion transfer since it was unlikely to be driven by a thermodynamic gradient as described by the previously mentioned ESI-MS experiments.

NMR and crystallographic studies of Atx1 show distinct changes in structure from the apo to the holoprotein, with Cu(I) forming a nearly linear two coordinate structure using the two Cys residues in the MxxCccC domain. This same work found that a lysine residue, poised near the metal binding site, might serve as a trigger for either the stabilization or the release of metal by moving the Cys residues outward,

toward solvent (Arnesano *et al.* 2001a). Subsequent studies of the protein-protein interaction between Atx1 and Ccc2 by nuclear magnetic resonance techniques supported a role for lysine, and found strong, specific interactions between lysine residues on Atx1 and negatively charged residues on Ccc . However, the Cu(I) ion was in fast exchange between the two proteins, which led to speculation as to how metal was finally transferred.

Cu –edge x-ray absorption spectroscopy (XAS), and heteronuclear single quantum coherence nuclear magnetic resonance (HMQC-NMR) data of the ^{199}Hg-loaded Atx1 variant had initially indicated a trigonal geometry for the Cu(I) center of Atx1, in which the third ligand was possibly exogenous. However, the continuing investigation of the Atx1/Ccc2 pair, determined via XAS of model inorganic complexes, was that Ccc2 was indeed linear two-coordinate as thought previously, but that the Cu(I) center would readily accept an exogenous phosphine or sulfur ligand to adopt a strained trigonal geometry. The follow-up work by the same group, which probed the six metal binding subdomains (MBS) of the Ccc2 counterpart ATP-7B, showed conclusively that metal transfer occurs exclusively to domain 2 of ATP-7B, which has a very similar biscysteinate coordination geometry to Atx1 (Ralle *et al.* 2003; Walker *et al.* 2004). This domain specificity was a surprising result, because exhaustive x-ray absorption, metal competition, and fluorescence labeling studies indicated no straightforward reason for this clear preference in domains.

The missing perspective on this dilemma was given when a combination of mutagenesis and NMR structural work was applied to the yeast Atx1/Ccc2 chaperone pair. The NMR data, which could not directly observe the metal ion, *could* be

combined with the detailed x-ray absorption data on the metallocenter to form what is now the current working mechanism. Individual Cys mutations in Atx1 or Ccc2 allowed for the NMR detection (by ^{15}N-^{1}H chemical shift mapping) of the actual residues responsible for successful Atx1-Cu(I)-Ccc2 complexation. NMR of the complex also lead to the observation of 25 discrete intermolecular Nuclear Overhauser Effects (NOEs), which gave key evidence of transient, electrostatic interactions on the surfaces of the proteins (Banci *et al.* 2006). This additional data allows for a scenario in which a nucleophilic attack of the Atx1-Cu(I) center by a thiolate ligand in Ccc2 leads to *a short-lived three-coordinate Cu(I) species*, and eventual Cu(I) transfer to Ccc2 (**Figure 1.2**).

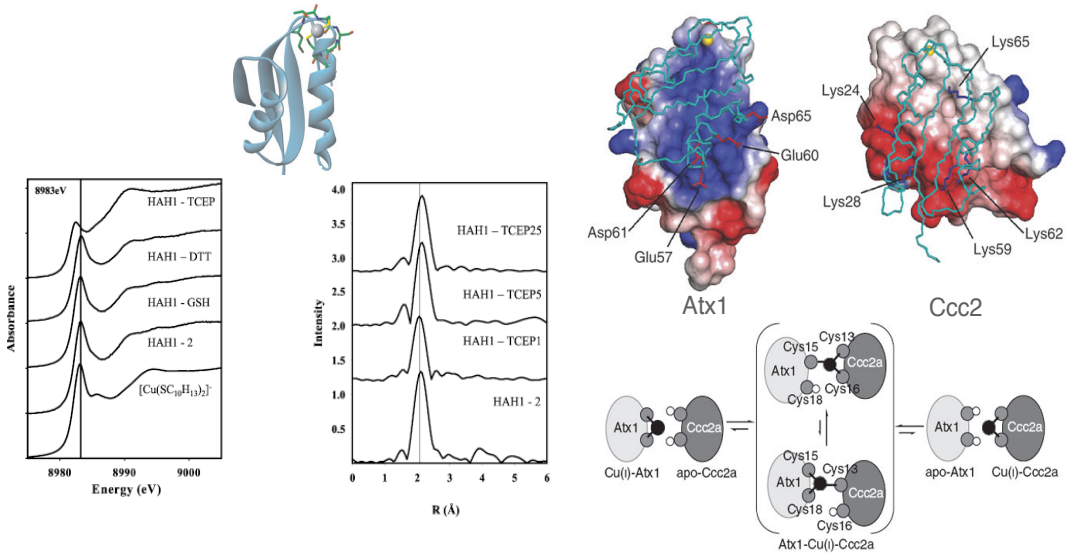

Fig 1.2 EXAFS and NMR studies of the Atx1/Ccc2 pair.
A) (Left) Absorption edges for unligated HAH1 reconstituted in the presence of GSH, DTT, and TCEP, showing an additional phosphine ligand for HAH1 in the presence of TCEP. The absorption edge of bis-2,3,5,6-tetramethylbenzenethiolate Cu(I) is included for reference. The solid vertical line corresponds to 8982.5 eV. (Right) EXAFS of the titration of HAH1 with TCEP. TCEP was titrated into Cu(I)-reconstituted HAH1 with ratios of 1:1, 5:1, and 25:1 TCEP/protein. Panel A reproduced from (Ralle *et al.* 2003). B) (Top) NOE-based electrostatic maps of Atx1 and Ccc2 showing the complementary charges of each active site region. (Bottom)

The mechanism for Cu(I) transfer between Atx1 and Ccc2a. Panel B reproduced from (Banci *et al.* 2006).

This kind of ligand "sampling", in which an adduct is formed between two nearly identical protein sites until metal has found the best resting site among the shared ligands, has now been offered as an alternative, kinetically-driven mechanism to describe chaperone-to-partner metal transfers that appear to act similarly to the Atx1/Ccc2 pair.

1.6 Challenges to the study of metal ions in proteins: Selenomethionine labeling as a means to track metal-ion recognition, loading and transfer:

Determining the mechanism of how a metal ion is incorporated into a protein or enzyme of interest often depends entirely upon the techniques available to "track" the metal ion. Fortunately, for many biologically relevant metal ions, the UV-Vis and microwave energy regions provide many ways to characterize and monitor metal ion capture by a protein, or to observe metalloenzyme activity. However, it is very difficult to find methods of tracking metal ions which have either completely full or completely empty d-shells – such as Cu(I), Zn(II) or Ag(I) – because they lack a spectroscopic signature at those energies.

By turning to extremely high energies, made possible by synchrotron radiation, these spectroscopically "quiet" metals can be fully examined. Hard X-rays can be harnessed in order to eject a core photoelectron from a metal and produce multiple scattering resonances between ligands and the metal ion, in a technique known as x-ray absorption spectroscopy (*vide infra*). However, this technique is insensitive to heterogeneity, and will only provide an *average* of all of the binding states in the

sample. This frustrates any effort to analyze proteins that have more than one metal binding site, or in an experiment that requires multiple, unique metalloproteins to be in the same sample.

Nevertheless, XAS becomes ideal for the investigation of redundant metallosites, as well as metalloprotein interactions, when combined with selenomethionine (Se-Met) labeling of active site methionine (S-Met) residues. By observing the Fourier transform (FT) spectra derived from the Se extended X-ray absorption fine structure (EXAFS), specific holo and apo metallosites within a given protein can be clearly distinguished. Se-Met labeling allows metallobiochemistry to be tracked both from the vantage point of Se, as well as from the vantage point of the bound metal ion.

This technique was first utilized in the CuA center of *Thermus thermophilus*, as a means to unambiguously determine Se−S(thioether) distances and thereby gain information on the Se−Cu−Cu and Se−Cu−S(thioether) angles (Blackburn *et al.* 1999). It was subsequently used to determine the role of the axial methionine in the blue copper center of azurin (Berry *et al.* 2003). Both of these are examples of the use of Se-Met labeling as a means to determine thioether distances and angles in a static site, but this method has also been used in order to track direct metal transfer between the periplasmic metal efflux proteins CusF and CusB. In this dissertation, I will describe further applications of the Se-Met labeling which have allowed for the kinetic and spectroscopic study of metal containing proteins, and have thus contributed to the ongoing quest to understand the nature of metal homeostasis.

1.7 Questions that will be addressed in this dissertation:

The overarching goal of our research is to better understand the mechanisms by which metalloproteins obtain and transport their target metal ions. To that end, we have selected cuproprotein systems for study that are poorly understood in terms of either their maturation pathway (i.e. from apo to holo protein), or in terms of the overall mechanism of metal transfer. In Chapters 3 and 4, I describe use of spectroscopy to investigate the assembly of the CuA center of *Thermus thermophilus* from inorganic Cu ions, as well as the possible roles for known biological accessory proteins in the in vivo assembly of the CuA center. In Chapters 5 and 6, I describe the use of multi element x-ray absorption spectroscopy and fluorescence spectroscopy to understand the mechanism of metal ion efflux in the periplasmic Cus system of *E. coli,* as well as the future directions of research on these systems.

CHAPTER 2

SPECTROSCOPIC METHODS UTILIZED IN THE STUDY OF METALLOPROTEINS

In order to facilitate the ease of reading in subsequent chapters, a chapter is devoted here to very briefly describe the spectroscopic methods implemented in the work that follows, with some experimental examples.

2.1 UV-visible spectroscopy of cupric metalloproteins

A key characteristic of many Cu(II)-binding proteins is that the copper ion will primarily form tetrahedral complexes with preferred amino acid ligands (His, Cys, Asp, Tyr, Met, or sulfide). Due to the $3d^9$ electronic configuration of Cu(II), an unpaired *d* electron and therefore unfilled *d* orbital allows for interesting, observable behavior upon excitation in a wide range of energies. In particular, the electrons in cupric centers can be excited into higher energy *d* orbitals, allowing for both weak and at times quite strong $d \rightarrow d$ transitions. Ligand to metal charge transfer (LMCT) transitions, which arise from the interaction of high-valent metal ions and electron-rich ligands, can also have large energy absorptions. Therefore, LMCTs and $d \rightarrow d$ transitions can be recorded as a spectrum by sweeping across a given energy range, as is carried out in UV-vis spectroscopy. UV-visible spectroscopy includes light in the visible and adjacent regions (near-UV and near-IR). Generally, the UV region is scanned from 200 to 400 nm, and the visible region is scanned from 400 to 800 nm.

In the case of biological metallocenters with partially full d orbitals, the identity of the ligands in the metal binding site have major influence of the intensity and shift in observed energy. Steady state UV-visible spectroscopy is therefore ideal for probing the electronic structure of a cupric protein site.

UV-visible spectroscopy is also useful in determining the affinity of a metal for a given protein so long as care is taken in what chemical methods are used (Xiao and Wedd 2010). Cu-specific, colormetric copper chelators such as bicinchoninic acid (BCA) and bathocuproinedisulfonic acid (BCS) can be complexed with metal ion, and slowly titrated into a solution of the metalloprotein under study. In the case of BCA, two originally uncolored molecules will chelate a single Cu(I) ion, forming a purple, water-soluble complex that absorbs light at 562 nm. BCS is a stronger chelator that binds either Cu(I) or Cu(II), and strongly absorbs light at 483 nm. The resulting binding curve can be fit in order to arrive at the association or dissociation constant for the metalloprotein, depending on whether the colorimetric ligand is being used to remove the metal ion, or to deliver the metal ion to the protein.

Finally, UV-visible spectroscopy can be used to probe the kinetics of a given metalloprotein system by the use of stopped flow measurements. Stopped-flow measurements can be made by rapidly mixing two components, such as an apo protein and a given metal ion. Once mixed, UV-vis spectra are taken on the millisecond timescale via high sensitivity photo diode array detectors or the like (**Figure 2.2**).

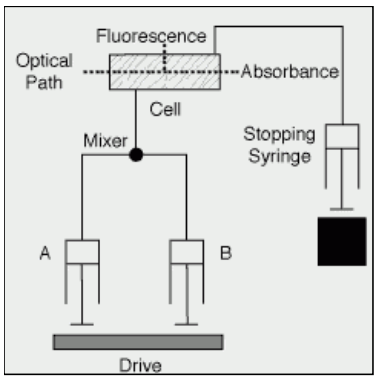

Fig 2.1 Schematic of a stopped flow UV-vis apparatus

Multiple species occurring during the time course of the reaction can be resolved to arrive at a kinetic scheme by the single value decomposition approach, as well as global fitting techniques. An example of this will be shown in section 3.4.4 of this dissertation.

2.2 Electron Paramagnetic Resonance Spectroscopy of cupric metalloproteins

Electron paramagnetic resonance (EPR) spectroscopy as used in biological systems has been described thoroughly in other work (Que *et al.*, *Physical Methods in Bioinorganic Chemistry,* 2010, University Science Books). In short, EPR measures the energy differences of an unpaired electron when placed in an external magnetic field. The basic concept of EPR is analogous to nuclear magnetic resonance (NMR), but instead of exciting the spin of an atomic nuclei (like a proton), it is the electron spins in the material that are excited. The essential equations are represented by

$$\mu = -g\beta \mathrm{S}$$

$$E = -\mu \cdot \mathbf{B}$$

$$E = h\nu$$

Where the first equation relates the magnitude of the magnetic moment (μ) of the electron to the electron spin, which are represented by g and β. β is the Bohr magneton, defined as

$$\beta = \frac{e}{2m}\frac{h}{2\pi}$$

Where m is the mass of a classical particle with charge e, and h is Planck's constant, here divided by 2π. The Bohr magneton has magnitude 9.285×10^{-21} ergG^{-1} (1Tesla=10^4 G). The value g, also called the spectroscopic splitting factor or the g factor, takes into account the local environment of the spin system. This value is equal to 2.0023 in an unperturbed system; however in metal systems, the g-values can significantly deviate from that number and therefore the g-value can be related to the characteristics of the ligand set near the unpaired electron. The experimentally obtained value of g depends heavily on the orientation of the unpaired electron in the magnetic field. In fact, depending on the angle at which a given spin system's absorption is measured, the obtained g-value will vary greatly, giving rise to the unique EPR spectrums observed in bioinorganic systems. After accounting for the averaging of anisotropy contributions in a given system, 4 limiting cases arise:

$$g_x = g_y = g_z$$

isotropic; magnetic moment is independent of orientation

$$g_x = g_y < g_z$$

axial; magnetic moment resembles prolate ellipsoid

$$g_x = g_y > g_z$$

axial; magnetic moment resembles oblate ellipsoid

$$g_x \neq g_y \neq g_z$$

rhombic; magnetic moment exhibits three unique values

In axial cases, the two common *g* values will be referred to as $g_{\parallel}$ ("*g* parallel") and the unique *g* value referred to as $g_{\perp}$ ("*g* perpendicular") (**Figure 2.3)**.

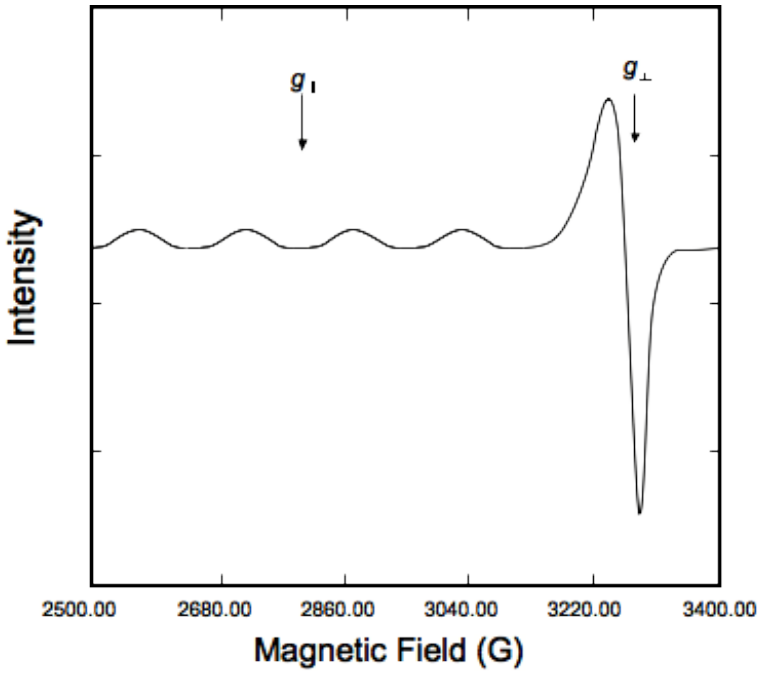

Figure 2.2 Typical axial EPR spectrum for a Cu(II) compound.

There are additional contributions to these types of EPR spectral envelopes – hyperfine splitting, and super-hyperfine splitting. As an electron is perturbed, the unique hyperfine couplings between the electron and nearby ligands produce a hyperfine splitting pattern that can be seen in the EPR spectra. As for the super hyperfine case, ligand nuclei which themselves have nuclear spins split the resonance into a multiple line pattern with the number of lines given by **2n I + 1,** where **n** is the

number of nuclei with nuclear spin **I**. These patterns may be subsequently simulated and quantified to gain information on the material under study.

Because Cu(II) complexes often contain an unpaired electron, some cupric proteins can be studied by EPR to better understand their structure and reactivity, as well as to quantify the amount of paramagnetic material in a sample. To analyze a given EPR spectrum, one must first define the type of spectral envelope it exhibits by establishing the *g* anisotropy of the system. While this can be difficult to determine due to complex hyperfine and super- hyperfine contributions, one can recognize familiar splitting patterns due to common nuclei and with the help of simulation software such as SimPip or EasySpin, a system can be characterized relatively easily.

EPR is often used on static protein samples, at very low temperatures (~ -160 °C). Additionally, transient structural as well as kinetic information about a cupric metalloprotein can be obtained when EPR is combined with the method of rapid freeze quenching of metalloprotein sample mixtures (*vide infra).*

2.3 X-ray absorption spectroscopy of metalloproteins

As was discussed previously, UV-vis and EPR spectroscopy are not of much use on metal ions such as Cu(I), Zn(II) or Ag(I) – because they lack a spectroscopic signature at those energies. Fortunately, the excitation of these and many other metals at extremely high energies is made possible by synchrotron radiation.

X-rays have wavelengths that are on the atomic size scale, making them ideal to use in interactions with molecules – much like in x-ray crystallography, which uses diffraction of x-rays to arrive at a 3D structure. However, in contrast to x-ray crystallography, x-ray absorption spectroscopy measures the energy dependent

absorption coefficient of a material, rather than its diffractive properties. While XAS for biological applications generally uses x-rays in the energy range of ~2400 – 30000 keV, XAS can in fact be used on a large number of elements in the periodic table. A common phrase used to describe the questions that XAS is able to answer is: *How many* of *what type* of atom are at *what distance* from the absorbing atom?

An XAS spectrum (**Figure 2.4**) is helpful to illustrate the phenomena that occur.

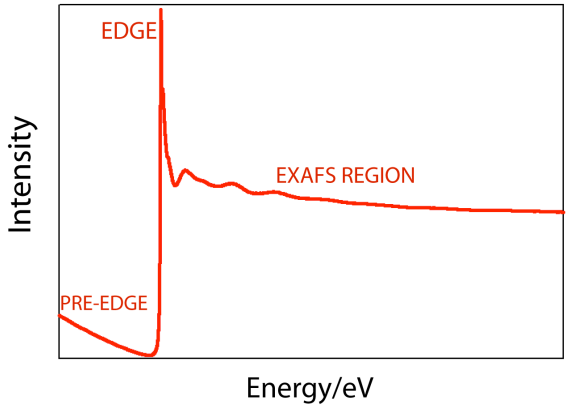

Fig. 2.3 A typical x-ray absorption spectrum, shown here at the Se edge

At discrete x-ray energies, energy is absorbed by an atom and a core electron is ejected from the atom to produce a photoelectron, which results in a sharp increase in the absorption coefficient as seen on the plot. This increase is known as the "edge" and its appearance and energy location provide information as to the local geometry and oxidation state of the atom. As the x-ray energy is increased, interactions between the produced photoelectron and the immediate neighbors of the absorbing atom produce many single scattering events. The many resonances result in oscillatory patterns in the plot, which is broadly referred to as the extended x-ray absorption fine structure (EXAFS) region. The EXAFS region provides a wealth of direct structural information regarding the radial distance from the absorbing atom to its neighboring

atoms, as well as the identity of those atoms. Importantly, XAS may only provide an average of all structures in a sample, and for this reason it is usually key that a sample is as homogenous as possible – i.e. that the sites in which the atom under study are nearly identical.

The physical description of the properties of χ (the EXAFS quantity) as a function of k (the photoelectron wave vector) will not be derived here, but the overall description of all factors that contribute to an EXAFS spectrum can be conveniently described in the EXAFS equation:

$$\chi(k) = \sum_j \frac{N_j f_j(k) exp[-2k^2\sigma_j^2] exp[-2R_j/\lambda]}{kR_j^2} sin[2kR_j + \delta_j(k)] \quad (2)$$

The EXAFS equation is the theoretical single scattering expression for χ. The summation is over the number of shells of scattering atoms, N, as well as over the individual expressions for the contributions of the amplitude, phase, and Debye-Waller (dampening factor, σ) to the semi-periodic behavior of the EXAFS.

An x-ray absorption spectroscopy experiment is set up similarly to a UV-Vis spectrophotometry experiment (**Figure 2.5**)

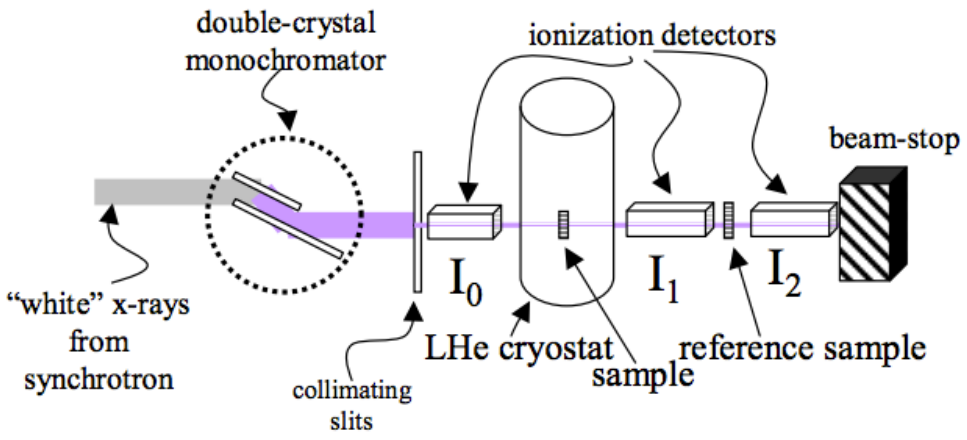

Fig. 2.4 Simple schematic of a typical x-ray absorption spectroscopy instrumental setup (fluorescence detector, which faces the sample on the x-axis, is not shown).

Key differences include: the source of energy is in the hard x-ray region, a mirror is needed to reject unwanted harmonics of the x-ray beam arising from Bragg diffraction effects, and a series of ionization chambers are used to record changes in intensity (I) as the x-ray beam passes though the slits, sample, and a reference material.

Applications of XAS are broad, and samples can range from solid to liquid. Additionally, one may choose to carry out transmission XAS (which will provide the absorption coefficient proportionally to ln (I_0/I), much akin to UV-vis) or fluorescence XAS. For most biological applications, however, fluorescence XAS is the preferred method to study a given absorbing atom. The technique of x-ray fluorescence utilizes extremely sensitive fluorescence detectors that are able to count fluorescent x-ray photons *whose origin is only from the absorbing atom*. This fluorescence arises from the energy surplus produced upon an outer shell electron dropping into the hole left by the ejection of the core electron. Importantly, there are

multiple fluorescence lines that can result from this event, and the most commonly selected line to detect is that of k α1 ("k alpha"), followed by L-edge fluorescence. These lines are primarily chosen for their relatively large signals relative to other nearby lines. The fluorescence detectors needed to detect these lines are commonly made from germanium, and the sensitivity can be altered depending on the number of detector channels available, as well as physical changes to the beam line setup (e.g. filters and slit size). A final key advantage to the technique of x-ray fluorescence is that the Ge detector can be efficiently "windowed" to the fluorescent peak of interest, which adds a higher level of signal to noise as well as selectivity.

While some information can be derived directly from the energy vs. absorption plot of an XAS spectrum, an EXAFS spectra must be processed by averaging, reducing, and Fourier transform (FT). A final FT will have a unitless y-axis, and an x-axis that corresponds to the distance from the absorbing atom in Ångstroms. Each peak present in the FT will directly correspond to a frequency present in the original EXAFS oscillation, and thus represent a neighboring atom to the absorber. At this point, these frequencies can be simulated by computational methods and the distance and identity of these contributions can be resolved. XAS provides extremely accurate interatomic distances (± 0.02 Å), and as such can be used to refine crystal structure interatomic distances, for example. Coordination numbers are less defined (± 20%), and determining the identity of the scattering atom is generally accurate for Z = 6-17 and less so for Z= 20-35. The use of SeM labeling is extremely useful in improving the accuracy of a simulation, because the fit parameters of the Se edge data must mirror that of the bound metal ion's edge data. With the additional Se data, therefore,

some parameters may be fixed to improve other parameters that are allowed to float during fit refinement, such as scattering atom distances and coordination number.

XAS can be used to address a diverse range of experimental questions, and in this dissertation, has been used as a primary means to understand physical mechanisms of metalloprotein maturity and metal ion transfer. As previously discussed in the introduction, SeM labeling can be exploited to probe not only the bound metal ion (such as copper, silver, and so on), but also neighboring Met ligands, which provides multiple vantage points that are useful to answer mechanistic questions. Furthermore, the technique of XAS can be combined with rapid freeze quench methods in lab in order to obtain time resolved structural and kinetic data simultaneously (*vide infra)*.

2.4 Rapid Freeze Quench

Rapid freeze quench (RFQ) is the process of arresting a rapidly mixed chemical reaction by extreme cold temperatures. It was pioneered by Bray in 1961 and has been used increasingly in spectroscopy as a means to trap chemical intermediates for spectroscopic study without the need to alter the reaction conditions, which would alter the phenomenon one wishes to study (Bray 1961; George *et al.* 1986). RFQ has been used in Resonance Raman, EPR, and XAS, and in other techniques where it would ordinarily be difficult to monitor a reaction in real time and native temperature (George *et al.* 1986;(Matsumura and Moenne-Loccoz 2014).

In essence, the setup is analogous to that of stopped flow, but unlike in stopped flow, which can collect time points optically, the time points collected in RFQ are

done so manually, and must be calculated in advance. Varying the syringe displacement rate from 2-8 cm/s, which varies the speed of solution ejection from the system, controls reaction times. In conjunction with variable displacement rates, the volume of the reactor hose after the mixer can be varied to achieve different reaction times. 5 ms are added to the calculated reaction time to account for time of flight and freezing in liquid ethane. Samples of 125 to 250 μL are ejected into a glass funnel attached to XAS or EPR tubes filled with liquid ethane at ≤ -140° C. The frozen sample is packed into the tube as the assembly sits within a Teflon block cooled with liquid nitrogen to ≤ -100° C (**Figure 2.6**). Once packed, the frozen samples are stored in liquid nitrogen until analysis.

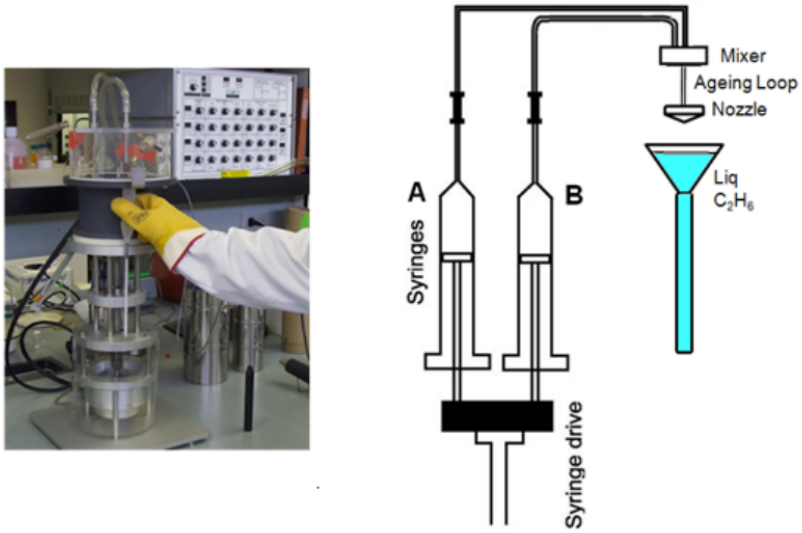

Figure 2.5 Update Instruments Inc. System 1000 Chemical/Freeze Quench apparatus photograph (left) and schematic (right). *Photograph/figure credit, P. Moënne-Loccoz.*

2.5 Fluorescence Spectroscopy of tryptophan-containing proteins

The final spectroscopic technique that has been employed in this dissertation is that of fluorescence spectroscopy. At room temperature, most molecules occupy the lowest vibrational level of the ground electronic state, and on absorption of light they are elevated to produce excited states. Once excited, the molecule may reach any number of vibrational sub levels. Having absorbed energy and reached one of the higher vibrational levels of an excited state, the molecule rapidly loses its excess of vibrational energy by collision and falls to the lowest vibrational level of the excited state. In addition, almost all molecules occupying an electronic state higher than the second undergo internal conversion and pass from the lowest vibrational level of the upper state to a higher vibrational level of a lower excited state, which has the same energy. From there the molecules again lose energy until the lowest vibrational level of the first excited state is reached. From this level, the molecule can return to any of the vibrational levels of the ground state, emitting its energy in the form of fluorescence (**Figure 2.6**).

Fluorescence in proteins is largely due to aromatic amino acid residues, such as tryptophan (Trp) or tyrosine (Burstein *et al.* 1973). Trp residues, which contain an indole group, are particularly sensitive to their local environment, and therefore are an extremely sensitive chemical probe. As a Trp rotates and moves, the resulting fluorescence can decrease, increase, or shift energy, all results which inform ongoing biochemistry (Vivian and Callis 2001). Most Trp residues will be excited by a photon at an energy of approximately ~280 nm, and emit the photon at ~ 350 nm.

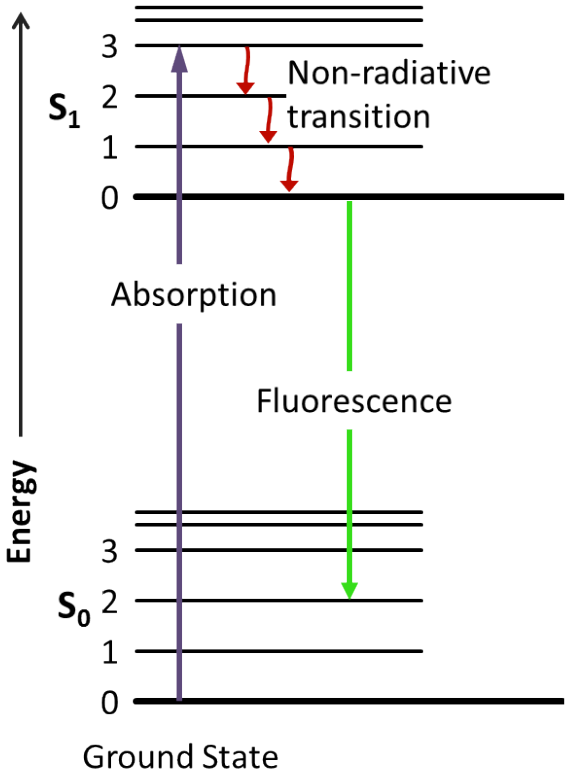

Fig 2.6 Generalized Jablonski diagram

Fluorescence quenching can be used to probe the extent of a small molecule or atom binding to an active site, to find the number of binding sites in a protein, as well as to probe the accessibility of an active site to solvent or a partner protein.

There are a wealth of studies utilizing Trp fluorescence to determine intermolecular distances, solvation, and global effects on enzyme mechanism. However to date, there have been limited fluorescence studies of the interaction of metal ions with binding site Trp residues. A study of note, which will be referenced here, is a Trp quenching experiment on the CusF Cu(I)/Ag(I) metallochaperone (**Chapter 5.2**).

CHAPTER 3

STABLE MONONUCLEAR INTERMEDIATES IN *TT* CUA

3.1 Introduction:

Cytochrome c oxidase (CcO) is a large terminal respiratory enzyme, belonging to the heme copper oxidase superfamily, and is present in all eukaryotes, and some aerobic prokaryotic organisms. Generally, cytochrome oxidases contain an Fe-Cu_B catalytic center that is responsible for the four electron reduction of molecular oxygen to water with concurrent driving of the proton gradient necessary for ATP production (Tsukihara *et al.* 1995);(Liu *et al.* 2009; Ostermeier *et al.* 1997; Soulimane *et al.* 2000; Svensson-Ek *et al.* 2002). The electrons required for this essential process must first be delivered to the Fe-B catalytic site via a series of transfers through the cofactor heme *a* in subunit 1, and in the *a3*-type oxidase, electron transfer occurs through the CuA binuclear Cu center in subunit 2 (Savelieff and Lu 2010). The CuA center is a unique, binuclear Cu center which by virtue of its short, cysteine-bridged Cu-Cu bond (~2.45 Å), is able to delocalize a single electron between the two Cu atoms, maintaining a mixed valence redox state of net +1.5 (1 Cu^{2+} and 1 Cu^{1+}). This short bond distance, coupled with the finely-tuned residues of the CuA metal-binding site, impart a remarkably efficient electron transport ability (Blackburn *et al.* 1994; Blackburn *et al.* 1999) (**Figure 3.1**).

---

* Material in this chapter has been published in this or similar form in the Journal of the American Chemical Society, and is used here with the permission of the American Chemical Society.

Chacón K.N., Blackburn N.J. (2012) Stable Cu(II) and Cu(I) Mononuclear Intermediates in the Assembly of the CuA center of *Thermus thermophilus* Cytochrome Oxidase. *Journal of the American Chemical Society* **39**, 15373-8

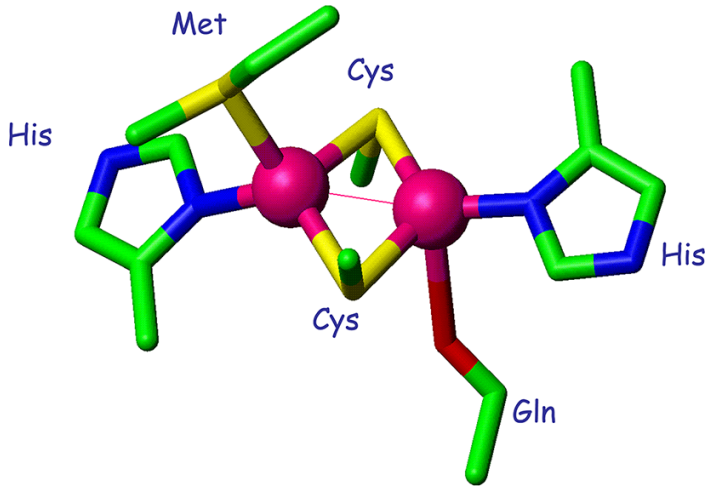

Fig. 3.1. Structure of the dinuclear CuA center (taken from pdb file 2CUA).

CuA cofactors have as of yet only been found in cytochrome *c* oxidase as well as in nitrous oxide reductases, where they perform essential tasks for the organism – radical mutations in the CuA metal binding sites, or in the ability to otherwise produce mature CuA prove fatal. The multiple copper chaperones and complex copper transport pathways necessary to produce the mature CuA are therefore of great interest in biology and chemistry. Currently to our knowledge, only two metalloproteins have been directly implicated in the loading of Cu into apo CuA. One of these metalloproteins is Sco, a red copper protein that is present in the inner membrane of mitochondria and can bind either Cu(I) *or* Cu(II) in a $(Cys)_2His$ motif. The variant Sco1, present in mammals and yeast, is directly implicated in CuA assembly, but its role is still poorly understood (Leary 2004; Leary *et al.* 2007; Leary *et al.* 2009). In *Bacillus subtilis*, it has been shown that the △*sco* mutant eliminates

oxidation of a dye, tetramethylphenylenediamine (TMPD), that directly indicates a defect in electron transfer to the CuA center present in aa_3 cytochrome c oxidase (Mattatall 2000; Siluvai *et al.* 2010; Siluvai *et al.* 2009). While the work in *B. subtilis* is a strong indicator that Sco is implicated in CuA assembly, whether Sco acts as a direct metallochaperone that loads metal into CuA or whether Sco simply acts as an oxidoreductase to reduce the cysteine residues in CuA to allow it to bind metal from some other chaperone is still unclear. The latter hypothesis was shown to have some support via a series of NMR studies utilizing *Thermus thermophilus* Sco and a truncated version of the *Tt* CuA protein subunit, which has its N-terminal membrane binding domain removed, yielding the soluble protein. In that study, the bis-thiol form of apo Sco was able to reduce the disulfide form of apo CuA. Further to this, that work introduced a separate, putative metalloprotein *Tt* PCuAC that was capable of loading Cu(I) into reduced CuA (Abriata *et al.* 2008). While that work was an intriguing addition to the CuA assembly story, PCuAC has as of yet only been found in prokaryotes, such as *Rhodobacter spheroides* (Thompson et al. 2012) and does not address how CuA is metallated in the many other eukaryotic organisms that require it for survival.

Model protein systems have been long employed as a robust method to understand the underlying chemistry of biological metallation processes. As such, the CuA center has been introduced into protein scaffolds via protein engineering (Andrew *et al.* 1995; Wilmanns *et al.* 1995), and metallated using inorganic ions in an effort to determine a mechanism of metal binding. In one such system, a CuA-Azurin construct, the addition of inorganic Cu(II) ions led to the discovery of three

mononuclear species (Wilson *et al.* 2011). The earliest intermediate had an absorption maxima at 390 nm and resembled an early red type-2"Sco-like" intermediate (Savelieff *et al.* 2008), the second was a novel species I_x, which presented at λ_{max} 410 nm, and the final was a blue intermediate with λ_{max} of 640 nm, which soon gave way to the final mature purple CuA center . However, attempts to isolate and characterize these intermediates were mostly unsuccessful.

While model complexes introduced to a protein scaffold have been invaluable, the use of the *Tt* CuA soluble domain has shown to be a soluble protein that in the apo form, can be reacted with Cu(II) ions to produce holo mixed-valence CuA (Slutter *et al.* 1996; Williams *et al.* 1999). Further to this, holo CuA can be reduced using dithionite to yield a di-Cu(I) form under anaerobic conditions – making *Tt* CuA a robust biological model.

Previous work utilized selenomethionine (Se-Met) incorporation in place of the axial Met 160 residue to probe the CuA center by x-ray absorption spectroscopy (XAS)(Blackburn *et al.* 1997). The remarkably short Cu-Cu distances in both the mixed valence and di-Cu(I) forms of CuA were determined by monitoring the extended absorption fine structure (EXAFS) of both the Se and Cu edges (Bagai *et al.* 2008; Barry and Blackburn 2008; Barry *et al.* 2008). Here we extend that work by reacting the apo S-Met and Se-Met labeled CuA protein with Cu(II) or Cu(I) ions and monitoring the formation of both the mixed valence and di-Cu(II) CuA by UV-vis, stopped flow, EPR, and XAS. Importantly, we were able to observe Cu(I) bound to CuA, which is silent to many forms of spectroscopy, by analyzing the Cu EXAFS. We found key differences between the CuA-Az and *Tt* CuA reactions with copper

ions, elucidated mechanisms of the metallation of CuA that may be biologically relevant, and homogenously isolated a novel green intermediate species with λ_{max}460 nm. This green intermediate has been shown to be mononuclear Cu(II)−(His)$(Cys)_2$ species with no observable Cu(II)−(Met) interaction. Reduction with dithionite generates the Cu(I) homologue which is again mononuclear but now shows a strong interaction with Met160. We suggest that pathways for Cu(I) and Cu(II) loading into apo CuA are distinct, with important implications for how CuA may be metallated in vivo, by its as of yet undetermined copper chaperones.

3.2 Experimental Methods

Expression of wild-type His6-Tt CuA

Ten milliliters of culture medium (LB and 50mg/mL kanamycin) was inoculated from a freshly streaked plate of BL21(DE3) cells containing the wild-type (WT) His6-Tt CuA plasmid. After overnight incubation, this culture was used to inoculate a 1L flask of culture medium. After approximately 3-4 hours of incubation at 37° C with shaking, the OD600 of the cell culture reached 0.6 - 0.8. At this point, the cell culture was induced by addition of IPTG to a final concentration of 0.4 mM and incubated for 4 hours at 37° C. Cells were harvested by pelleting via centrifugation at 5000 × g for 15 minutes. Typically, 1L of culture produced 8-10 grams of cells.

Expression of selenomethionine (SeM) His6-Tt CuA

Ten milliliters of culture medium (LB and 50mg/mL kanamycin) were inoculated from a freshly streaked plate of BL21(DE3) Met auxotrophic cells containing the His6-Tt CuA plasmid. After overnight incubation at 37° C, 100 microliters of this

culture was used to inoculate a 10 milliliter flask of minimal culture medium which included L-methionine. After overnight incubation at 37° C with shaking, this culture was used to inoculate a 1L flask of minimal medium that contained SeM in place of methionine. After approximately 8 hours, the OD600 of the cell culture reached 0.6 - 0.8. At this point, the cell culture was induced by addition of IPTG to a final concentration of 0.4 mM, and incubated for 6 hours at 30° C. Cells were harvested by pelleting via centrifugation at 5000 × g for 15 minutes. Typically, 1L of culture produced 4 grams of cells. Purification of wild-type and selenomethionine Tt CuA Pelleted cells were resuspended in lysis buffer, lysed using a French Press, and the cell debris pelleted by centrifugation. The lysate was passed through a 0.45 micron syringe filter. Tt CuA was purified from the lysate by chromatography on a nickel-NTA affinity column. The His6 tag was cleaved by overnight incubation with r-TEV protease followed by dialysis against imidazole-free buffer, and a second metal affinity chromatography step was used to remove the cleaved His6 tag. Sodium dodecyl sulfate-polyacrylamide gel electrophoresis (PAGE) (8-12% gradient stained with Coomassie brilliant blue R-250) showed a single band. Following purification, the protein was dialyzed into 50mM phosphate buffer, pH 7.0 with 10% glycerol and immediately stored at 80° C. Both the WT and SeM Tt CuA protein concentrations were routinely determined by the bicinchoninic acid (BCA) assay, and Inductively Coupled Plasma Optical Emission Spectroscopy (ICP-OES) was used to accurately determine selenium content in the SeM Tt CuA. Protein yield of the WT Tt CuA was ~25 mg per liter of culture medium, and yield of the SeM variant was generally ~12 mg per liter. Before use, apo-Tt CuA samples were thawed, dialyzed into the desired

buffer, and then incubated anaerobically with 3 mM tris(2 carboxyethyl)phosphine (TCEP) for up to 1 hour to reduce any disulfide crosslinks at the CuA site. The reduced protein was then dialyzed into excess anaerobic phosphate buffer (50 mM, pH 7) overnight to remove the TCEP.

Reconstitution of wild-type and SeM apo-Tt CuA with Cu(I) and Cu(II)

Reconstitution was carried out in a Coy anaerobic chamber to prevent oxidation of the cysteine residues. Reduced and dialyzed protein was incubated with up to a 3-fold excess of Cu(II) using an aqueous Cu(SO4) solution, or up to a 3-fold excess of Cu(I) using tetrakis acetonitrile copper (I) hexafluorophosphate ([Cu(CH3CN)4]PF6) in acetonitrile solvent. The protein was stirred while using a syringe pump which was set to deliver the given metal ion solution at a rate of 1 microliter per minute. The final concentration of acetonitrile did not exceed 10% of the total volume of protein solution. The reconstituted protein was then dialyzed exhaustively with metal free anaerobic buffer. Upon reconstitution with Cu(II), both wild-type and SeM apo-Tt CuA exhibited the expected purple color and remained stable indefinitely. Reconstitution with Cu(I) gave colorless solutions which were found to oxidize back to the purple mixed-valence species on removal of excess Cu(I) by dialysis. Therefore, for Cu(I) reconstitution, excess Cu(I) was removed by passing through three successive desalting columns equilibrated with buffer that contained decreasing concentrations of acetonitrile. The resulting samples were then flash-frozen in liquid N2 to prevent oxidation. Bound metal concentrations were determined by ICP-OES. Partial reconstitution of WT and SeM-Tt CuA with Cu (II) was performed on reduced and dialyzed proteins, by slow, anaerobic addition of metal solution using a syringe

pump set to deliver a pre-determined molarity of metal ions at 0.8-0.9:1 (SeM) or 0.5:1 (WT) copper to protein mole ratios.

UV-vis and EPR Spectroscopic measurements

Electronic spectra were recorded on a Cary 50 spectrophotometer. Electron paramagnetic resonance measurements were carried out on a Bruker ER085CS spectrometer under the following conditions: 9.4 Ghz frequency, 120 K, 2mW power, 25 db gain, 4 G modulation amplitude and a sweep time of 42 s. To determine the relative concentrations of paramagnetic copper in a given sample, a series of standard solutions containing 100-600 μM Cu(II)-EDTA in 50 mM phosphate buffer at pH 7.0 were measured in the same tubes as were used for protein samples. The concentrations of paramagnetic copper were determined by double integration. EPR spectra were simulated using SIMPIP as previously described (Nilges 1979)

X-ray absorption data

X-ray absorption data were collected at the Stanford Synchrotron Radiation Lightsource. The extended X-ray absorption fine structure (EXAFS) and X-ray absorption near-edge structure (XANES) of Cu (9.8 keV) and Se (12.6 keV) were measured on beamline 9-3 and 7-3 using a Si 220 monochromator with crystal orientation $\varphi = 90°$, and a Rh-coated mirror located upstream of the monochromator set to 13 keV (Cu) or 15 keV (Se) cutoff to reject harmonics. Samples were measured as frozen aqueous glasses in 20-25% ethylene glycol at temperatures between 7 and 15 K, and the XAS was detected as Kα fluorescence using either a 100-element (beamline 9-3) or 30-element (beamline 7-3) Canberra Ge array detector. A Z-1 metal oxide filter (Ni, As) and Soller slit assembly was placed in front of the detector to

attenuate the elastic scatter peak. Four to six scans of a buffer blank were measured at each absorption edge and subtracted from the raw data to produce a flat pre edge and eliminate residual Ni/As Kβ fluorescence of the metal oxide filter. Energy calibration was achieved by placing a Cu or Se metal foil between the second and third ionization chamber. Data reduction and background subtraction were performed using EXAFSPAK 31. The data from each detector channel were inspected for drop outs and glitches before being included into the final average. Spectral simulation was carried out using the program EXCURVE 9.2 as previously described (Binsted and Hasnain 1996; Gurman *et al.* 1984, 1986)

Stopped-flow spectrophotometry

SeM-Tt CuA Cu(II) binding kinetics were followed by stopped-flow using an Applied Photophysics SX-20 stopped flow spectrometer. In the first series of experiments, TCEP reduced anaerobic apo protein was rapidly mixed with an excess of anaerobic Cu(SO4)(aq) to form the SeM Tt CuA-Cu(II) intermediates and final mixed valence form. In a second series of experiments TCEP-reduced apo protein was rapidly mixed with 0.4 molar equivalents Cu(II) with the purpose of following the formation and decay of the green mononuclear intermediate under copper limiting conditions which precluded binding of a second Cu atom in the dinuclear site. Kinetic data were analyzed using the program DYNAFIT 34 (Kuzmic 1996) and by the Pro-K II global analysis software package (Applied Photophysics).

3.4 Results

Identification of a green copper intermediate in Tt CuA

Slow addition of Cu(II) ions to TCEP-reduced, anaerobic apo CuA led to a rapid conversion to an intense green species absorbing at 460 nm with a shoulder at ~410 nm, and less intense absorptions at 660 and 790 nm. This green species was stable at copper to protein ratios at or below 0.5:1 under anaerobic conditions for the WT protein, but showed greater stability in the M160SeM derivative where the 460 nm species persisted to 0.8-0.9 Cu:P. For both derivatives, further addition of Cu(II) ions converted the green species to the native purple of the mixed valence state, with the characteristic bands at 360, 480, 530, and 790 nm. **Figure 3.2** shows the UV/vis spectrum due to the formation of the green intermediate from WT, while **Fig. 3.2(b)** shows its subsequent conversion to purple product. The UV/vis spectral bands attributable to the green species increase monotonically in the formation phase reaching a maximum, and thereafter convert to purple CuA with isosbestic behavior. This suggests that the green species in **Fig. 3.2(a)** corresponds to an intermediate which can be isolated as a single species at molar ratios of ~0.5 or below for WT or 0.9 or below for the SeM derivative.

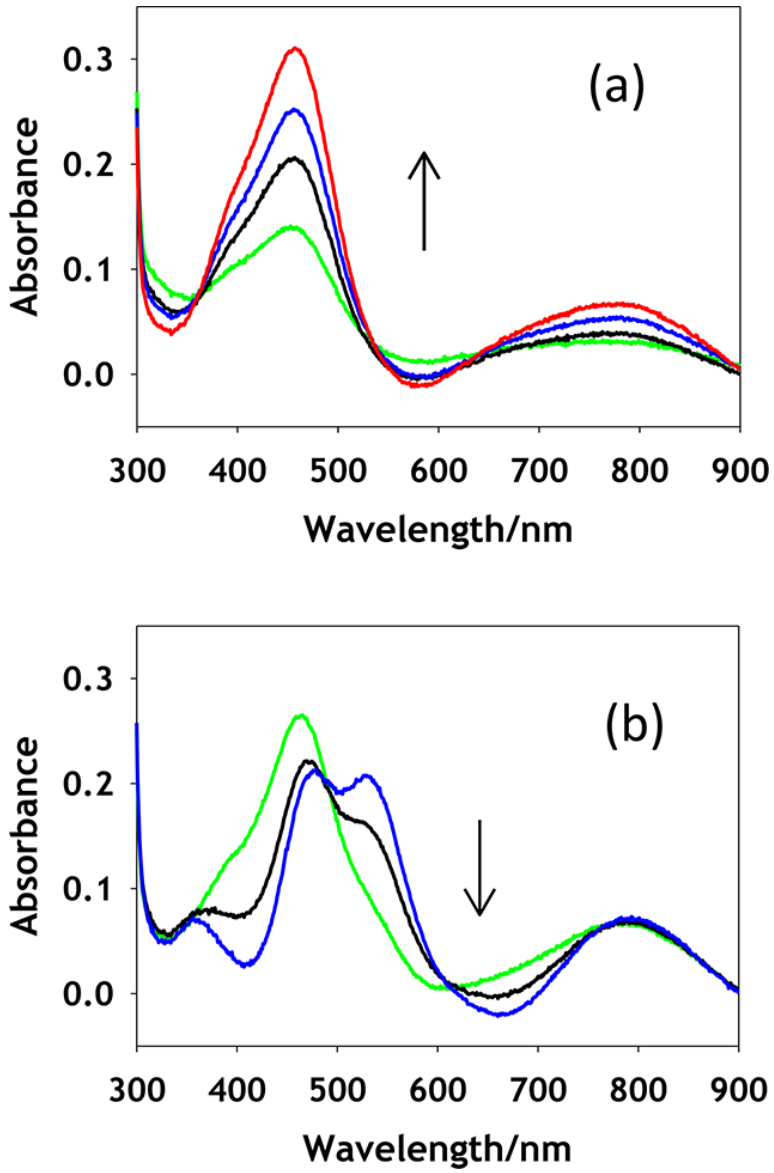

Figure 3.2 Titration of apo WT [M160S(Met)] CuA with increasing equivalents of aqueous Cu(II) sulfate. The spectra in (a) represent increase in formation of the green intermediates with Cu(II) to protein values (mM) of 0.2 (green), 0.3 (black), 0.4 (blue), and 0.5 (red) and in (b) represent conversion of the intermediate to mixedvalence product with Cu(II) to protein values (mM) of 0.7 (green), 0.9 (black), and 1.25 (blue).

Electron Paramagnetic Resonance Spectra

To investigate the nature of the green species, an EPR sample of apo SeM CuA was prepared by incubation with Cu(II) at 0.5 coppers to protein and then flash frozen to ensure stability in the open atmosphere. The resulting spectrum is shown in Fig. 3(a). A copper concentration that was less than stoichiometric was selected in order to minimize the possible presence of the mixed valence species, which would complicate extraction of the EPR signal of the intermediate. The spectrum is characteristic of a mononuclear type 2 cupric center with well-resolved hyperfine in both the parallel and perpendicular regions of the spectrum. Double integration of the signal versus Cu(II)-EDTA as standard resulted in an unpaired spin concentration of 98 per cent of the total copper, indicating that the intermediate was fully in the cupric state. The assignment as a mononuclear species was confirmed by simulation of the spectrum using the program SIMPIP which resulted in spin Hamiltonian parameters listed in the legend to **Figure 3.3**. The spectrum is axial, with $g_x = g_y < g_z$, corresponding to a mononuclear Cu(II) species and differs significantly from the mixed valence CuA spectrum, particularly with respect to the partially resolved seven-line parallel hyperfine splitting pattern observed in the M160SeM CuA center (Fig.3 (b)) which results from coupling of the single unpaired spin over two copper nuclei. Instead, a tetragonally distorted four-line splitting pattern is observed with $g_x = 2.0127$, $g_y = 2.0521$, and $g_z = 2.1344$. The anisotropy of the hyperfine interaction is calculated to be $A_x = A_y = 47$ MHz and $A_z = 326$ MHz (116 G), respectively. The g_z value is similar to that reported recently for red Cu(II)-Sco ($g_z = 2.1501$, $A_z = 572$ MHz) (Andruzzi *et al.* 2005) which is classified as a type II copper-thiolate ligated by

two cysteines and one histidine residue (Balatri *et al.* 2003; Williams *et al.* 2005). The value of A_z in the green intermediate places its coordination between type 1 and type 2, and differentiates the spectrum from both the Sco-like red copper thiolates and the "green" cupredoxin sites such as that found in nitrite reductase (A = 188 MHz (67 G)) (Olesen *et al.* 1998).

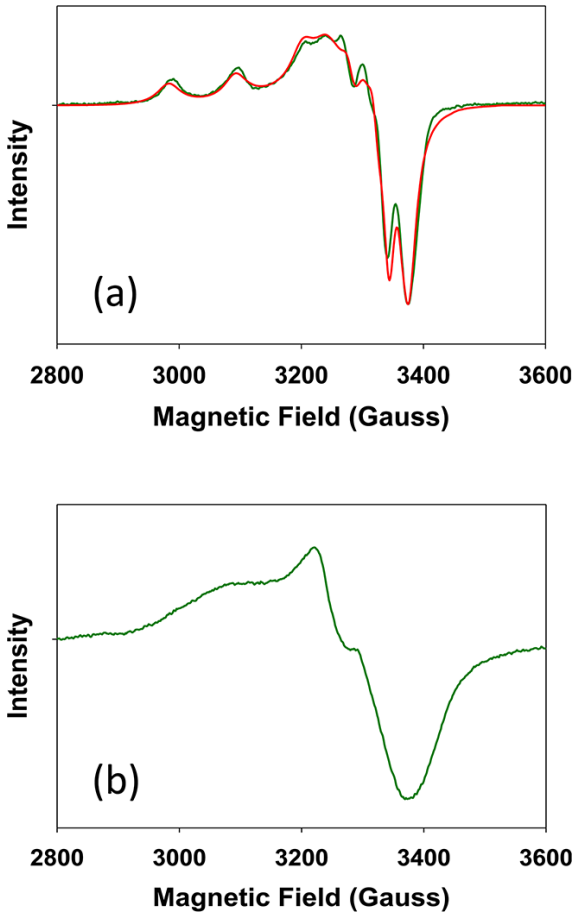

Figure 3.3 (a) Experimental and simulated X-band EPR spectrum of the green intermediate. The spectrum was simulated with the following Hamiltonian parameters: $g_x = 2.0127$, $g_y = 2.0521$, $g_z = 2.1344$ and $A_x = A_y = 47$ and $A_z = 326$ MHz (116 G). (b) X-band EPR spectrum of purple mixed-valence CuA for comparison. Experimental conditions were as follows: frequency 9.400 GHz, temperature 120 K, microwave power 2mW, modulation amplitude 4 G, instrument gain 25 db, and sweep time 42 s.

X-ray Absorption Spectroscopy

The nature of the intermediates formed in the metallation process was probed by X-ray absorption spectroscopy. To calibrate the system, we first re-measured and simulated EXAFS spectra for the mixed-valence and di-Cu(I) forms of the WT, and the SeM160 Tt CuA at both the Cu and Se edges. The results of these studies were similar to those previously reported, and are shown for reference in **Figure 3.4** and **Table 3.3**.

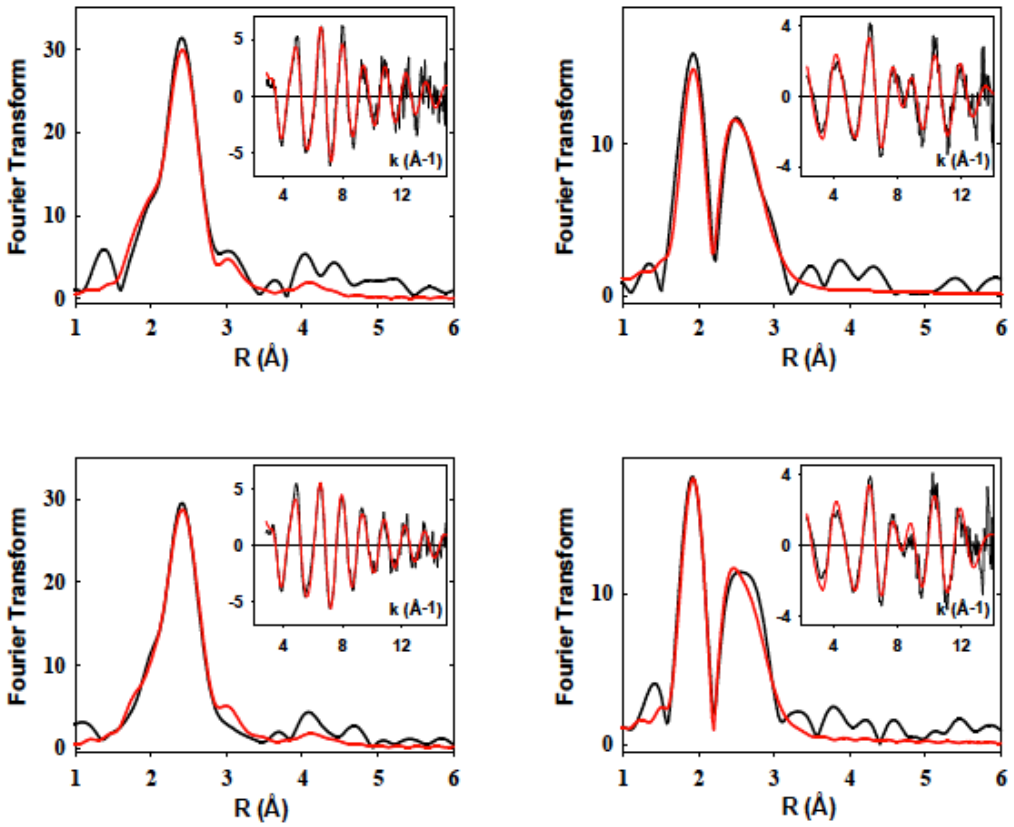

Fig 3.4 Fourier transforms and EXAFS (insets) for experimental (black) and simulated (red) spectra of the fully metallated dicopper forms of M160SeM T. thermophilus soluble CuA. Plots on the left are Cu EXAFS, while plots on the right are Se EXAFS. Top two panels are the mixed-valence spectra while the bottom two panels are the di-Cu(I) spectra.

The coordinate structure of the green intermediate formed in both WT and SeM derivatives was also probed by X-ray absorption spectroscopy at both the Cu and Se edges. Experimental and simulated data are shown in **Figure 3.5** with the parameters used in the fits listed in Table 1.

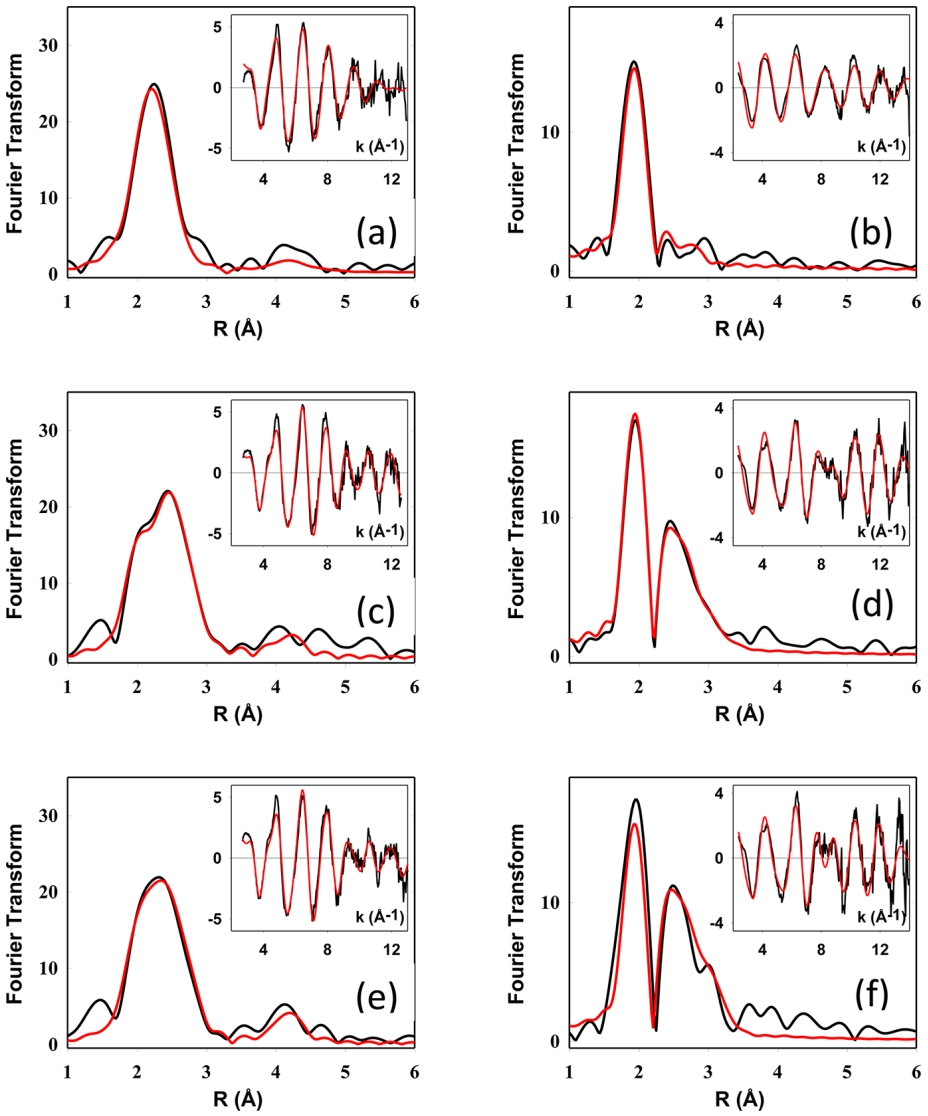

Figure 3.5. Experimental and simulated FTs and EXAFS (insets) for the Cu and Se EXAFS of mononuclear intermediates in the metallation of M160SeM CuA. Spectra (a,c,e) on the left are Cu EXAFS, and spectra (b,d,f) on the right are Se EXAFS. Spectra represent the following samples: top (a,b), green mononuclear Cu(II) intermediate; middle (c,d), mononuclear Cu(I) intermediate prepared by dithionite reduction of the green intermediate; and bottom (e,f), mononuclear Cu(I) intermediate prepared by reconstitution of apo bis-thiol CuA with $[Cu(I)(CH_3CN)_4]PF_3$.

Cu K-edge spectra for the SeM intermediate (**Fig. 3.5 (a)**) could be simulated by 1 Cu-His ligated at 1.98 Å together with 2 Cu.S(Cys) ligated at 2.22 Å. This coordination suggests that the SeM160 ligand is not coordinated in the mononuclear Cu(II) intermediate. A maximum of 0.15 Cu-Se could be tolerated by the simulation accompanied by ~0.2-0.3 Cu-Cu suggesting a small contaminating fraction of the mixed-valence product. Measurements at the Se edge confirmed this result as shown in **Fig. 3.5(b)**, where the Se EXAFS consists entirely of a single Se-C shell from the methyl and methylene C atoms covalently bound to Se in the selenomethionine residue. Consistent with the Cu data, a small component (~0.2) of Se-Cu could be fitted to the data again suggesting the presence of a small percentage of mixed-valence product. Studies on the WT green intermediate (at the Cu edge only) were also consistent with these conclusions, refining to 1 Cu-His at 1.98 Å, and 2 Cu-S at 2.27 Å, although in this case the S shell cannot be unambiguously assigned to the Cys residues such that Met coordination is not excluded by the data (**Table 3.3**).

We next inquired as to the whether a similar mononuclear intermediate could form from apo-enzyme and Cu(I). Cu(I) species were prepared by (i) reduction of the green Cu(II) mononuclear species with sodium dithionite and (ii) by reconstitution of apo protein with sub-stoichiometric amounts of tetrakis acetonitrile Cu(I) hexafluorophosphate [$Cu(MeCN)_4.PF_6$], using established protocols (Ralle *et al.* 2003). For WT where Se XAS is absent, the intermediate was formed using 0.5 mole equivalents. For the SeM derivative, mole ratios of 0.9:1 were employed so as to maximize the formation of the intermediate and avoid contribution from apo SeM protein at the Se edge.

sample/fit	F^a	Cu–N(His)^b no.^{c}	Cu–N(His)^b R (Å)^d	Cu–N(His)^b DW (Å^2)	Cu–Se no.^{c}	Cu–Se R (Å)^d	Cu–Se DW (Å^2)	Cu–S no.^{c}	Cu–S R (Å)^d	Cu–S DW (Å^2)	$-E_0$
Cu edge (S-Met)											
Cu(II)	0.540	1	1.98	0.003				2	2.27	0.013	1.1
Cu(I)-Dithio Fit A	0.514	1	2.10	0.030				2	2.20	0.015	0.3
								1	2.33	0.003	
Cu(I)-Dithio Fit B	0.478	1	1.99	0.012				1	2.21	0.007	1.7
								1	2.33	0.002	
Cu edge (Se-Met)											
Cu(II)	0.615	1	1.99	0.020	0.15	2.48	0.012^e	2	2.22	0.013	1.0
Cu(I)-Dithio Fit A	0.443	1	1.98	0.030	1	2.47	0.007	2	2.21	0.014	−1.9
Cu(I)-Dithio Fit B	0.465	1	1.96	0.004	1	2.47	0.006	1	2.23	0.002	−0.4
Cu(I)-ACN Fit A	0.442	1	1.93	0.025	1	2.46	0.007	2	2.21	0.011	−3.0
Cu(I)-ACN Fit B	0.408	1	1.97	0.003	1	2.47	0.008	1	2.23	0.002	0.2

sample/fit	F^a	Se–C(met) no.^{c}	Se–C(met) R (Å)^d	Se–C(met) DW (Å^2)	Se–Cu^f no.^{c}	Se–Cu^f R (Å)^d	Se–Cu^f DW (Å^2)	Se–S no.^{c}	Se–S R (Å)^d	Se–S DW (Å^2)	$-E_0$
Se edge (Se-Met)											
Cu(II)		2	1.96	0.006	0.2^e	2.49	0.012				
Cu(I)-Dithio	0.703	2	1.97	0.004	0.9	2.48	0.007	1	3.09	0.025	5.1
Cu(I)-ACN	1.15	2	1.96	0.005	0.9	2.49	0.008	1	3.07	0.014	4.2

Table 3.1 Fits obtained to the EXAFS of mononuclear intermediates formed during the metallation of the M160SeM variant of *Tt* Cu_A.

Cu K edge Fourier transform and EXAFS data for the Cu(I) species formed from the SeM derivative by each of these methods are shown in **Fig.3.5(c) and (e)** with Se K edge data shown in **Fig 3.5 (d) and (f).** Parameters used in the simulations are listed in **Table 3.1**. Inspection of the Se data show a clear difference relative to the Cu(II) intermediates, namely that a strong Se-Cu interaction is now visible as an intense second-shell peak at ~2.5 Å in the FTs. This provides unambiguous evidence that Cu(I) recruits the Met ligand. The Cu data confirm the presence of a Cu-Se interaction for both dithionite reduction and Cu(MeCN)4 reconstitution at the same (2.46-2.49 Å) distance. Whereas the green Cu(II) intermediate is clearly mononuclear both from the EPR and XAS data, a similar assignment for the putative Cu(I) mononuclear species is not as definitive. Dithionite reduction of the Cu(II) intermediate would be expected to generate a mononuclear Cu(I) species, but the coordination is different for the two oxidation states, since the Se edge data clearly

shows Cu(I) coordinated by the M160 ligand. However, detailed analysis of the XAS data reveals ambiguities in distinguishing between two possible structural models for the Cu(I) coordination. The first of these involves a simple Cu(I) mononuclear species in which the Cu(I) ion adopts a similar structure to the Cu(II) mononuclear species but increases its coordination by binding the M160 S or Se donor. In this scenario, it we expect the Se edge data to show 1 Se-Cu interaction, and the Cu-edge data to show 1 Cu-Se (at the same distance) and no Cu-Cu interaction. This is modeled in Table 1 for both the dithionite reduced form and the Cu(I) reconstituted form and is consistent with a mononuclear assignment. The second possibility is that the Cu(I) mononuclear species is unstable relative to formation of the di-Cu(I) product, such that at 1:1 Cu(I) to P, equal amounts of di-Cu(I) and apo protein are present. Here we expect the Se data to show 0.5 Se-Cu (since half the Se in the sample is apo), while the Cu data should show 0.5 Cu-Se and 1 Cu-Cu, similar to the fit observed for the di-Cu(I) (**Figure 3.4**). Put in another way, comparison of the Se edge data for 1:1 with the fully formed 2:1 Cu(I):P species should show equal intensity of the Se-Cu peaks in the FT if the 1:1 species is mononuclear, but be half as intense if the species is a mixture of 2:1 and apo protein. **Fig 3.6 (a)** compares Se edge FTs for the Cu(I) species generated by dithionite reduction of the green intermediate (Cu(I):P = 0.9:1) and purple mixed valence (Cu(I):P = 2:1), from which it can be seen that the Se-Cu peaks are (i) of comparable intensity and (ii) have very different shapes, suggesting differences in the identity of the species and favoring the mononuclear model.

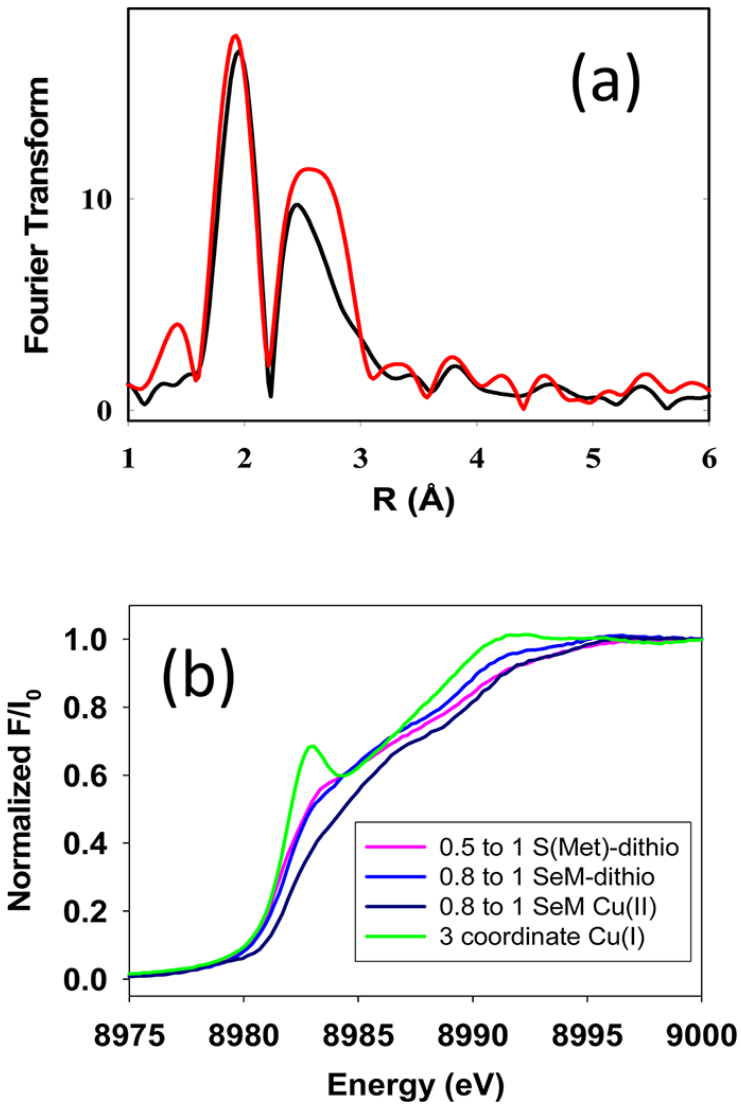

Figure 3.6. Evidence that 1:1 Cu(I) to protein species is mononuclear. Top panel, comparison of FTs of the Se EXAFS of the M160SeM species at Cu(I) to protein ratios of 1:1 and 2:1 showing nearequivalency of the intensity of the Se−Cu peaks in the FT expected for a mononuclear Cu(I) species. Bottom panel, absorption edges of Cu(I) mononuclear species compared with the three-coordinate Cu(I) derivative of the H135A variant of B. subtilis Sco [where Cu(I) is bound by 2 Cys and 1 Met residue]. The low intensity of the 8983 eV peaks of the mononuclear Cu(I) CuA intermediates suggest four coordination.

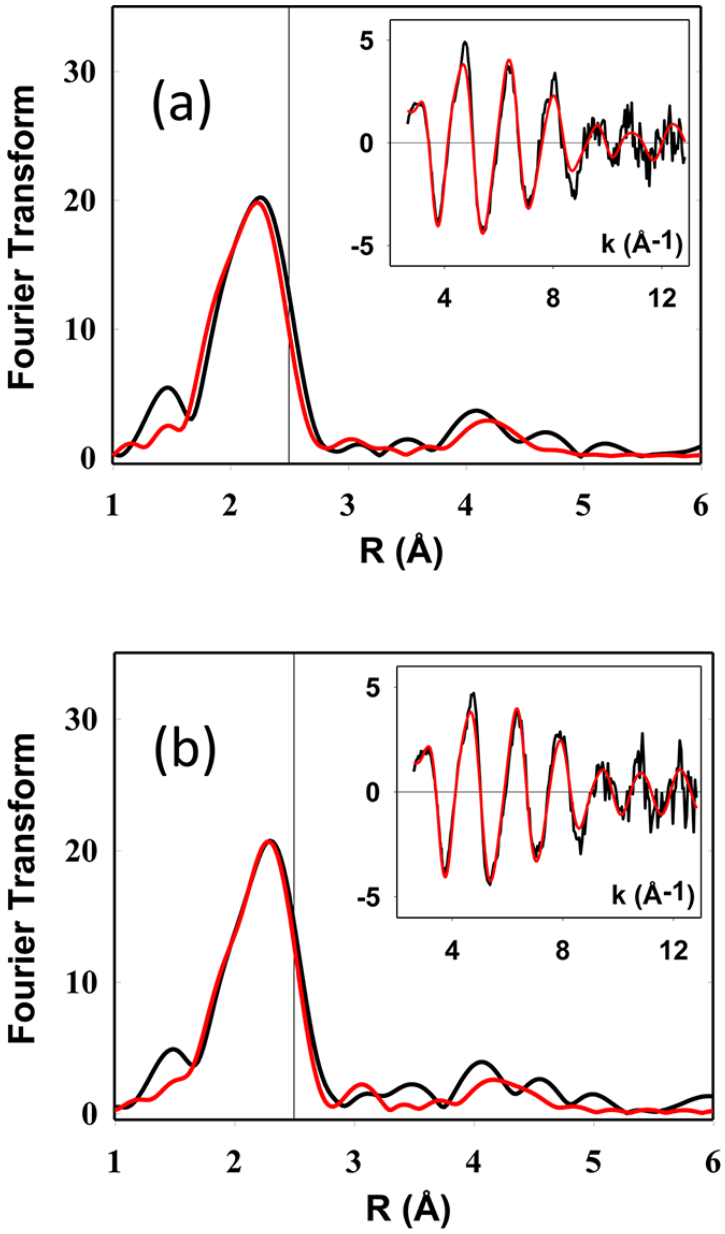

Figure 3.7. Experimental and simulated FTs and EXAFS (insets) for the Cu EXAFS of mononuclear intermediates in the metallation of the WT [M160S(Met)] CuA. Top spectra, mononuclear Cu(I) intermediate prepared by dithionite reduction of the green intermediate; and bottom, mononuclear Cu(I) intermediate prepared by reconstitution of apo bis-thiol CuA with $[Cu(I)(CH_3CN)_4]PF_6$. Parameters used in the fits are listed in Table 1. The vertical reference lines in each FT are drawn to illustrate the absence of a strong Cu−Cu interaction at 2.5 Å.

Additional evidence comes from analysis of the Cu EXAFS data, where good fits are obtained with 1 Cu-Se and no Cu-Cu. However this latter result is subject to uncertainty since the Cu-Se and Cu-Cu interactions have the same distance and similar phase shifts, making them difficult to distinguish and quantify. Paradoxically, distinguishing between mononuclear and dinuclear species is easier for the WT (S-Met) forms of CuA, since the species now differ only in the presence of the Cu-Cu. **Figure 3.7** compares the Cu FTs and EXAFS for M160M (S-met) CuA prepared by dithionite reduction of its green mononuclear intermediate, and by reconstitution with 0.5:1 $[Cu(MeCN)_4]^+$. The data are well simulated by a mononuclear species with Cu(I) bound by 1 His, 1-2 Cys residues (vide infra) and 1 S(Met). The vertical line at ~2.5 Å represents where Cu-Cu is expected, and the lack of intensity at this distance indicates Cu-Cu scattering at 2.5 is absent from the spectra. These data confirm the assignment as mononuclear species. A final ambiguity arises with respect to the number of coordinated cysteine residues in the mononuclear Cu(I) entities. Comparable fits (as judged by the value of F) can be obtained for S-Met and SeM derivatives using either 1 or 2 Cys residues, and are labeled Fits A and B for each species in Table 1. For the SeM derivatives where the Met donor atom is Se, Fit A (2 Cys residues per Cu) produces a very large and chemically unreasonable Debye-Waller factor for the Cu-His shell, whereas in Fit B (1 Cys) the DW values for both Cu-N and Cu-S are smaller and well within the expected limits. We also examined the absorption edges where the 8983 eV edge feature is often used as an indicator of coordination number. 3- coordinate species (corresponding to the 1 Cys model) have well resolved low-intensity peaks on the rising edge, whereas 4-coordinate species

have featureless edges. **Figure 3.6(b)** compares the absorption edges of the mononuclear Cu(I) species with that of a genuine three coordinate Cu(I) species, the H135M variant of B. subtilis Sco which is coordinated to 2 Cys and 1 Met residue (Siluvai *et al.* 2011). The lack of 8983 eV peaks on the mononuclear CuA(I) are more suggestive of 4-coordination favoring the 2-cys model. Although this observation seems to contradict the modeling, one possibility is that the mononuclear Cu(I) may sample all the ligands in the coordination environment in a fluxional fashion, or be held in a pseudo tetrahedral structure by the influence of the fourth ligand.

Stopped Flow Kinetic Analysis of CuA Assembly

To gain further insight into the mechanism of CuA assembly, we studied the kinetics of the metallation process using stopped flow spectrophotometry. The rates of formation of the mixed-valence product and its mononuclear intermediates were determined, starting from the bisthiolate apo protein and aqueous Cu(II) ion. The results of a typical experiment starting from 170 μM apo protein and 500 μM Cu(II) are shown in **Figure 3.8(a)** with the complete kinetic analysis given in **Fig. 3.8(b)-(d)**. **Fig. 3.8(a)** shows the time course of the reaction on a time scale of 0 -10 s (10-104 ms) where the evolution of the spectra is color coded from red (0.04 – 84 ms) to green (1 – 1.64 s) to blue (2.84 – 9.64 s) to purple (final products above 10 s). It can be seen that a spectrum similar to the green mononuclear intermediate with λmax= 460 forms initially and is then cleanly converted to the mixed valence product. **Fig. 3.8(b)** shows the absorbance versus time kinetic trace at 462 nm which is characterized by an increase to a sharp maximum followed by a slower decrease, corresponding to the

respective formation and decay of the intermediate species.

Absorbance versus time data was fit to trial mechanistic models using the program DYNAFIT which solves the series of differential and mass balance equations which define any particular mechanism for the associated rate constants. First, we tested a simple $A \rightarrow I \rightarrow P$ reaction scheme, where apo protein (A) reacts with Cu(II) to form intermediate I, which subsequently converts into the mixed-valence product P, but this reaction sequence failed to reproduce the sharpness of the maximum. The fact that the green mononuclear Cu(II) intermediate was converted into the mixed-valence product suggested that the latter was formed by addition of Cu(I) to I. This prompted us to include steps that could generate Cu(I) including reaction of Cu(II) with the bis-thiolate apo protein to form Cu(I) and oxidized apo protein A(S-S), or

$$A(S{-}H)_2 + 2Cu(II) \rightarrow A(S{-}S) + 2Cu(I) + 2H^+$$

or disproportionation of I,

$$I{-}Cu(II) + I{-}Cu(II) \rightarrow P + A(S^{\bullet}{-}SH) + H^+$$

$$A(S^{\bullet}{-}SH) + Cu(II) \rightarrow A(S{-}S) + Cu(I) + H^+$$

$$Cu(I) + I \rightarrow P$$

However, neither set of Cu(I) generating reactions improved the fit. The solution to the problem came from two experimental observations, first that very early in the reaction an additional species (the early intermediate) was present (Figure 8, vide infra), and second that the subsequent green intermediate was stable at sub-stoichiometric ratios of Cu(II), but converted to purple mixed-valence when the molar equivalents of Cu(II) rose above a threshold (**Fig. 3.2**). This latter result implied that Cu(I) is formed when the green intermediate reacts with Cu(II) and this Cu(I) may either react further with the green intermediate to form purple product or react with

apo protein to form the Cu(I) mononuclear species. A mechanism incorporating all of these observations was tested,

$$A + Cu(II) \rightarrow I_{early}$$

$$I_{early} \rightarrow I$$

$$I + Cu(II) \rightarrow A(S{-}S) + 2Cu(I)$$

$$I + Cu(I) \rightarrow P$$

$$A + Cu(I) \rightarrow I{-}Cu(I)$$

and after refinement of the rate constants for each step, gave an excellent fit to the data as shown in **Fig 3.8(b).**

The PRO-K II software of the Applied Photophysics stopped flow instrument was used to complete the kinetic analysis. The mechanism determined above was used to undertake global fitting of the complete data set at all wavelengths and time points. This analysis generated the set of rate constants listed in **Table 3.2**, together with the spectra of each intermediate **(Fig 3.7(c))** and the time course of their formation and decay **(Fig 7(d)).** Fits to the absorbance versus time curves for a selected number of wavelengths are given in **Figure 3.9**. The excellent quality of the fits over the complete wavelength range gives a high level of confidence in the postulated mechanism.

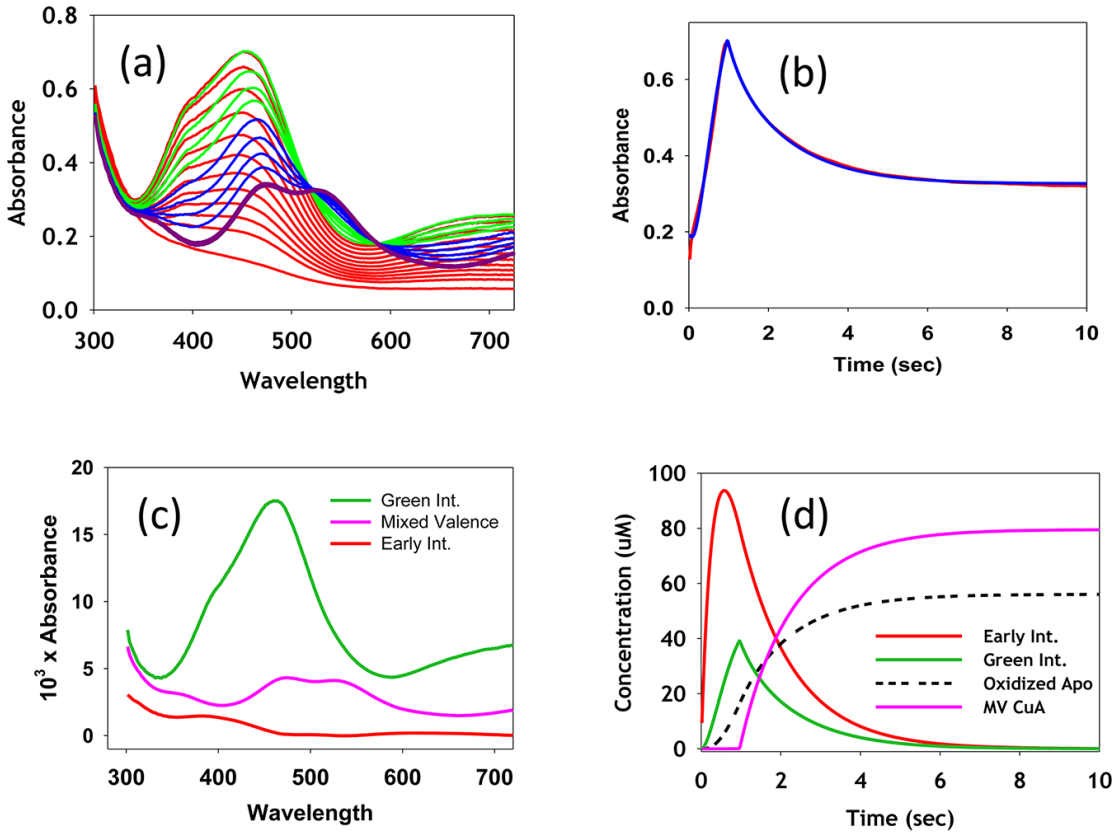

Figure 3.8. Stopped-flow kinetic analysis of the reaction of the bis-thiol apo M160SeM CuA with aqueous Cu(II) sulfate. (a) Transient spectra collected at increasing time intervals color coded as follows: red, 4−84 ms; green, 1−1.64 s; blue, 2.84−9.64 s; and purple, final products above 10 s. (b) Fit to the absorbance versus time data collected at 462 nm. (c) Absorption spectra of colored species (including intermediates) derived from a global kinetic analysis of data at all wavelengths, using the Pro-K II software package. (d) Time dependence of the formation and decay of colored species during the reaction. Fits, spectra of intermediates, and formation−decay curves were derived using the mechanism and rate constants listed in **Table 3.2**. Concentrations were apo protein, 170 **μ**M, and Cu(II), 500 **μ**M.

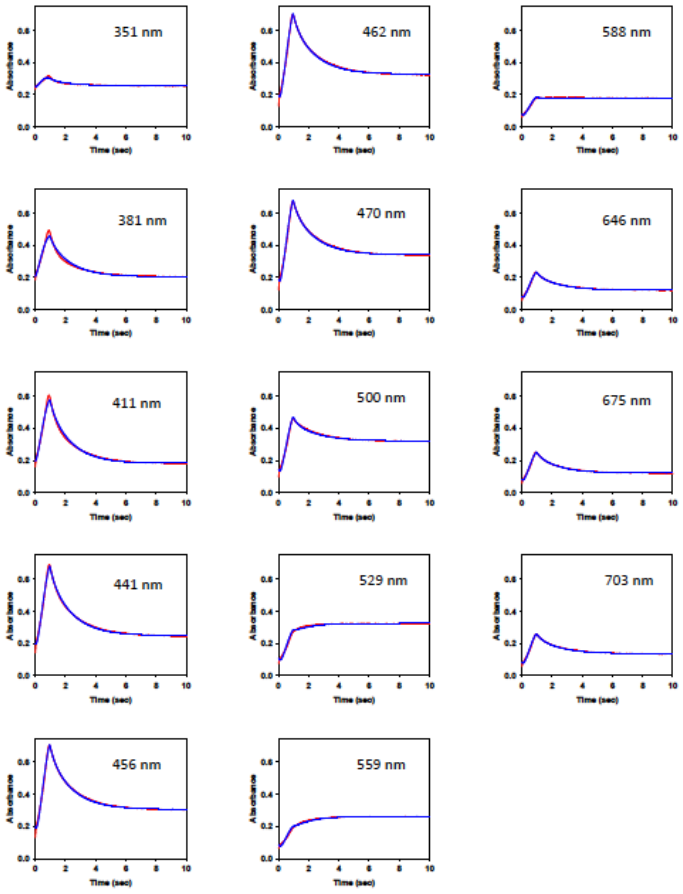

Fig 3.9. Multiwavelength fits to the kinetic data for the reaction of 175 μM apo M160SeM CuA with 500 μM Cu(II) at 23°C. Fits were based on the mechanism and rate constants listed in **Table 3.2**.

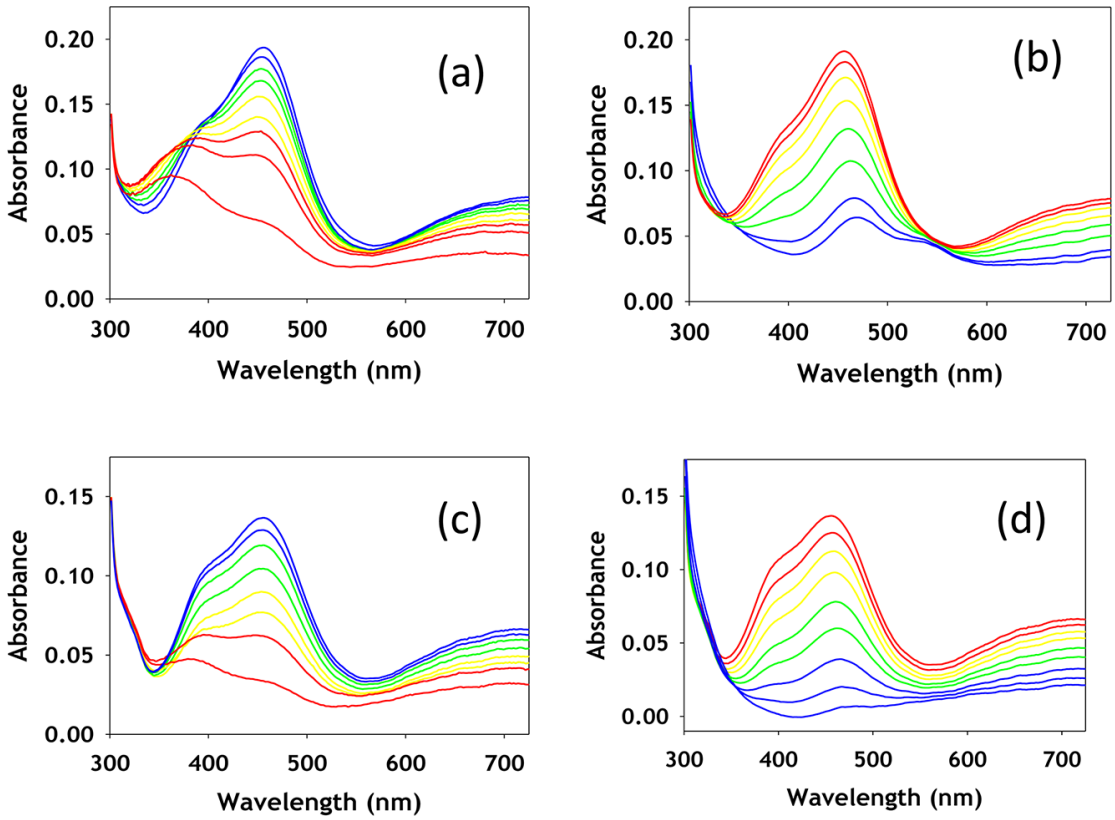

Figure 3.10. Stopped-flow data at substoichiometric Cu to protein (0.4:1) for WT (left) and M160SeM (right). Top spectra (a,b) show an increase of the green intermediate at 460 nm, while bottom spectra (c,d) show the decay of the 460 nm green intermediate.

As a further test of this mechanism, we followed the time course of the reaction under conditions of limiting Cu(II) at low temperature (10°C). These data (**Fig. 3.10**) confirmed the presence of the early intermediate as a species with λmax in the 350-400 nm range. Significantly, the S(Met) and SeM derivatives give rise to early intermediates with different absorption maxima at λmax = 360 and 380 nm respectively. In contrast, the absorption maxima of the green intermediates do not change although small differences in the ratio of the 460 nm main absorption to the 400 - 410 nm shoulder are apparent. As fully predicted by the mechanism, when

Cu(II) is limiting, the mixed-valence product does not form (except in very low amounts for the S(Met) derivative late in the reaction), confirming that major route to its formation is by addition of Cu(II) to the green intermediate. We may speculate that addition of cupric ion to the green intermediate initially forms an unstable di-Cu(II) species which then rapidly decays to Cu(I) and oxidized apo protein, perhaps via the intermediacy of Cu(I)-thiyl radicals. However in the absence of excess Cu(II) this reaction cannot proceed: instead, the green intermediate loses intensity over longer time periods, suggesting that it undergoes slow autoreduction.

reaction step[a]	rate constant
$\mathbf{A + Cu(II) \rightarrow I_{early}}$	$7.5 \pm 1.1 \times 10^3\ mol^{-1}\ s^{-1}$
$\mathbf{I_{early} \rightarrow I}$	$0.81 \pm 0.18\ s^{-1}$
$\mathbf{I + Cu(II) \rightarrow A(S{-}S) + 2Cu(I)}$	$3.0 \pm 0.31 \times 10^3\ mol^{-1}\ s^{-1}$
$\mathbf{I + Cu(I) \rightarrow P}$	$11.0 \pm 3.8 \times 10^6\ mol^{-1}\ s^{-1}$
$\mathbf{A + Cu(I) \rightarrow I{-}Cu(I)}$	indeterminate

[a] A is the bis-thiol apo protein, A(S–S) is the disulfide bridged apo protein, P is the mixed-valence product, I_{early} is the red copper intermediate, I is the green copper intermediate, and I–Cu(I) is the mononuclear Cu(I) intermediate. I–Cu(I) may react with Cu(I) to form the di-Cu(I) product, but no information on this step could be extracted from the data. The rate constant for reaction of A with Cu(I) is also not well-defined.

Table 3.2 Rate constants for the individual reaction steps leading to the formation of the mixed-valence form of M160SeM *Tt* CuA

Cu edge	F[a]	C-N(His)[b]			Cu-Se			Cu-S			Cu-Cu			E_0
		No[c]	R (Å)[d]	DW ($Å^2$)	No[c]	R (Å)[d]	DW ($Å^2$)	No[c]	R (Å)[d]	DW ($Å^2$)	No[c]	R (Å)[d]	DW ($Å^2$)	
Mixed-Valence	0.541	1	1.93	0.009	0.5	2.49	0.012	2	2.23	0.016	1	2.46	0.006	3.2
di-Cu(I)-dithio	0.561	1	1.93	0.013	0.5	2.51	0.012	2	2.24	0.016	1	2.47	0.006	2.5
di-Cu(I)-ACN	0.297	1	1.93	0.020	0.5	2.52	0.011	2	2.25	0.016	1	2.48	0.007	0.6

Se Edge	F[a]	Se-C(met)			Se-Cu[f]			Se-S			$-E_0$
		No[c]	R (Å)[d]	DW ($Å^2$)	No[c]	R (Å)[d]	DW ($Å^2$)	No[c]	R (Å)[d]	DW ($Å^2$)	
Mixed_Valence	0.949	2	1.96	0.005	1	2.48	0.011	1	3.06	0.025	4.7
di-Cu(I)-dithio	0.914	2	1.95	0.002	1	2.49	0.012	1	3.06	0.023	4.5
di-Cu(I)-ACN	0.734	2	1.95	0.005	1	2.51	0.010	1	3.05	0.025	4.7

[a] F is a least-squares fitting parameter defined as $F^2 = \frac{1}{N}\sum_{i=1}^{N} k^6 (Data - Model)^2$

[b] Fits modeled histidine coordination by an imidazole ring, which included single and multiple scattering contributions from the second shell (C2/C5) and third shell (C3/N4) atoms respectively. The Cu-N-C_x angles were Cu-N-C2 126°, Cu-N-C3 -126°, Cu-N-N4 163°, Cu-N-C5 -163°.

[c] Coordination numbers are generally considered accurate to ± 25%

[d] In any one fit, the statistical error in bond-lengths is ±0.005 Å. However, when errors due to imperfect background subtraction, phase-shift calculations, and noise in the data are compounded, the actual error is probably closer to ±0.02 Å.

Table 3.3. Parameters used to fit the Cu and Se EXAFS spectra of the dinuclear forms of M160SeM T. thermophilus CuA at the Cu and Se edges. The mixed valence form was prepared by addition of an excess of aqueous Cu(II) sulfate to the bis-thiol apo protein, followed by dialysis to remove excess Cu(II). The reduced di-Cu(I) forms were prepared either by dithionite reduction of the mixed-valence derivative, or by addition of a 3-fold excess of $[Cu(I)(CH_3CN)_4]PF_6$ followed by removal of excess Cu(I) using a desalting spin column.

3.5 Discussion:

Biological mechanisms of metal transport have been the subject of intense investigation. In particular, the metallation reactions of the CuA center of cytochrome oxidase have generated special interest because of (i) the uniqueness of its mixed-valence $Cu^{1.5} – Cu^{1.5}$ electronic structure (Gamelin *et al.* 1998; Williams *et al.* 1999), and (ii) the role played by the putative chaperone Sco in its assembly (Siluvai *et al.* 2011) . Whereas Sco has been shown to be essential for CuA assembly in vivo (Horng *et al.* 2005; Mattatall 2000; Nittis *et al.* 2001), direct transfer between copper-loaded Sco and apo CuA has never been observed. On the other hand, transfer of Cu(I) center from the mononuclear periplasmic protein PCuAC has been shown to

generate the dinuclear di-Cu(I) CuA (Abriata *et al.* 2008). We undertook a detailed study of the metallation reactions of the T. thermophilus CuA with the goal of answering fundamental questions relating to the chemical mechanism, for example is CuA metallated via mononuclear intermediates, which redox state of copper binds preferentially, and what are the structures of the putative mononuclear intermediates in each oxidation state. The dinuclear mixed-valence end product could be generated from the reaction of apo protein with aqueous Cu(II). Slow titration of sub-stoichiometric amounts of Cu(II) formed a green species with λmax=460 nm, which was clearly a mononuclear entity as judged by its UV-vis, EPR, and XAS spectral properties. However, stopped-flow kinetics showed that this was not the first intermediate to form. Early in the reaction, a species with an absorption maximum between 360 and 380 nm was observed which rapidly converted into the green intermediate. This early intermediate has also been observed in the metallation of nitrous oxide reductase and purple copper azurin, where it has been ascribed to a "red copper" center (Arciero *et al.* 2002; Basumallick *et al.* 2005; Clark *et al.* 2010), typical of a cupric thiolato species coordinated in a tetragonally distorted environment.

Nature of the intermediates

The binding of Cu(II) in both the intermediates is best discussed within the framework of the "coupled distortion" model for understanding the electronic structure in type 1 and type 2 copper thiolates, of the kind found in blue, green and red cupredoxin sites (Clark *et al.* 2010; Solomon 2006). Blue copper centers of the type found in azurin (Adman 1991) or plastocyanin (Penfield *et al.* 1985) are characterized by intense visible absorption around 600 nm, a weaker band at around

400 nm, and narrow A // hyperfine splittings, assigned to a trigonal planar coordination of two His residues and a Cys residue, with weak axial interaction to a Met and/or a carbonyl main chain O. The spectroscopic features have been assigned to a strong S p(π) interaction with the Cu $d_{x\ 2-y2}$ giving rise to the intense Cu-S CT band at 600 nm, and a weaker S p(σ) interaction of lower intensity at higher energy. The π-interaction results in a highly covalent Cu-S(Cys) interaction corresponding to 38% S(Cys) 3p in the Cu $3d_{x\ 2\ -y\ 2}$ orbital for plastocyanin (Shadle *et al.* 1993; Solomon *et al.* 1992). As the axial interaction strengthens, the site undergoes an increase in ligand field strength together with tetragonal distortion which is coupled to a rotation of the $dx_{\ 2\ -y\ 2}$ orbital. The coupled distortion causes the π-interaction to weaken and shift to higher energy while the σ- interaction achieves better overlap and gains intensity resulting in the green T1 center found in nitrite reductase with two absorptions of almost equal intensity at 460 and 495 nm. In the limit of strong axial interaction, a 5-coordinate pseudo square pyramidal (type 2 copper) structure is formed, as exemplified by the red copper sites of nitrosocyanin where four ligands (2 His, 1 Cys and a water) occupy the equatorial plane with a strong 2.1 Å interaction to an axial Glu residue (Lieberman *et al.* 2001). Another example is found in Sco where 1 His, 2 Cys, and an endogenous 0/N (non-His) act as equatorial ligands. In these systems the Cu-S p(σ) interaction is now the dominant absorption at 350 -400 nm with much weaker S p(π) around 450 nm and much lower Cu-S covalency (20% for nitrosocyanin 44, 22% over both Cu-S bonds in Sco (Siluvai *et al.* 2010). As further confirmation of the validity of the coupled distortion model, it has been possible to convert green copper into blue copper by mutation of the axial Met in NIR to

threonine (Basumallick *et al.* 2003), and a blue site into a red site via increasing the axial ligand field strength in azurin from Met to homocysteine. The protein derived ligand set available for binding Cu(II) in the early intermediate of CuA is one or two His residues, one or two cysteines and the Met or Gln residues which act as axial ligands in the mixed-valence product. The absorption maxima of 360 nm for the S(Met) and 380 nm for the SeM derivative places the species in the category of a red copper center, where the axial interaction is strong enough to induce a 5-coordinate tetragonally distorted structure. An important observation is the fact that the absorption maxima are dependent on the donor atom in the M160 residue, undergoing a red shift when S(Met) is substituted by SeM. This effect has been reported previously in the H135M and H135SeM variants of B. subtilis Sco, where Se edge XAS confirmed the coordination of the SeM ligand to Cu(II) (Siluvai *et al.* 2011). Therefore it is likely that the early intermediate coordinates the two Cys residues in the equatorial plane with a strong axial interaction to M160. The identity of the remaining equatorial ligands is unclear but since this is an early capture complex, two water ligands would not be unreasonable. In the Sco system, the coordinated H135 ligand has been shown to stabilize the Cu(II) center (Siluvai *et al.* 2009) and its mutation to either Ala or Met results in autoreduction of the Cu(II) and concomitant oxidation of the two thiolates to a disulfide. This chemistry suggests that the initial red copper center would be unstable but could stabilize itself via a rearrangement to bind the His residue and generate the green intermediate, which we have shown by EXAFS to have a N(His)+$S(Cys)_2$ ligand set. While this coordination is similar to the WT Sco, the UV-vis spectrum is quite different, resembling more closely the green

copper center of NIR. This suggests that the rearrangement that results from binding of the His residue may induce a tetragonal to trigonal perturbation which would increase the amount of S p(π) interaction, and increase the Cu-S covalency, and it is notable in this regard that the mixed-valence product is also highly covalent (DeBeer George *et al.* 2001). A ∥ values from EPR spectra provide a further point of comparison with values for the green intermediate and NIR of 326 and 188 MHz respectively (Olesen *et al.* 1998), relative to the red copper sites of BSco (533 MHz) and nitrosocyanin (387 MHz). From this comparison, the green intermediate lies between the cupredoxin-like NIR spectrum and the tetragonally distorted nitrosocyanin, suggesting that the rearrangement induced by His binding decreases the axial interaction below that found in typical red copper centers. The absence of observable Cu-Se interactions in the XAS supports this view, since T1 sites with axial Met ligands seldom show any contribution from the Met S in the EXAFS (Berry *et al.* 2003). However, the value of A ∥ is at best an approximate indicator of axial ligand strength since the WT NIR (green) has an identical A ∥ to that of its M182T variant (blue) in which the moderately strong axial interaction with S(Met) has been eliminated (Olesen *et al.* 1998). The structure of the Cu(I) mononuclear intermediate is easier to formulate. Here EXAFS at both the Cu and Se edges provide good evidence for thioether coordination from M160 together with one of the available His residues. The coordination sphere is completed by addition of 1 or both of the Cys residues. Interestingly, detailed analysis of the XAS parameters suggested that the Cu(I) may sample all of its available ligands in a fluxional fashion, perhaps suggesting that the metal is "rattling around" in the site. This may reflect one reason

why addition of a second Cu(I) to form the di-Cu(I) species is a facile reaction, whereas larger ions such as Hg(II) appear to form mononuclear sites preferentially (Hay and Lu 2000).

Reaction Mechanism

Stopped-flow kinetic studies have suggested a mechanism in which the early red intermediate converts to the green intermediate, the fate of which is dependent on the availability of additional copper in the system. Excess copper in either oxidation state converts the green intermediate into mixed-valence. Addition of Cu(I) is straightforward mechanistically as the excess metal will populate the additional binding site and generate the mixed-valence product. Addition of excess Cu(II) also forms mixed-valence, and our kinetic analysis shows that this step is obligatory in the conversion of green to purple product. This suggests that Cu(II) can bind in the second site to form a transient di-Cu(II) species which is unstable with respect to disproportionation to form oxidized disulfide, and Cu(I). The Cu(I) can then rapidly react with residual green mononuclear species to form the purple product. The different stoichiometry at which the green intermediate is maximally populated varies between the S(Met) and SeM derivatives, and we believe that this reflects differences in the rates at which the S(Met) and SeM green mononuclear species react with excess copper. The rate of this reaction is likely to be influenced by the presence or absence of a coordinated Se-methionine residue, since the latter will have differing stabilizing influence on the Cu(II) monomer. It is unclear why the di-Cu(II) species is so unstable, but Hay and coworkers have argued that the site is destabilized if the overall charge exceeds +3. This empirical observation explains the formation of

Hg(II)Ag(I) derivatives which appear to be stable, and is consistent with the formation of mononuclear but not dinuclear Co(II) derivatives in CuA-azurin at high pH.

Comparisons with other CuA systems

The intermediates characterized in the present study show both similarities and differences from those described for other CuA systems such as purple CuA azurin and N2O reductase (Wilson *et al.* 2011). The early intermediate appears to be similar, and is formulated as a red copper species. In CuA azurin under conditions of excess copper, the red copper species converts to a blue type 1 copper species with λ_{max} = 640 nm, which clearly differs from the green intermediate of *Tt* CuA with λ_{max} = 460 nm. This may be the result of small differences in the copper sites imposed by the different protein matrices, and is not inconsistent with the observed differences in Cu-Cu distances, where the azurin model exhibits a shorter Cu-Cu in the mixed-valence state than *Tt* CuA (2.39 versus 2.44 Å respectively ,57). At low copper, a new species I_x is observed in the azurin model, which is only transiently stable, and converts either aerobically to the T1 site or anaerobically to a Cu(I) species. The spectral properties of I_x show similarities to the *Tt* green intermediate, with absorptions at 410, ~460 and 760, but the relative intensities of the 410 and 460 nm bands are reversed. However, whereas the $A_{//}$ values are similar (326 versus 345 MHz; 116 versus 123 G) the g_z values differ significantly (2.13 versus 2.25) for the green intermediate and I_x respectively. Wilson and coworkers propose a structure for I_x based on similarities to imidazole and pyrazole adducts of horse liver alcohol dehydrogenase with a suggested $(His)(Cys)_2$ ligand set similar to that of the green intermediate presented

above. However, the large differences in g_z values suggest differences in electronic structure which are clearly manifest in the decreased stability of I_x over the green intermediate.

Biological Implications

The pathway for CuA metallation in vivo is still poorly understood. Whereas Sco-type proteins appear to be essential, direct transfer from Sco to CuA has not been demonstrated. The periplasmic Cu(I)-binding protein PCuAC remains the only protein copper donor shown to successfully metallate CuA (Abriata *et al.* 2008). The reaction of T. thermophilus Cu(I)-loaded PCuAC with *T. thermophilus* apo CuA generated a NMR spectrum characteristic of the fully metallated di-Cu(I) CuA species, but the study did not detect mononuclear intermediates, nor any protein-protein interactions. PCuAC homologues are not universally present in prokaryotes, and are absent from eukaryotes, calling into question a direct role in CuA metallation. A recent study of CuA assembly in Rhodobacter spheroides which expresses both PCuAC and Sco (PrrC) homologues showed that deletion strains of either or both proteins lowered the accumulation of the CuA-containing aa3-type oxidase but showed a stronger phenotype for PrrC (96%) than for PCuAC (86%) (Thompson *et al.* 2012). The data indicated distinct roles for each chaperone, as overexpression of PCuAC in a ΔPrrC background did not compensate for the defect. The defects in both deletion strains could be partially restored in cells grown at high (1.6 μM) added Cu(II) which mitigated against the role suggested for PrrC/Sco by Abriata et al.. as a disulfide reductase. The two scenarios most consistent with the findings on R. spheroides CuA assembly were (i) each chaperone could add one copper or (ii) PrrC

adds both coppers but is itself metallated by PCuAC. In mitochondria where PCuAC is absent, it has been shown that Sco1 is metallated by Cox17 (absent in bacteria) which would explain the lack of a universal requirement for PCuAC in CuA assembly (Banci 2005; Horng *et al.* 2004). While the evidence is compelling for metallation of both copper sites by Sco/PrrC, the inability to demonstrate this chemistry in vitro is worrisome. It is possible that removal of the membrane anchor to produce soluble Sco constructs perturbs its transfer chemistry, or destabilizes mechanistically-relevant oligomers, but in the absence of such effects, the lack of transfer chemistry suggests a missing component, and argues in favor of a mechanism in which each of the two copper ions is added sequentially by a separate chaperone. In previous work, we showed that *Bacillus subtilis* Sco variants that lack the coordinating His residue (H135) are inactive in assembly of the aa3 oxidase. This His residue stabilizes the Cu(II) state as shown by the large increase in reduction rate for the H135A variant. The Cu(I) state is stabilized in the H135M variant, which has properties similar to those of the reduced WT protein, but this derivative is completely inactive. These data suggest that the Cu(II) state of Sco is important for CuA assembly, and when this oxidation state is inaccessible or unstable as in H135A or H135M variants, the transfer is impeded. These observations support the idea that Sco may provide a cupric ion to generate the green mononuclear intermediate, but the assembly of the site by Cu(I) addition may occur via a different pathway. Like those of others, our own efforts to metallate CuA in either oxidation state using copper loaded WT Sco or its H135A variant have been unsuccessful, leading instead to a dead-end complex with unusual UV-vis properties (*vide infra*). Given the facile metallation chemistry of

CuA from inorganic ions, and the weakened binding affinity of the H135A variant of Sco, these findings seem difficult to reconcile. Further work is underway to use the techniques described herein to probe the transfer chemistry of CuA with Sco and PCuAC with the goal of resolving these issues.

CHAPTER 4

INVESTIGATIONS OF POSSIBLE METALLOCHAPERONES IMPLICATED IN CUA ASSEMBLY

4.1 Introduction

In our work described in the previous chapter, we determined that both Cu(I) and Cu(II) oxidation states were present during the assembly of the *Tt* CuA site from inorganic Cu ions. This allows for an in vivo assembly pathway that requires both a Cu(I) donor and a Cu(II) donor. It has been shown that Sco binds a single Cu, in either the (I) or (II) oxidation state, while Abriata and coworkers have isolated and shown a putative CuA chaperone, PCuAC, which can bind a single Cu(I) ion (**Figure 4.1**).

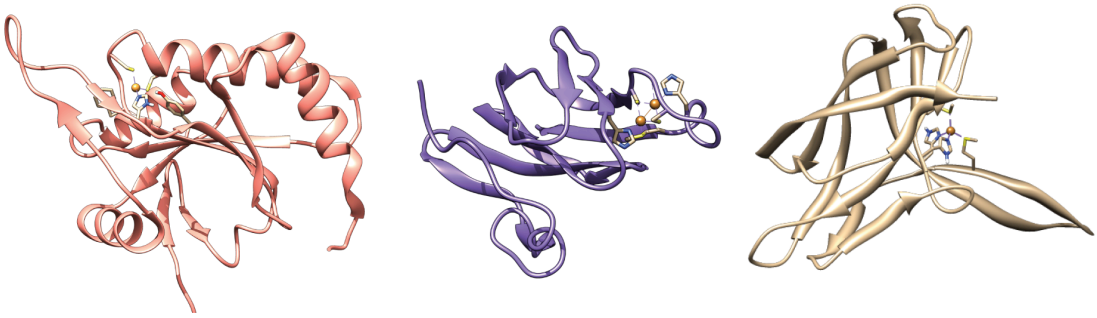

Fig 4.1 Structures of *Tt* CuA and its putative metallochaperones. From left: *Tt* Sco, *Tt* CuA (soluble fragment), and *Tt* PCuAC. PDB files 2RLI, 2CUA and 3PIK.

While Sco-type proteins appear to be essential, direct transfer from Sco to CuA has not been demonstrated, and periplasmic Cu(I)-binding protein PCuAC remains the

only protein copper donor shown to successfully metallate CuA (Abriata *et al.* 2008). However, as discussed in the previous chapter, a recent study of CuA assembly in Rhodobacter spheroides which expresses both PCuAC and Sco (PrrC) homologues showed that deletion strains of either or both proteins lowered the accumulation of the CuA-containing aa3-type oxidase but showed a stronger phenotype for PrrC (96%) than for PCuAC (86%) (Thompson *et al.* 2012). The data indicated distinct roles for each chaperone, as overexpression of PCuAC in a ΔPrrC background did not compensate for the defect.

With the mechanistic information we have obtained on CuA assembly from inorganic Cu ions in hand, we have sought to further investigate these putative biological chaperones in vitro, in the hopes of determining how they may be responsible for CuA assembly in vivo.

4.3 UV-Vis and EXAFS studies on the interactions between *Tt* Sco and *Tt* CuA

We have obtained and isolated *Thermus thermophilus* Sco in good purity and yield as expressed in *E. coli*, using methods described previously (Chacón and Blackburn 2012a) , and have begun a series of protein-to-protein binding and metal affinity experiments.

Thus far, our attempts to titrate Cu(II)-loaded Sco into a solution of apo CuA have resulted in a dead-end protein complex which is pink (red-purple) in color. This complex exhibits a small peak at ~365 nm, and another more intense peak at ~520 nm, and these peaks do not resemble the UV-vis signatures of either protein (**Figure 4.2)**. The pink color is thought to arise from the 520 nm peak, which is consistent with absorption in the green energy region.

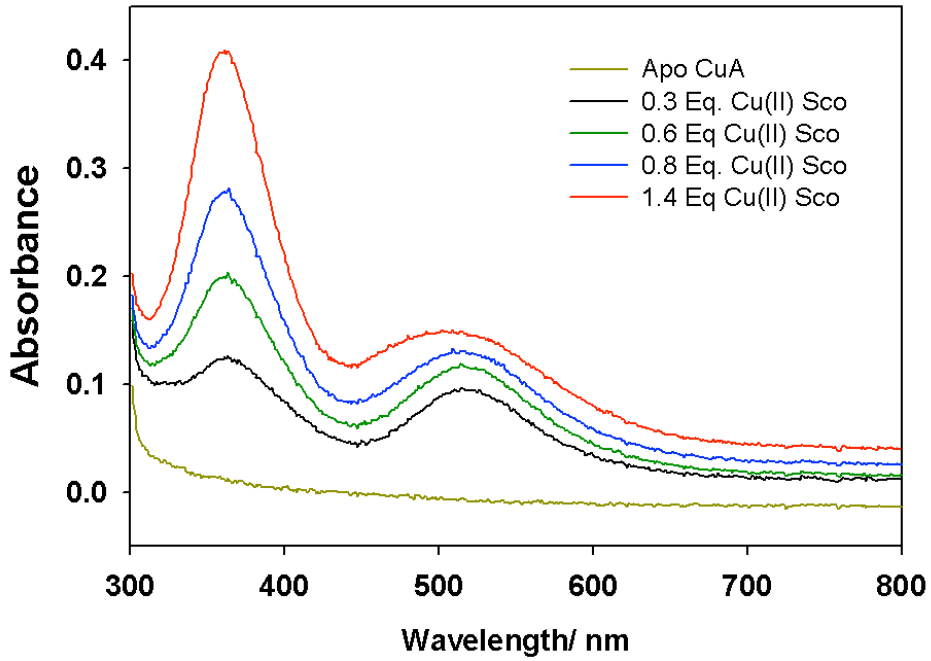

Fig 4.2 Titration of WT Cu(II)-loaded *Tt* Sco and apo CuA.

In the hopes of encouraging successful transfer, based on data obtained previously which showed a higher reactivity of Sco upon removal of its active site His, (Siluvai *et al.* 2009) we designed a H139A Cu(II)-loaded Sco mutant and performed the identical titration as shown above, with limiting Cu(II) Sco. The dead end-complex was shown to increase as additional equivalents of Cu(II) H139A Sco were added, similar to the WT Sco titration. Of note, however, is that while the relative intensity of the peaks were proportional in each experiment to the concentration of Cu(II) in the system, the actual peaks were red-shifted, and a new peak appeared at 333 nm in addition to the previously observed features (**Figure 4.3)**. The color of the incubation was more deeply pink than that of the WT Sco – CuA incubation, edging toward the canonical purple color of CuA.

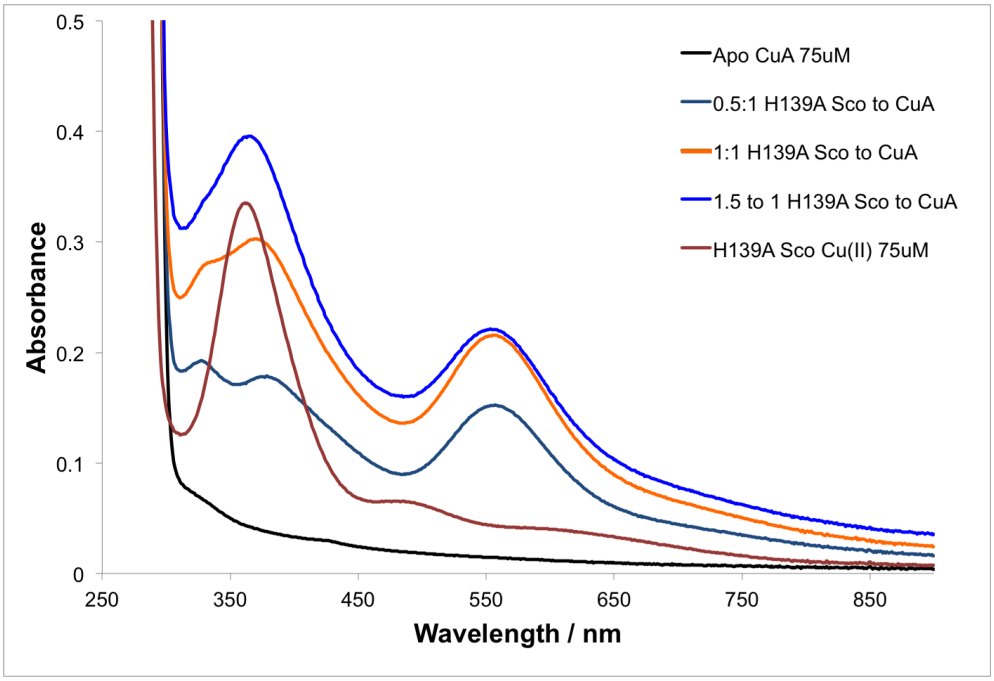

Fig 4.3 Titration of Cu(II)-loaded H139A *Tt* Sco and apo CuA. Addition of substoichiometric Cu(II) loaded H139A Sco to apo CuA led to the appearance of a more deeply pink, edging toward purple-colored, complex at ~560 nm. Peaks were also present at 333 nm and 386 nm.

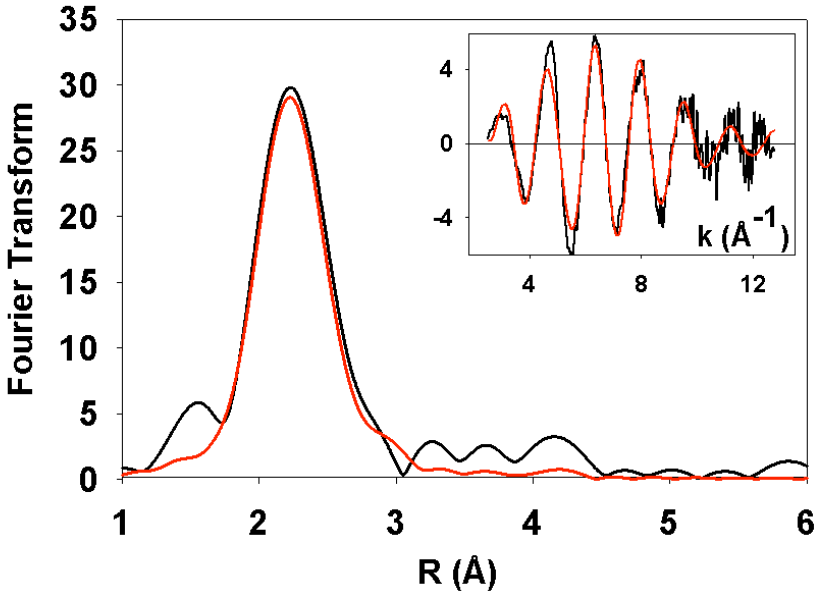

Fig 4.4 Cu K-edge FT and EXAFS of the pink Cu(II) Sco and SeM CuA incubation. Simulation of the EXAFS gave a FI of 0.90 – 1 His at 1.97A (DW 0.003), 2 S(Cys) at 2.23A (DW 0.008).

We next turned to x-ray absorption spectroscopy, hoping to further characterize the Cu(II) Sco – CuA complex, using SeM 160 labeled CuA as a spectroscopic probe (**Figure 4.4**). The Cu K-edge EXAFS fit best to the well-known Sco environment of 2 Cys, and 1 His (**Table 4.1**). It initially appeared that the fit was improved by the addition of a Se atom, which would have been attributed to involvement by the apo CuA center. However, when we collected the Se edge data for the same mixture, no Se-Cu interaction was detected, with only the 2 carbons of Se-Met presenting themselves in the Se edge FT. These conflicting results lead us to believe that the Sco-CuA complex will require extensive further analysis. We have begun the design of a streptavidin tagged construct of Sco, which will be incubated with CuA in a series of experiments designed to react the two proteins to form the dead end complex.

We then will separate the reacted proteins by the use of a streptavidin column for further analysis by UV-vis, and XAS.

4.4 Spectroscopic studies on the interactions between *Tt* PCuAC and *Tt* CuA

Our next aim was to understand better the possible role of *Thermus thermophilus* PCuAC in CuA assembly. To do so, we need to determine if PCuAC delivers its cargo to both sites of the CuA center, or if it instead only delivers to a single site. The importance of a Cu (II) Sco state in CuA maturation has been well established (Siluvai *et al.* 2011), and because those results seem to conflict with the finding that PCuAC is capable of loading CuA with two equivalents of Cu(I) (Abriata *et al.* 2008), more insight is needed.

We have expressed *Tt* PCuAC in *E. coli* using the methods described previously (Chacón and Blackburn 2012b) . Therefore, we designed a set of "oxidation-quench" experiments. Cu(I)-loaded PCuAC was incubated at a 1:1 ratio with apo CuA to produce a colorless solution, and then a solution of potassium ferricyanide was added up to 1 equivalent. Ferricyanide is readily reduced, and will result in ferrocyanide by the following reaction:

$$[Fe(CN)_6]^{3-} + e^- \rightleftharpoons [Fe(CN)_6]^{4-}$$

While ferricyanide has an extinction coefficient of 1040 M^{-1} cm^{-1} at 420nm, the reduced form has a negligible absorption in the UV-vis range. This would therefore allow us to monitor the UV-vis spectrum of only Cu(II)-loaded CuA. As shown in our previous work, mononuclear Cu(II)-bound CuA has a distinctive spectrum at ~460 nm.

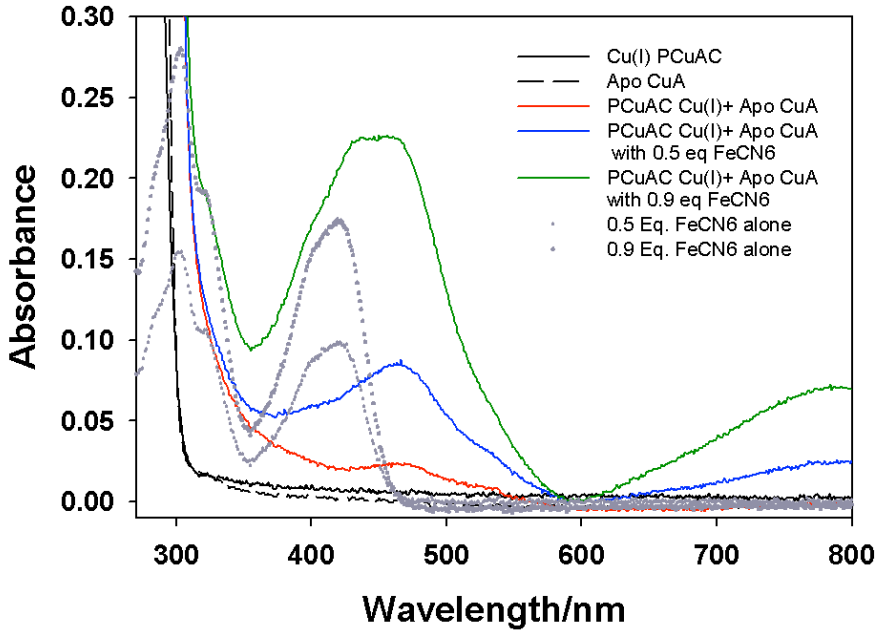

Fig 4.5 Oxidation quench, via ferricyanide, of the 1:1 mixture of Cu(I) Tt PCuAC with apo CuA. Addition of ferricyanide led to the immediate appearance of the green mononuclear Cu(II) intermediate of CuA, indicating that metallation by PCuAC is specific to a single site of CuA.

If PCuAC is discriminating as to which apo site of CuA it will load Cu(I) into, then we would see only the signature Cu(II) mononuclear species in the UV-vis upon oxidation quench. If, however, PCuAC is non-specific, we will observe a mixture of Cu(II) mononuclear and mixed valence species (provided that the added ferricyanide has been completely consumed in the redox reaction). In our preliminary experiments, we observed only the Cu(II) mononuclear species formed upon oxidation (see **Figure 3.2** for comparison), which provides evidence that PCuAC is specific to one site of CuA (**Figure 4.4**).While it has been shown by Abriata and coworkers that PCuAC will load an additional Cu(I) ion under in vitro conditions, this does not explain when or how the necessary oxidation event occurs that would produce mature mixed

valence CuA in vivo, and also does not exclude Sco or some other Cu(II) chaperone from playing an equal role in CuA assembly.

4.5 X-ray absorption studies of Cu(I) M350, 59I PCuAC to *Tt* CuA transfer

The UV-vis results provide evidence that PCuAC is specific to a single site of CuA. However, these results do not necessarily reflect the Cu(I) binding chemistry that is occurring, because of the very nature of oxidation quench. Fortunately, Cu edge XAS can be used to confirm Cu(I) transfer, and can determine the destination of the Cu(I) in CuA. The existence of two additional Met residues in Tt PCuAC had previously interfered slightly with the Se K-edge EXAFS signal in preliminary scans of SeM labeled, Cu(I) loaded PCuAC. We designed a M350,59I PCuAC double mutant (hereafter referred to as "PCuAC DM") that is spectroscopically identical to WT PCuAC, but lacks a slight, unwanted Se contribution in the EXAFS waveform. Unfortunately, we found that the SeMet labeled PCuAC has an extremely stable 2Se-Cu bond and is to our current knowledge, nearly unreactive upon incubation with apo CuA. We currently are working to characterize the chemistry of this tight bonding, by metal competition assays. As we could not use the SeM labeled PCuAC DM for transfer experiments, we chose to simply invert which protein contained the SeM label. We incubated Cu(I)-loaded PCuAC DM with apo, SeMet labeled CuA, at a ratio of 1 to 1. We observed full Cu(I) transfer to CuA, as shown in both the Se and Cu edge (**Figure 4.6, Table 4.1**), and further to this, the resulting Cu(I) CuA monomer was entirely consistent with our previously prepared mononuclear Cu(I) CuA, and appears to bind selectively in the identical site (See **Figure 3.5**).

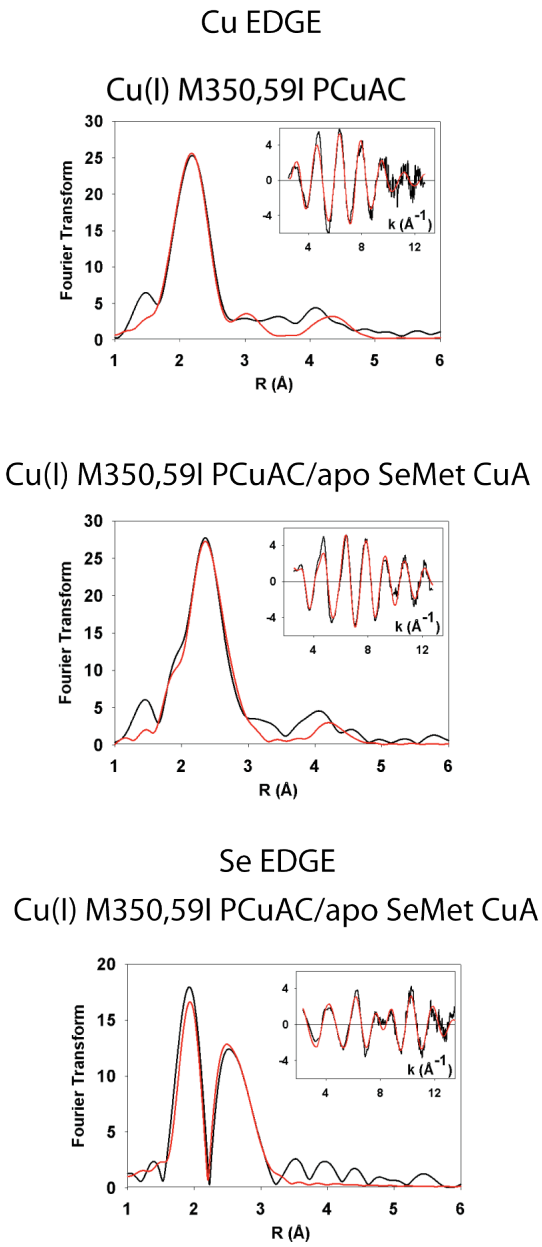

Figure 4.6 Cu and Se K-edge FTs of the transfer of Cu(I) from PCuAC DM to apo SeMet CuA. **Top panel**, Cu K-edge of Cu(I)-loaded PCuAC DM. **Middle panel**, Cu K-edge of the incubation of equal amounts Cu(I)-loaded PCuAC DM and spo SeMet labeled CuA. **Bottom panel**, Se K-edge of the incubation of equal amounts Cu(I)-loaded PCuAC DM and spo SeMet labeled CuA.

4.6 Metal binding competition studies probe the Cu(I) binding behavior of CuA

The oxidation-quench results led us to probe the relative metal binding affinities for Cu(I) in PCuAC and CuA, as compared to that of Sco, which has been previously determined, in order to provide further insight into possible site-specific Cu ion loading into CuA by metallochaperones. To do so, we designed a series of metal competition experiments that would provide us with metal binding affinities for CuA as compared to PCuAC. To do this, we prepared 30μM solutions of mature, Cu-loaded CuA and Cu(I) loaded PCuAC that were rapidly stirred in a UV-vis cuvette. Next, a solution of either 100mM BCA or BCS with 100 mM ascorbate was smoothly added to the metalloprotein at a rate of 0.5 μL/minute using a syringe pump. UV-Vis scans were taken every thirty seconds until full chelation of metal ion by BCA or BCS had occurred, as indicated by the leveling of the colorometric curve.

We had initially attempted to outcompete the Cu ions in the CuA site using BCA. However, we found that the BCA did not reach a binding plateau at 60 μM Cu (the concentration of Cu in the CuA center) and instead was only chelating approximately half of the Cu ions. This indicated the presence of two distinct Cu(I) binding affinities in CuA. We therefore turned to the stronger Cu colorimetric chelator, BCS, which removed both Cu ions easily. By using the DynaFit program to model the BCA-Cu(I) binding as related to the first, lower affinity site, and using these obtained values in the multi-step BCS chelation experiment, we arrived at satisfactory fits for binding affinities in CuA (**Figure 4.6**).

Similarly to the high affinity Cu(I) site in CuA, BCA was unable to remove any appreciable amount of metal ion from Cu(I)-loaded PCuAC, and BCS was used to

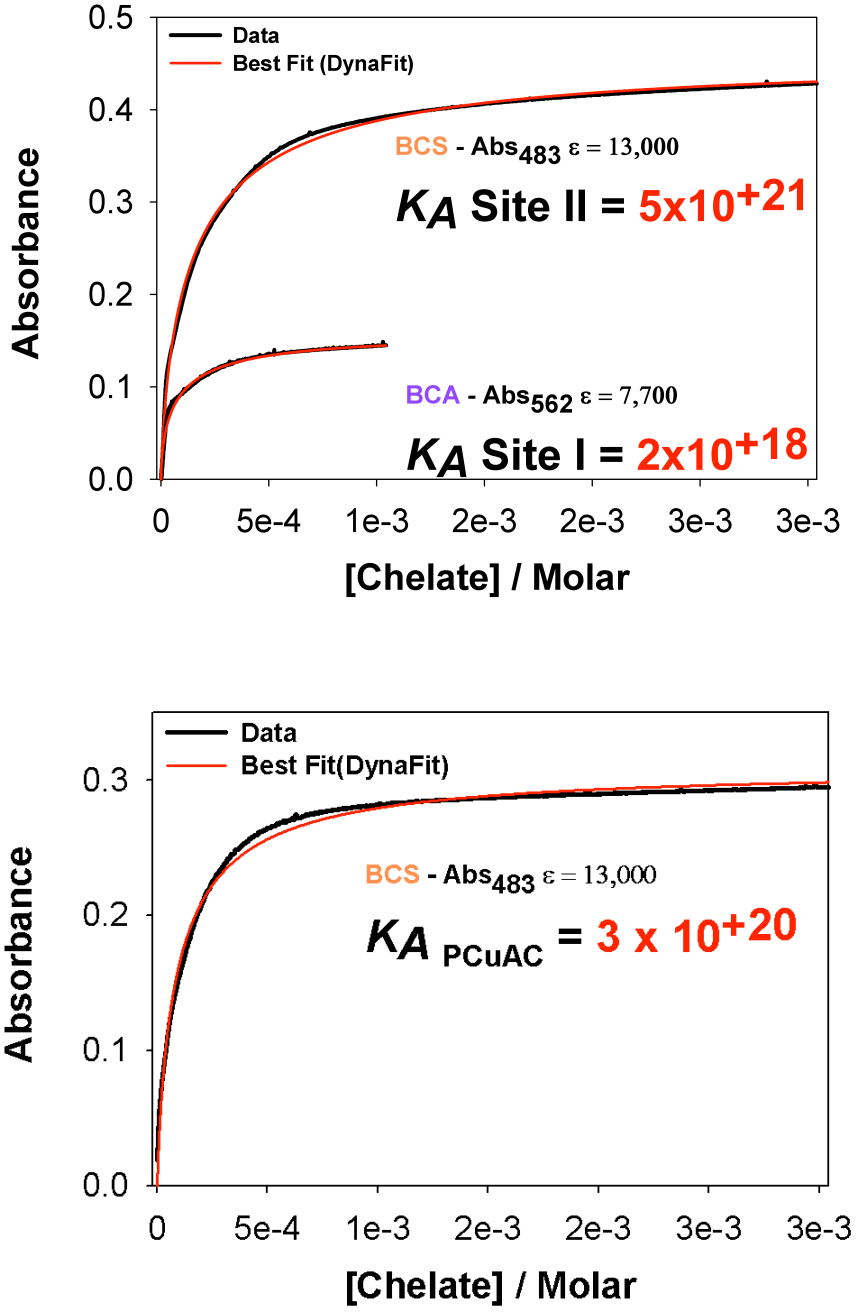

Fig 4.7 BCA and BCS, Cu(I) competition assays of the metal binding sites of Tt CuA and PCuAC. Top panel, BCA and BCS competition assay for CuA. Bottom panel, BCS Cu(I) competition assay for PCuAC.

obtain a chelation curve.

As discussed above, our preliminary results indicate that the two metal binding sites of CuA have distinctly different affinities for Cu(I). The binding curve for the first site, arbitrarily named "site I", was fit to a Cu(I) affinity constant of ~2 x 10^{+18}, while "site II" has an affinity constant three orders of magnitude higher at ~5 x 10^{+21} (**Figure 4.6**). Interestingly, the Cu(I) affinity constant for PCuAC is ~3 x 10^{+20} , and the published value for Cu(I) affinity in Sco is ~1 x 10^{+16}.

We suggest that these results support an "affinity gradient" model (Banci *et al.* 2010), and that and the lower affinity of Sco for Cu(I) indicates that it may interact with CuA first, loading Cu(II) into the lower Cu(I) affinity site of CuA. We observed strong evidence that PCuAC prefers to load Cu(I) to the high Cu(I) affinity site in CuA, as the oxidation-quench results indicate, and we posit that PCuAC may unload its Cu(I) cargo to CuA *after* Sco, to produce the mature protein. Future work is directed at repeating these experiments, as well as designing a series of rapid freeze quench XAS experiments using SeM labeled CuA and Cu(I) PCuAC to determine the site Cu(I) is being loaded into.

		Cu-S (Cys)			Cu-N (His)			Cu-Se (1)			
Sample/Fit	FI	No	R(Å)	DW(Å^2)	No	R(Å)	DW(Å^2)	No	R(Å)	DW(Å^2)	Eo
											-3.33
Tt Sco/SeM CuA	0.9	2	2.23	0.008	1	1.97	0.0023	0			
Cu(I) PCuAC DM	0.38	2	2.30	0.012	2	2.04	0.01	0			-4.65
Cu(I) PCuAC DM/Apc	0.35	1.6	2.29	0.01	1	2	0.01	0.5	2.45	0.005	-3.913

		Se-C			Se-Cu			Se-S (Cys)			
Sample/Fit	FI	No	R(Å)	DW(Å^2)	No	R(Å)	DW(Å^2)	No	R(Å)	DW(Å^2)	Eo
Cu(I) PCuAC DM/Apc	0.74	2	1.95	0.004	0.8	2.5	0.008	0.3	3.03	0.004	-5.08

Table 4.1 Fit Parameters used in Chapter 4.

CHAPTER 5

THE ROLES OF THE PERIPLASMIC PROTEINS IN CUS(CFBA) AG / CU EFFLUX

5.1 Introduction

As a consequence of its inherent toxicity, unbound copper is not encountered within the living cell (Rae *et al.* 1999). Mammals have evolved to exploit this by exposing bacterial pathogens to high concentrations of copper as part of the innate immune response (Braymer and Giedroc 2014; Chaturvedi and Henderson 2014; Samanovic *et al.* 2012; White *et al.* 2009; Wolschendorf *et al.* 2011). While this will often kill the invading species, copper tolerance pathways have co-evolved in many bacteria (Botella *et al.* 2012; Hernandez-Montes *et al.* 2012; Hood and Skaar 2012). In *E. coli*, the chromosomally encoded CusS (Cu sensing) copper-responsive regulator responds to low micromolar concentrations of free periplasmic copper and silver (Franke *et al.* 2003; Gudipaty *et al.* 2012; Gudipaty and McEvoy 2014; Lok *et al.* 2008; Outten *et al.* 2001) and activates the cytoplasmic transcription factor CusR. Activation of CusR results in the production of the periplasmic copper efflux pump CusCFBA, which is specific to cuprous and argentous ions (Conroy *et al.* 2010) and is essential to copper resistance in *E. coli* under anaerobic conditions (Mealman *et al.* 2012a). CusCFBA is composed of the inner membrane bound proton-substrate antiporter CusA, the periplasmic adapter protein (PAP) CusB, and the outer membrane factor (OMF) CusC

---

* Material in this chapter has been published in this or similar form in the Proceedings of the National Academy of Sciences, and is used here with the permission of PNAS.

Chacón KN, Mealman TD, McEvoy MM, Blackburn NJ (2014) Tracking metal ions through a Cu/Ag efflux pump assigns the functional roles of the periplasmic proteins. The Proceedings of the National Academy of Sciences. **43** 15373-15378.

(Arguello *et al.* 2013; Mealman *et al.* 2012a).

The Cus system is distinguished from other RND-type efflux pumps such as AcrB-TolC and its homologs (Tseng *et al.* 1999) both by its association with the periplasmic metallochaperone CusF (Loftin *et al.* 2007; Xue *et al.* 2007), and by the active involvement of its periplasmic adapter protein. Unlike other PAPs, which are thought to primarily provide structural support, CusB is conformationally flexible and also possesses a metal-binding site within its N-terminal region (Bagai *et al.* 2007). Additionally, *cusB* knockout strains produce a Cu-sensitive phenotype (Mealman *et al.* 2012b). CusF and CusB have been shown to freely exchange Ag(I) and Cu(I) toward equilibrium in highly specific protein-protein interactions (Bagai *et al.* 2008; Mealman *et al.* 2011).

Crystal structures of CusA (Long *et al.* 2010), CusB (Su *et al.* 2009), and the outer membrane protein CusC (Kulathila *et al.* 2011) have been reported in recent years together with a structure of the CusBA complex (Su *et al.* 2012), revealing a stoichiometry of 2:1:1 for the B:A:C components. While these structures have provided enormous insight into possible modes of metal efflux (Kim *et al.* 2011; Long *et al.* 2012), the dynamic mechanism of periplasmic metal detoxification by Cus is still undetermined. This is in part due to disorder in the metal-binding site of CusB, as shown by crystallography and extensive molecular dynamics simulations (Ucisik *et al.* 2013), and the difficulty of creating an *in vitro* scenario that includes CusA, CusB, and CusF in biologically relevant conditions. The purpose of our study was to create such a scenario, and to determine the method of activation of the CusA pump, thereby defining the exact roles of CusF and CusB in periplasmic Ag and Cu efflux. Recently,

a truncated N-terminal CusB fragment (CusB NT, hereafter CusB) that behaves similarly to native CusB *in vivo* has been developed, facilitating its study (23).

X-ray absorption spectroscopy (XAS) is ideal for the investigation of metalloprotein interactions when combined with selenomethionine (Se-Met) labeling of active site methionine (S-Met) residues (Blackburn *et al.* 1999); (Chacón and Blackburn 2012b). By observing the Fourier transform (FT) spectra derived from the Se extended x-ray absorption fine structure (EXAFS), specific holo and apo metallosites within a mixture of proteins can be clearly distinguished. In the Cus efflux system the metal-binding ligand sets known as of yet are two Mets, one His and a weakly coordinating tryptophan for CusF, and three Mets each for CusB and CusA, respectively. Therefore, the Cus system is an excellent candidate for Se-Met labeling, because all three of the Cus proteins under investigation contain at least two active site Met residues. We have used this technique previously to monitor metal transfer between labeled and unlabeled versions of CusF and CusB. We now extend this to combine the three key Cus proteins *in vitro,* in a series of experiments in which either CusF or CusB possess a Se-Met label (**Fig. 5.1**).

In this manner we were able to track the metal gain or loss by any Se-Met labeled Cus component. Further, we exploited the ability of the Cus system to bind and transport either copper or silver ions. With the ability to incubate copper-loaded CusF, silver-loaded CusB, and apo CusA in the same reaction, and with the Se-Met XAS spectroscopic probes sequentially placed on one or the other of the metal-loaded proteins, we accomplished a full account of metal transfer by a series of tri-metal (Cu, Se, and Ag) XAS experiments.

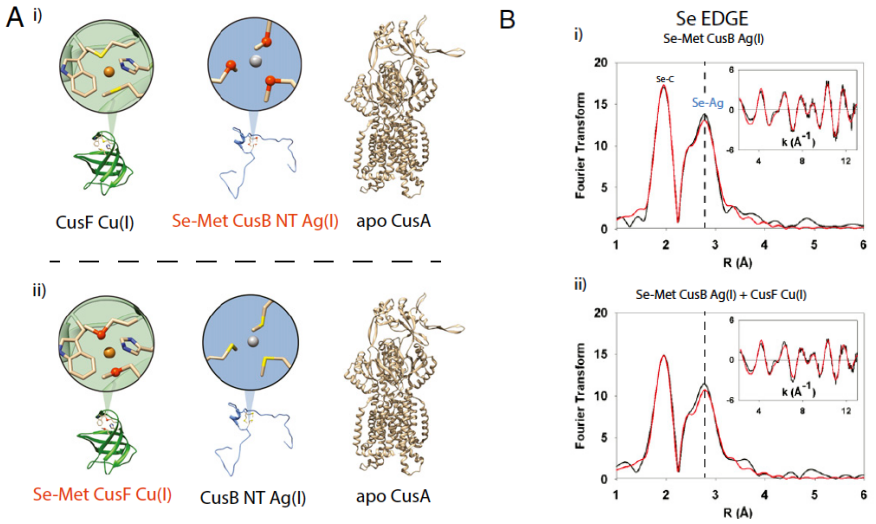

Fig. 5.1 (A) Trimetal edge XAS to determine metal transfer in CusF, CusB, and CusA. (Atom legend: sulfur, yellow spheres; selenium, dark orange spheres.) (i) Ag(I)-loaded Se-Met–labeled CusB (red typeface) incubated with unlabeled, Cu(I)-loaded CusF and apo CusA. With the Se-Met label on CusB, any change in Se-Ag coordination could be attributed to metal transfer from CusB to CusF or CusA. (ii) Cu(I)-loaded Se-Met–labeled CusF (red typeface) incubated with unlabeled, Ag(I)-loaded CusB and apo CusA. In these cases, any change in Se-Cu coordination could indicate metal transfer from CusF to CusB or CusA. (B) CusF and CusB do not exchangemetal ions when both are fully metal ion loaded. (i) Se K-edge FT of selenomethionine-labeled, Ag(I)- loaded CusB. The CusB Se-Ag interaction is represented in the FT by the peak at ~2.60 Å. (ii) Se K-edge FT of a stoichiometric mixture of selenomethionine labeled, Ag(I)-loaded CusB and unlabeled, Cu(I)-loaded CusF. No decrease was observed in the CusB Se-Ag signal intensity, nor did a Se-Cu signal appear. It is of note that the overall intensity of all signals was lowered in the FT of the CusB/CusF mixture; however, this dampening occurred by the same amount in both the Se-C and Se-Ag peaks and is not indicative of metal transfer.

5.2 Experimental procedure

Expression and purification of S-Met CusF and S-Met CusB-NT

E. coli BL21 (λDE3) containing the CusF(6-88) trx-his6-tev plasmid were grown from a freshly streaked plate into LB media containing 100 μg/mL ampicillin at 37 °C until they reached an OD600 of 0.8, at which point protein production was induced with 0.4 M of isopropyl β-D-1-thiogalactopyranoside (IPTG). Growth was allowed to continue at 37 °C for 4 hrs, whereupon the cells were harvested by centrifugation and pelleted. The cells were resuspended, lysed using the French pressure method, and centrifuged to remove cell debris. The filtered supernatant was poured over a Ni-NTA resin column, rinsed with buffer, and eluted using a 250 mM imidazole buffer rinse. To remove the His6-Trx tag, tobacco etch virus (TeV) protease and 5 mM β-mercaptoethanol was added to the protein solution and the mixture incubated at 20 °C overnight. After dialysis the protein solution was once again poured over a Ni-NTA resin column to yield cleaved, pure apo CusF. SDS-PAGE analysis of the purified protein showed the final product to be in a single band at the appropriate molecular weight (~10 kDa), with no visible impurities.

E. coli BL21 (λDE3) containing the CusB NT trx-his6-tev plasmid was prepared in exactly the same manner as for CusF. The SDS-PAGE analysis of the purified CusB-NT showed the final product to be in a single band at the appropriate molecular weight (~7 kDa), with no visible impurities.

Both purified proteins were then dialyzed and stored in HEPES buffer (50 mM pH 7.5) for the subsequent metallation steps.

Expression and purification of Se-Met CusF and Se-Met CusB NT

The selenomethionine labeled variants of each of the aforementioned constructs were prepared as described previously (Blackburn *et al.* 1999). The Se-Met variants of CusF and CusB-NT were purified and stored as described above, and their Se-to-protein content was verified by ICP-OES and the BCA assay.

Expression and purification of CusA

E. coli BL21 (pLYS) containing the pASK CusA vector were grown in LB media containing 100 μg/mL ampicillin at 37 °C until they reached an OD600 of 0.8, at which point protein production was induced with 200 μg/L of anhydrotetracycline. Growth was allowed to continue at 30 °C for 5 hrs, whereupon the cells were harvested by centrifugation and pelleted. The cells were then resuspended and lysed using the French pressure method, and the cell debris was pelleted by centrifugation. The supernatant was then ultracentrifuged, at which point the membrane-containing pellet was collected. The pellet was resuspended and solubilized by homogenization, followed by dropwise addition of Cymal-6 detergent with stirring over ice. The remaining membrane was removed by ultracentrifugation, the supernatant poured over a streptavadin agarose affinity column, and the column washed before eluting the clean, tagged CusA protein using a solution of desthiobiotin. The protein was then dialyzed into transfer buffer and frozen for future use. SDS-PAGE of the final, dialyzed protein showed a single band at ~ 116 kDa with no visible impurities. The Bradford assay was used for protein quantification, and ICP-OES was used to analyze the purified CusA for transition metal (Cu, Zn) content to ensure the protein was in

apo form.

Metal reconstitution of Cus proteins

Cu(I) reconstitution of CusF , CusB NT, and CusA

To produce the Cu(I) forms of CusF, CusB-NT, and CusA the same protocol was carried out in all cases. The protein of interest was quantified by the BCA (for CusF and CusB-NT) or Bradford assay (for CusA), then prepared and kept chilled overnight in a Coy anaerobic chamber to give anaerobic protein. Tetrakis(acetonitrile)copper(I) hexafluorophosphate was dissolved in pure acetonitrile (Cu(I)-ACN hereafter) and the amount of Cu(I)-ACN to add to the protein calculated such that the ACN concentration was limited to 10% of the total protein solution by volume. The Cu(I)-ACN was added to the apo protein anaerobically by syringe pump (1μL/minute rate), with stirring, at a ratio of 1.5:1 metal to protein for CusF and CusB or 0.9 :1 for CusA. The mixture was then allowed to incubate one additional hour with stirring, over ice. The metallated protein was concentrated to the desired volume using a microconcentrator, and three cycles of desalting were accomplished using spin columns that had been equilibrated with transfer buffer containing 10%, 5%, and 0% acetonitrile, which removed excess metal and salt from the proteins. At this point the proteins were either used immediately in anaerobic transfer experiments, or flash-frozen and stored anaerobically in liquid nitrogen for a future single anaerobic thaw and use. Metal to protein concentrations were verified by ICP-OES and the BCA or Bradford assay.

Ag(I) reconstitution of CusF and CusB NT

Protein concentrations were first determined by the BCA assay. Silver nitrate stock solutions (10mM) were always prepared fresh, and kept covered in foil and on ice until ready for use. The Ag(I) solution was added to the cold apo protein in the absence of any competing salts in the dark by syringe pump (1 μL/minute rate), with stirring, at a ratio of 1.5:1 metal to protein. The mixture was then allowed to incubate one additional hour with stirring, over ice, in the dark, then desalted of excess metal by three cycles of equilibrated spin columns. The protein was kept covered in foil, and either used immediately in anaerobic transfer experiments, or flash-frozen and stored in liquid nitrogen for a future single thaw and use. Metal to protein concentrations were verified by ICP-OES and the BCA assay.

Metal transfer experiments

For a typical two-protein metal transfer experiment, freshly metallated CusF and CusB were buffer exchanged from HEPES into Cus transfer buffer (50 mM HEPES pH 7.5, 0.1% 6-cyclohexyl-1-hexyl-β-D-maltoside [Cymal-6] detergent, 50 mM NaCl), the components of which were needed specifically to maintain the solubility and structure of the membrane protein CusA. Protein concentration was kept to either 75 μM for di-protein experiments involving CusA, or 150 μM for di-protein experiments involving only CusF and CusB, and for the purposes of this work, the protein stoichiometry was kept at 1:1:1. In experiments that tested the metal transfer from CusF or CusB to apo CusA, an aliquot of metallated protein was added to the apo CusA with slow pipetting up and down to ensure adequate mixing, and then allowed to incubate for ten minutes at room temperature before adding ethylene

glycol to 20% and flash freezing in an XAS cuvette to produce a liquid glass for future EXAFS analysis. In experiments that tested metal transfer from metal ion loaded CusF and CusB, metallated CusF was added in a small aliquot to a vial of metallated CusB and mixed thoroughly, whereupon the reaction was allowed to incubate for ten minutes before adding glassing agent and freezing as previously described. An aliquot from these mixtures was then tested by ICP-OES to confirm that the metal ion concentration was as calculated.

For a typical three-protein metal transfer experiment, concentration was maintained at 150 μM for each protein. Metallated CusB was always added first to a vial of apo CusA, mixed well, and incubated for ten minutes to allow CusB to interact with CusA. Before adding any metallated CusF, a control sample of CusB and CusA was then prepared and frozen using an aliquot of this mixture. At this point, an aliquot of metallated CusF was added to the vial, mixed again, and allowed to incubate for an additional 5 minutes before adding glassing agent and flash freezing as previously described.

EXAFS data collection

Samples were measured as aqueous glasses in 20% ethylene glycol at 10K. Cu K-edge (8.9 keV), Se K-edge (12.5 keV) and Ag K-edge (25.5 keV) extended x-ray absorption fine structure (EXAFS) and x-ray absorption near edge (XANES) data were collected at the Stanford Synchrotron Radiation Lightsource operating at 3 GeV, with currents near 500 mA maintained by continuous top off.

All edges were measured on beamline 9-3, using a Si[220] monochromator. All data were collected in fluorescence mode using a high-count rate Canberra 100-

element Ge array detector with maximal count rates per array element of <120 kHz. For each edge, four to six scans of buffer blank were averaged and subtracted for all protein samples in order to remove the Z-1 filter Kβ fluorescence and produce a flat pre-edge baseline. At each metal edge a Cu, Se, or Ag foil, respectively, was placed between the first and second ionization chamber in order to provide energy calibration.

Cu K-edges were collected using an Rh-coated mirror upstream with a 12.5 KeV energy cutoff to reject harmonics, and a nickel oxide filter and Soller slit inserted in front of the detector in order to reduce elastic scattering relative to the Cu Kα fluorescence. Se K-edges were collected using an Rh-coated mirror upstream with a 15 KeV energy cutoff to reject harmonics, and an arsenic oxide filter and Soller slit inserted in front of the detector in order to reduce elastic scattering relative to the Se Kα fluorescence. Ag K-edge data was measured using ion chambers operating at 1.5 kV, with the energy cutoff mirror removed in order to achieve the high energy. The amount of harmonic contamination from this setup was not expected to be significant. A Pd filter and Soller slit were inserted in front of the detector in order to reduce elastic scattering relative to the Ag Kα fluorescence.

EXAFS simulations

Data averaging, background subtraction, and normalization to the smoothly varying background atomic absorption were performed using EXAFSPAK (George 1995) For the experimental energy threshold energy (k=0), 8995 eV was selected for Cu K-edge, 12663 eV was used for the Se K-edge, and 25515 eV for Ag K-edge. Spectral

simulation was carried by least-squares curve fitting, utilizing full curved wave calculations as formulated by the SRS library program EXCURVE 9.2 as previously described (Binsted and Hasnain 1996; Gurman *et al.* 1984, 1986)

We refined the parameters of the fit as follows: E0, the photoelectron energy threshold, Ri the distance from the central metal atom (Cu, Se, or Ag) to atom i and 2σ2i the Debye-Waller (DW) term for atom i. We fixed the coordination numbers to those previously established from crystal structures whenever possible, or by other previously published values as in the case of CusB NT. Determination of residual metal bound to Se in transfer experiments was performed by refining the Se-Cu/Ag shell occupancy, using a DW factor determined from simulation of the EXAFS data from a fully metallated sample. The quality of the fits was determined using the least-squares fitting parameter, F, which is defined as:

$$F^2 = (1/N) \sum_i k^6(\chi_i^{theory} - \chi_i^{experiment})^2$$

and is hereafter referred to as the fit index (FI).

All EXAFS fit parameters can be found in **Table 5.1**, **Table 5.2**, and **Table 5.3**.

		Se-C			Se-Cu			Se-Ag			Se-Se			
Sample/fit	F*	No†	R, Å‡	DW, Å²	No	R, Å	DW, Å²	No	R, Å	DW, Å²	No	R, Å	DW, Å²	Eo
Se-Met Cu(I) CusB	0.51	2	1.96	0.006	1	2.42	0.006				0.2	2.82	0.017	−5.58
Se-Met Cu(I) CusB/Apo CusA	0.49	2	1.96	0.006	1	2.42	0.006				0.2	2.84	0.014	−5.53
Se-Met Ag(I) CusB	0.39	2	1.96	0.003				1	2.64	0.009				−6.11
Se-Met Ag(I) CusB/apo CusA	0.5	2	1.96	0.004				1	2.64	0.010				−5.60
Se-Met Ag(I) CusB/Cu(I) CusF	0.42	2	1.96	0.006				1	2.64	0.010				−5.26
Se-Met Ag(I) CusB/Cu(I) CusF/apo CusA	0.6	2	1.96	0.008	0.1	2.37	0.009	0.9	2.64	0.009				−5.71
Se-Met Cu(I) CusF	0.74	2	1.96	0.007	0.5	2.38	0.005				0.5	2.85	0.032	−6.04
Se-Met Cu(I) CusF/apo CusA	0.62	2	1.96	0.006	0.5	2.38	0.007				0.5	2.83	0.027	−5.82
Se-Met Cu(I) CusF/Ag(I) CusB/apo CusA	0.66	2	1.96	0.004	~0.05	2.38	0.005	0.19	2.60	0.005	0.5	2.80	0.02	−5.50
Se-Met Ag(I) CusF	0.92	1.5	1.96	0.003				0.45	2.62	0.008				−6.29
Se-Met apo CusF	0.93	1.5	1.96	0.003							0.5	2.79	0.025	−5.40

*F is a least-squares fitting parameter defined as follows:

$$F^2 = \frac{1}{N}\sum_{i=1}^{N} k^6(\text{Data} - \text{Model})^2.$$

†Coordination numbers are generally considered accurate to ±25%.
‡In any one fit, the statistical error in bond lengths is ±0.005 Å. However, when errors due to imperfect background subtraction, phase-shift calculations, and noise in the data are compounded, the actual error is closer to ±0.02 Å.

Table 5.1 Cus protein EXAFS fit parameters Selenium K-edge

		Cu-N (His)*			Cu-S			Cu-Se			Cu-O/N† or Cu-C			
Sample/fit	F	No	R, Å	DW, Å²	No	R, Å	DW, Å²	No	R, Å	DW, Å²	No	R, Å	DW, Å²	Eo
Se-Met Cu(I) CusF $k = 15$	0.46	2	1.93	0.006				2	2.38	0.021				−1.96
Se-Met Cu(I) CusF/Ag(I) CusB/apoA	0.56				2	2.24	0.018				1 O/N 2 C	1.85 3.12	0.009 0.017	0.28
Se-Met Cu(I) CusB $k = 16$	1.2							3	2.41	0.007				−3.50
S-Met Cu(I) CusB	0.39				3	2.30	0.007				1 C	2.06	0.003	−3.63
Cu(I) prepared CusA	0.59	1	1.891	0.012	1.5	2.18	0.016							−0.48

*Fits modeled histidine coordination by an imidazole ring, which included single and multiple scattering contributions from the second shell (C2/C5) and third shell (C3/N4) atoms, respectively. The Cu-N-C_x angles were as follows: Cu-N-C2, 126°; Cu-N-C3, −126°; Cu-N-N4, 163°; Cu-N-C5, −163°.
†Distances of the Cu-N(His) and Cu-N/O (non-His) shells were constrained to be equal in fits to the oxidized proteins.

Table 4.2 Cus protein EXAFS fit parameters Copper K-edge

		Ag-Se			Ag-S			Ag-N (His)			
Sample/fit	F	No	R, Å	DW, Å²	No	R, Å	DW, Å²	No	R, Å	DW, Å²	Eo
Se-Met Ag(I) CusB	2.8	3	2.63	0.005							6.23
Se-Met Ag(I) CusB/Cu(I) CusF/apo CusA	1.8	1.9	2.61	0.008	0.7	2.61	0.008	0.4	2.21	0.005	11.8

Table 5.3 Cus protein EXAFS fit parameters Silver K-edge

5.3 Results

CusF and CusB only exchange metal ions when one of the pair is an apo-protein. Previous work has showed that *partially*-loaded CusF and CusB will freely transfer Ag(I) and Cu(I) toward equilibrium, and that these metal-loaded proteins can form a specific protein-protein interaction, but only if one of them is in the apo-state. However, no work has yet investigated the extent of metal ion exchange when both are *fully* loaded with metal. To this end, we incubated Ag(I)-loaded, Se-Met labeled CusB with Cu(I)-loaded unlabeled CusF and monitored the Se-Met CusB Se-Ag EXAFS for any changes in the Se-Ag signal, such as a decrease in the Se-Ag signal or the appearance of a Se-Cu interaction (**Fig. 5.1 (b)**). However, we did not observe any evidence of metal ion exchange between the two metal-bound proteins. Any attempt in our models to simulate the presence of Cu in the Se environment resulted in an unrealistic Debye Waller (DW) factor of 0.040 $Å^2$ despite allowing the amount of Cu to float freely. While visually the intensity of the overall spectrum did decrease, this appears to be unrelated to metal transfer and may be due to protein-protein interactions between Se-Met CusB and CusF. These data provided an essential control that when Cu-loaded CusF was incubated with Ag-loaded CusB and apo-CusA in subsequent tri-protein transfer experiments (*vide infra*), any metal exchange that was observed must be between F and A, or B and A and not due to unproductive reversible exchange between F and B.

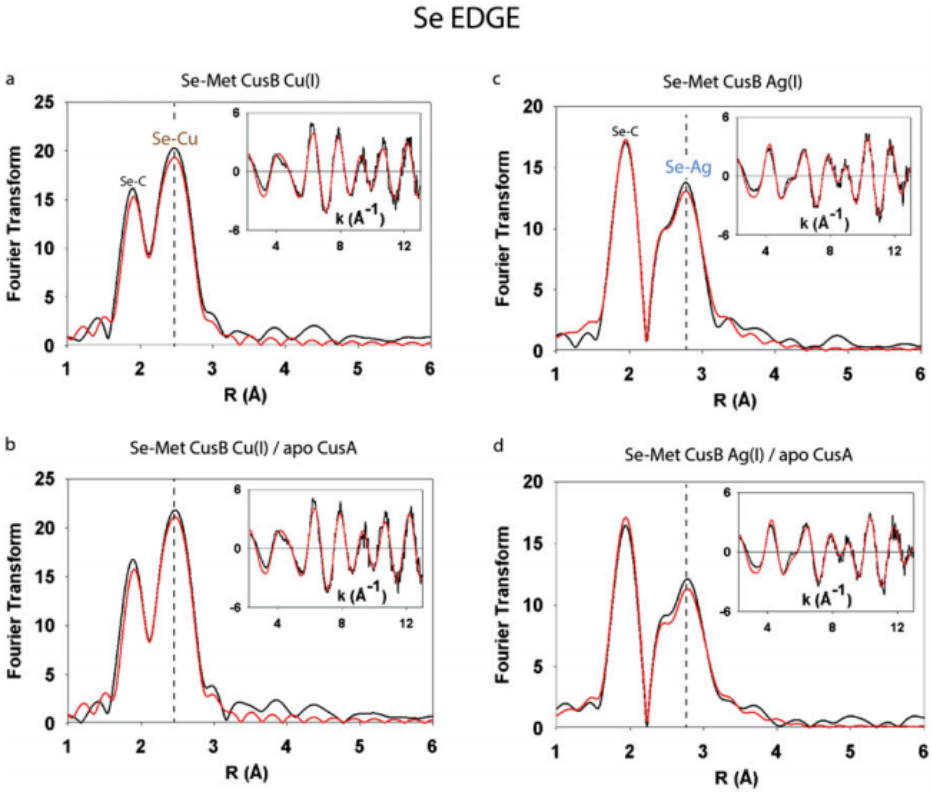

Fig. 5.2. CusB alone does not transfer metal ions to CusA. (A) Se K-edge spectra of Se-Met Cu(I) CusB. (B) Se K-edge spectra of Se-Met Cu(I) CusB incubated with apo CusA. No change in the Se-Cu signal of Se-Met Cu(I) CusB could be detected, indicating that no transfer occurs from CusB to CusA. (C) Se K-edge spectra of Se-Met Ag(I) CusB. (D) Se K-edge spectra of Se-Met Ag(I) CusB-incubated apo CusA. Although the Se-C and Se-Ag intensity both decreased upon the addition of apo CusA, both decreased by the same amount, indicating that no Ag(I) was removed from the Se-Met CusB metallosite.

Metal transfer experiments using Se-Met labeled CusB rule out a metal relay mechanism. To define a role for the CusB protein in Cus metal ion efflux, we first incubated apo unlabeled CusA with Se-Met labeled Cu(I)-loaded CusB to determine whether metal would be transferred from CusB to CusA. The Se-Met CusB Se-Cu interaction at 2.42 Å did not decrease in the Se K-edge Fourier transform (FT) upon the addition of apo-CusA as compared to Se-Met Cu(I) CusB alone. We also tested Ag(I)-loaded Se-Met CusB in place of the Cu(I)-loaded protein, and no metal transfer occurred, confirming that CusB alone is not capable of transferring either metal to apo-CusA (**Figure 5.2**).

We then sought to determine whether the presence of a metallochaperone activates the transfer of metal from CusB to CusA. We prepared Ag(I)-loaded Se-Met CusB, incubated it with apo CusA, and after five minutes, added Cu(I)-loaded CusF to the reaction. With the Se-Met label on CusB, we looked for any change in Se-Ag coordination at 2.63Å in the FT as compared to Se-Met Ag(I) CusB alone, at both the selenium and silver edges (**Fig. 5.3**).

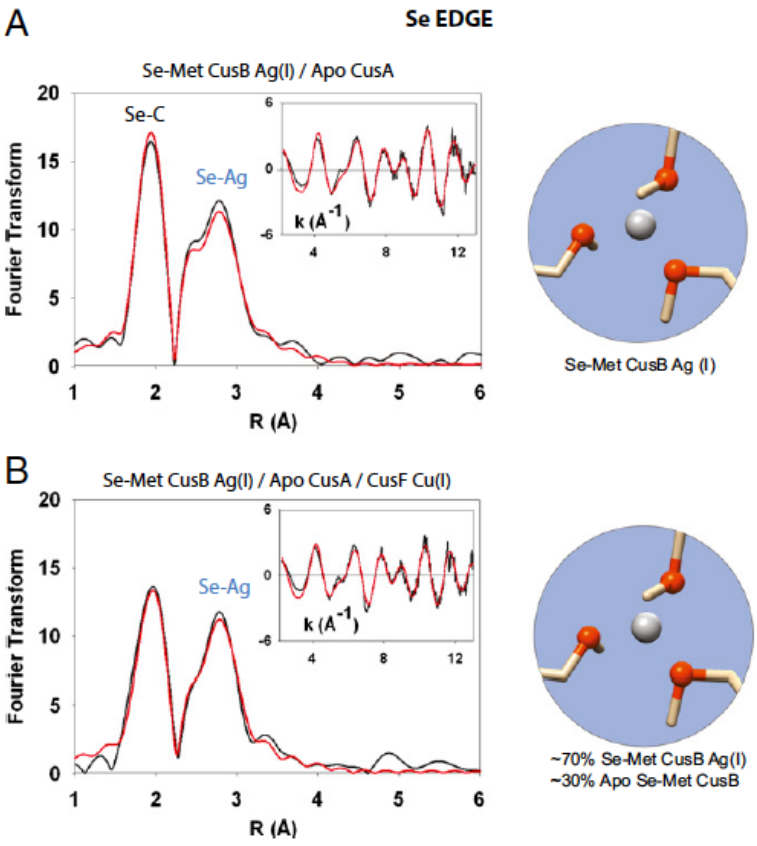

Fig. 5.3. Selenium K-edge EXAFS indicates that CusB is not a chaperone to CusA. Black spectra, experimental data; red spectra, simulated fit. (A) Se K-edge spectra of Ag-loaded Se-Met CusB incubated with apo CusA. The Se-Met CusB Se-Ag(I) interaction at 2.63 Å was not decreased in the FT upon the addition of CusA. (B) Se-Met Ag(I) CusB incubated with apo CusA and unlabeled Cu(I)-loaded CusF. The addition of CusF resulted in a small decrease (~30%) in the Se-Ag signal. However, no Se-Cu interaction could be observed or modeled in the EXAFS of the triprotein incubation, indicating that CusF did not relay metal to CusA via CusB.

The addition of CusF resulted in a ~30% decrease in the intensity of the Se-Ag signal in the Se K-edge FT. However, we did not consider this decrease to be evidence of transfer from CusB to CusA, because if CusB had transferred metal to CusA, a Se-Cu signal from Se-Met labeled, Cu(I)-CusB would appear as apo Se-Met CusB accepted Cu(I) from CusF (*vide infra*).

5.3.3 Metal transfer experiments using Se-Met labeled CusF indicates an activator role for CusB. These initial results described above indicated to us that metal-loaded CusB does not act as a metal relay to CusA but instead must perform the role of an activator of the pump or "on-off switch", as has been previously proposed (Kim *et al.* 2011). That is to say, CusB turns on the CusA pump when it accepts metal from holo CusF, and turns it off when the bound metal is released back to apo CusF. Thus the extent of metal ion binding to CusB will dictate the open or closed status of the CusA pump, and allows for the subsequent delivery of ions from the periplasm.

If CusB acts as a switch in the Cus system, then the metallochaperone CusF may be the primary vehicle of metal ion delivery to CusA during metal ion efflux, but CusF should only be able to deliver if it is also in the presence of metal-loaded CusB. To address this, we incubated Se-Met labeled, Cu(I) CusF with apo CusA and monitored the Se-Met CusF Se-Cu interaction at the canonical bond distance of 2.38 Å. No change in the Se-Cu intensity was detected as compared to the spectra of Se-Met Cu(I) CusF alone, indicating that CusF alone was insufficient for the transfer of metal to CusA (**Figure 5.4**).

However, when we added unlabeled, Ag(I)-loaded CusB to this reaction, a nearly

complete disappearance (~90%) of the Se-Met CusF Se-Cu interaction occurred in the Se FT within the ~5 min time frame of mixing and preparation of the XAS sample (**Fig. 5.5**). Concurrently, a new peak appeared in the Se FT at 2.63 Å, which we modeled to 0.3 equivalents of Ag(I) (**Figure 5.6**). The appearance of a silver signal was anticipated, and served as an important correlate to the previously described Se-Met labeled CusB data, in which there had been a ~30% decrease in the Se-Ag signal upon incubation with CusF and CusA (*vide infra*). These experiments confirm that metal ion is transferred from CusF, but only when CusB is in the metal-bound state. This suggests on-off switch behavior in CusB, and may show for the first time the *in vitro* activation of the Cus efflux pump.

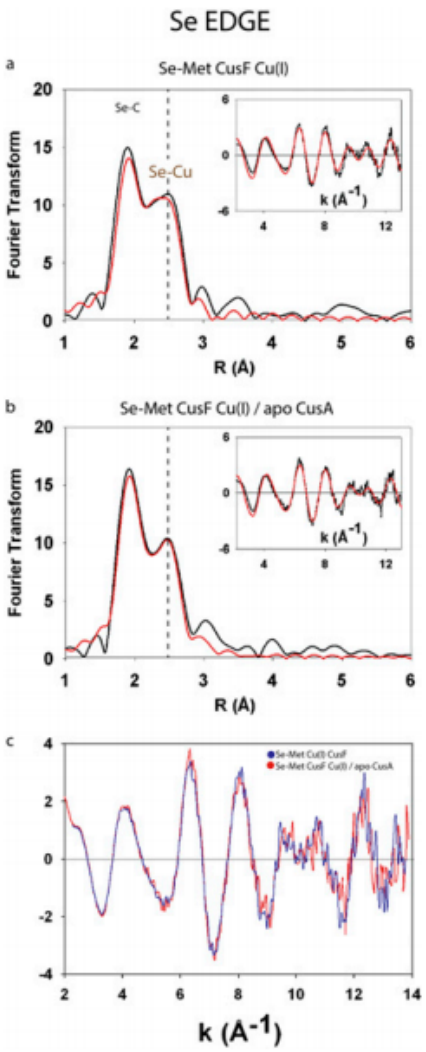

Fig. 5.4. CusF alone does not transfer metal ions to CusA. (A) Se K-edge spectra of Se-Met Cu(I) CusF. (B) Se K-edge spectra of Se-Met Cu(I) CusF incubated with apo CusA. No change in the Se-Cu signal of Se-Met Cu(I) CusF could be detected, indicating that no transfer occurred from CusF to CusA while not in the presence of CusB. (C) Overlay of the experimentally obtained EXAFS from A and B for clarity.

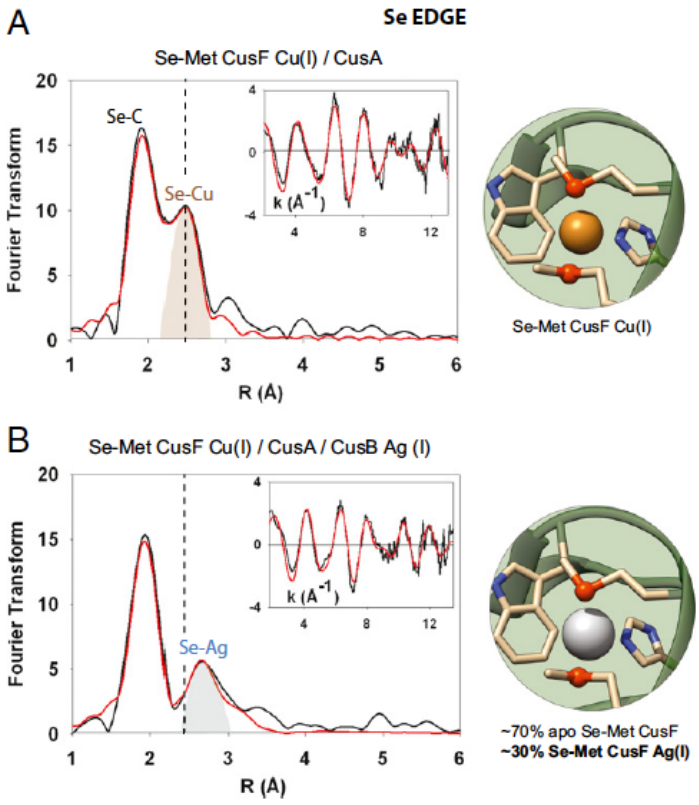

Fig. 5.5 Metal-loaded CusB activates the CusA pump. (A) Se K-edge spectra of Se-Met–labeled, Cu(I) CusF incubated with apo CusA. No change in the Se-Cu intensity at 2.38 Å was detected. (B) Se K-edge spectra of Se-Met–labeled, Cu(I) CusF incubated with unlabeled, Ag(I)-loaded CusB and apo CusA. A complete disappearance of the Se-Met CusF Se-Cu interaction occurred in the Se FT. Concurrently, a new peak appeared in the Se FT at 2.63 Å, which we fit to 0.3 equivalents of Ag(I). The vertical dashed line illustrates where a Se-Cu signal would have appeared in the spectra in B.

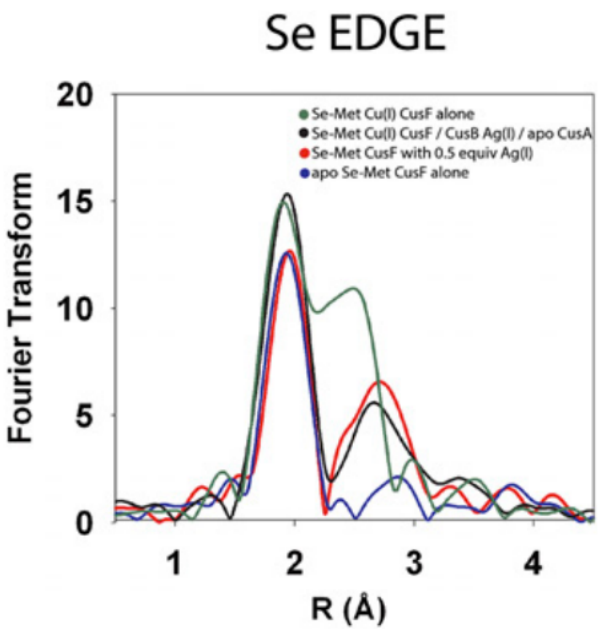

Fig 5.6 CusF accepts Ag(I) from CusB upon activation of CusA, confirming CusF/CusB interaction. Green spectrum , Se K-edge FT of Se-Met–labeled Cu(I) loaded CusF, which exhibits a Se-Cu peak at 2.40Å. Black spectrum, Se K-edge FT of the Se-Met Cu(I) CusF/Ag(I) CusB/apo CusA mixture, in which the Se-Cu peak has disappeared and is replaced by a Se-Ag signal at 2.60 Å. Red spectrum, Se-Met Ag(I)-loaded CusF. Blue spectrum, unreacted apo Se-Met CusF. The Ag(I)-loaded and apo CusF samples were from a separate preparation than the other Se-Met CusF protein used in the main work, and the intensity of the Se-C peak was lower than expected. This was likely due to detector oversaturation from excess Se k-α fluorescence.

Following the fate of the transferred cuprous ions by Cu-K edge XAS reveals a novel acceptor site on CusA. Having determined that CusF released its cuprous ion cargo upon exposure to the other two Cus components, we sought the final destination of the copper. EXAFS data of the Se-Met Cu(I) CusF / Ag(I) CusB / apo CusA mixture was collected at the Cu edge using the same sample as that used previously at the Se edge. The Cu edge FT revealed a new metallosite (**Figure 5.7**), which was quite distinct from the copper edge spectra of Cu(I)-loaded Se-Met CusF or unlabeled Cu(I) loaded CusB. This new spectrum could be modeled by one oxygen/nitrogen ligand at 1.85 Å and two S ligands (most likely from methionine residues) at 2.23 Å, and in all probability corresponds to the "entry" site for Cu(I) on the CusA pump.

Back transfer from CusB to apo-CusF implies regulation. Given that we had previously shown that CusF and CusB can only exchange metal ions when one of them is in the apo form, the prediction was that any apo CusF present after Cu(I) transfer to CusA would then accept silver from CusB. When we incubated Se-Met labeled, Cu(I)-loaded CusF with Ag(I)-loaded CusB and the apo CusA pump, the copper signal of CusF was replaced by a silver signal at the selenium edge, indicating back-transfer from Ag(I) CusB (**Fig. 5.5**). Importantly, this appearance of a silver signal in CusF could then be matched to the loss of silver signal in the Se-Met labeled CusB tri-protein incubation at both Se and Ag edges, underscoring the usefulness of monitoring all three metal edges (**Figure 5.8**).

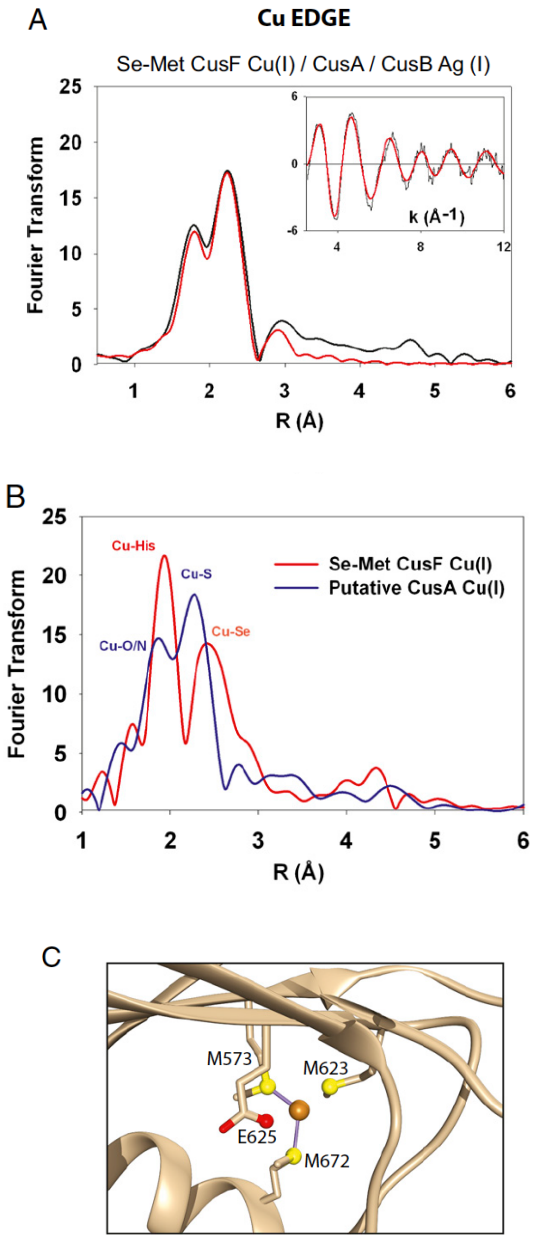

Fig. 5.7 Copper edge XAS reveals a putative CusA metallosite. (**A**) The Cu-K edge XAS spectra of Se-Met CusF Cu(I) incubated with apo CusA and Ag(I)-loaded CusB is distinctly different from the spectra of either Cu-loaded CusF or Cu-loaded CusB, and is best modeled as a Cu-loaded Met-Met-oxygen/nitrogen CusA metallosite. (**B**) For comparison, Cu K-edge XAS of Se-Met–labeled Cu(I)-loaded CusF (red spectra) overlaid with the spectrum from Fig. 4**A** (blue spectra). Upon mixing with Ag-loaded CusB and apo CusA, both the Cu-Se and Cu-His signals of Se-Met Cu(I) CusF disappeared and the spectrum in blue was observed, which is best fit to a single oxygen/nitrogen and two sulfur ligands. (**C**) The crystal structure of Cu(I)-soaked CusA (PDB ID code 3K01) shows that Met623 and Glu625 are nearly equidistant as ligands at ~3 Å and are therefore equally plausible ligands to Cu(I).

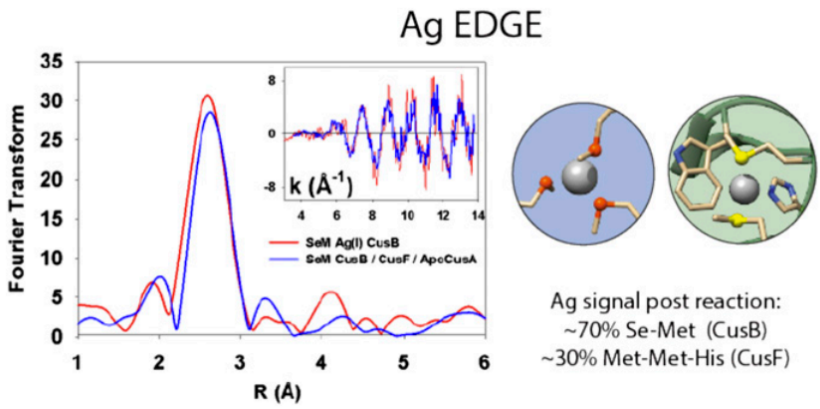

Fig. 5.8 Silver K-edge XAS supports the observed Se edge backtransfer of Ag(I) from Se-Met Ag(I) CusB to apo CusF. Analysis of the Ag K-edge of the Se-Met–labeled CusB triprotein incubation shows a mixed environment for Ag that is best fit to 80% Se-Met Ag(I) CusB (3 Se) and 20% CusF (2 Met, 1 His). CusF may only accept Ag(I) upon releasing its Cu(I) cargo, yet the Se-Met CusB spectra at the Se edge does not show a corresponding Se-Cu signal (Fig. 2B, main text). This one-way transfer of silver from Se-Met CusB Ag(I) to CusF indicates that, in the timescale of our reactions, CusB does not act as a metal relay toward CusA and instead operates as an on–off switch that activates the CusA pump for metal ion delivery from CusF.

5.4 Discussion

CusB is an activator or "switch". The detailed mechanism of the CusCBAF efflux system and in particular, the role played by the periplasmic adaptor protein CusB has been the subject of considerable debate. Two models have been proposed in the literature – the "funnel" model and the "switch" model. In the funnel model, excess periplasmic copper is sequestered by CusF, transferred to CusB, and then delivered to CusA for extrusion. In the "switch" model, copper loading of CusB induces a conformational change, which allows CusB to bind to CusA and open the entry site on the CusA pump, which is known to be located in its periplasmic cleft. While both models predict that either CusB deletion, or metal-site mutagenesis should lead to copper sensitive strains – an expectation that has been experimentally verified – definitive evidence for or against either model has been lacking, and is compounded by the fact that the copper-binding N-terminal domain of CusB is disordered in crystal structures of the isolated protein, or its complex with CusA. Existing evidence, though weak, has leaned more towards the switch model, based mainly on projections of the distance of the CusB metal binding site from the CusA periplasmic cleft, and analogy to structural data on other metal resistance RND adaptor proteins such as ZneB of *C. metallodurans* CH34. The predicted location of the N-terminal copper binding site of CusB close to the membrane would seem to preclude direct copper transfer to the CusA Met_3 acceptor site identified by crystallography (Su *et al.* 2012).

In the present work, we developed a new approach to distinguishing between funnel or switch. We took advantage of the fact that the RND efflux pump can extrude either copper or silver and labeled CusF and CusB with copper and silver

respectively, whose coordination environment could then be uniquely determined by x-ray absorption spectroscopy. In a further refinement of the method, we substituted the Met ligands on either CusF or CusB with selenomethionine, providing a third XAS-detectable label (Se) which would report on the fate of each metal as it interacted with and was transferred through the RND pump. For example if CusB acted as a funnel, Ag-loaded SeM substituted CusB should transfer its Ag(I) ion to apo-CusA resulting in the loss of the prominent Se-Ag signal in the Se EXAFS. On the other hand, if CusB acted as a switch, the Ag ion should remain bound throughout the transfer reaction, and no change in Se-Ag intensity should be observed. Our experimental data show that the latter scenario was indeed observed, thus providing the first definitive evidence for the mechanistic role of CusB as an activator or switch, which opens the entry site on CusA, thereby allowing copper access to the membrane extrusion channel.

CusF and CusB may exchange metal as part of a regulatory strategy for detoxification. Our previous studies of copper transfer from CusF to CusB have demonstrated that the transfer reaction is rapid and reversible (Bagai *et al.* 2008; Mealman *et al.* 2012a), suggesting that the degree of metallation of CusB is dictated by the overall copper flux within the periplasm as sensed by the CusF chaperone. The present observation of back-transfer from CusB to apo CusF after the latter has transferred its copper cargo to CusA strongly supports a mechanism for the Cus efflux system that is finely tuned and responsive to rapidly changing metal ion and environmental conditions. We posit that as copper and silver fill the periplasmic space under anaerobic conditions, the CusF chaperone acts as a scavenger of metal

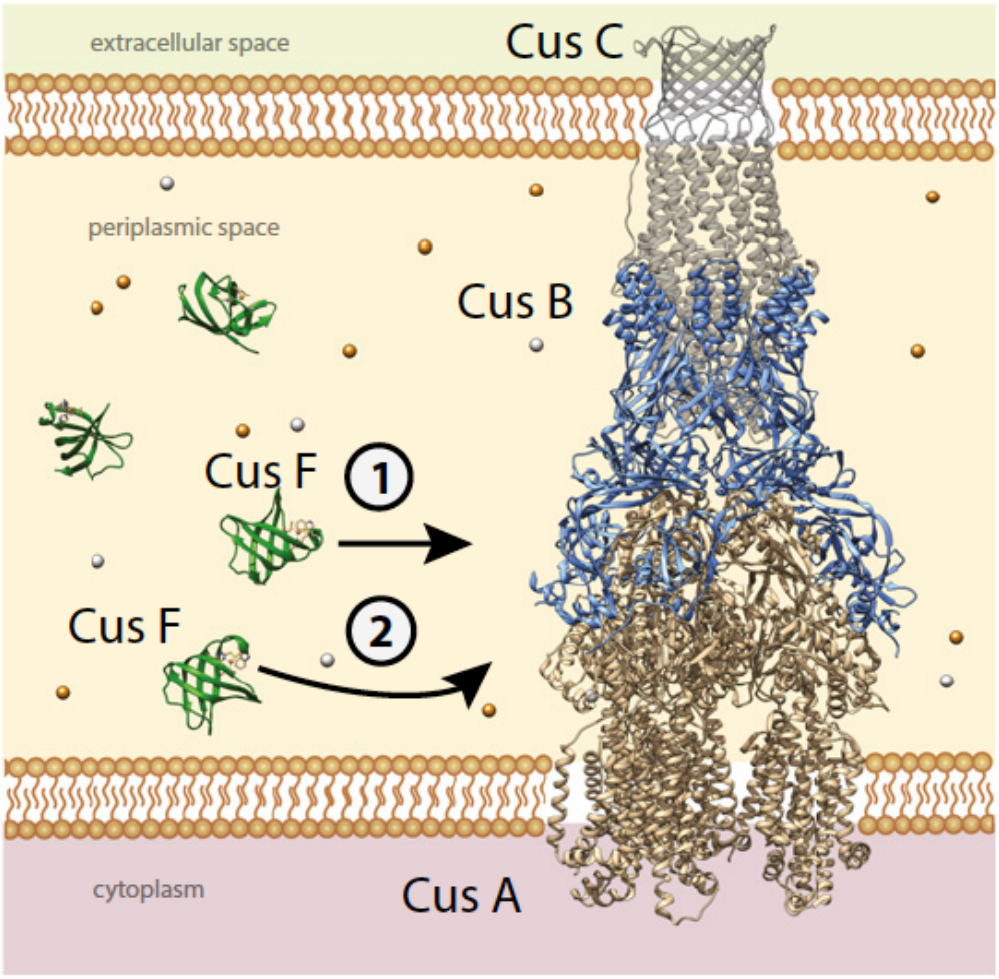

Fig. 5.9 Proposed mechanism of the CusCFBA Cu(I)/Ag(I) efflux system. The CusCBA complex spans the periplasmic space of Gram-negative bacteria during copper or silver stress and acts to pump out excess metal ions. CusF is believed to act as a metallochaperone to the complex, first delivering Cu(I) or Ag(I) to CusB metal-binding sites (1), which activates the CusA pump. This in turn facilitates delivery of metal ions by CusF to a previously unobserved binding motif in CusA (2). This mechanism would allow for the pump to be regulated by copper or silver: when excess metal in the periplasm falls to basal levels, CusF will backtransfer Cu or Ag from the CusB metal-binding sites, deactivating the pump and maintaining copper homeostasis.

and rapidly fills all available CusB metal-binding sites. Once activated in this manner, CusB affects a structural change, opening the CusA pump to the periplasm and allowing CusF to dock and release its cargo (**Figure 5.9**). As metal ion concentration in the periplasm begins to return to basal levels, CusF retrieves bound metal from CusB, closing CusA to the periplasm and inactivating efflux.

5.4.3 A proposed new binding motif in CusA. Our data also shows that metal-loaded CusB activates the pump to accept copper from CusF, as evidenced from the complete loss of Se-Cu signal in a mixture of Cu-loaded SeM-labeled CusF, Ag-loaded CusB and apo-CusA. The Cu EXAFS of this preparation then reports on the nature of the entry site on CusA when the system is actively transferring metal. The description of the CusA entry site revealed in these experiments contrasts with the $(Met)_3$ ligation determined previously from crystals of CusA soaked with excess cuprous ion (Long *et al.* 2010). Further, we have not been able to replicate the $(Met)_3$ ligand set in our own laboratory by incubation of the detergent-solubilized apo-CusA protein with inorganic cuprous ion (**Figure 5.10**). Rather, our transfer experiment strongly suggests a Met-Met-oxygen/nitrogen binding site as the product of the tri-protein incubation. Close examination of the Cu-incubated CusA crystal structure (PDB ID 3K01) reveals that a glutamate residue (E625) is almost equidistant with the longest proposed methionine ligand (M623) and appears poised to coordinate with Cu(I) (**Figure 5.9(c)**). Therefore, it is likely that at least two conformations and possibly more can exist within the copper-binding pocket of CusA. The novel $(Met)_2$ O/N motif observed in the present work suggests that a dynamic set of Met/oxygen metal binding sites may coexist and are available to bind the cuprous ion as it moves

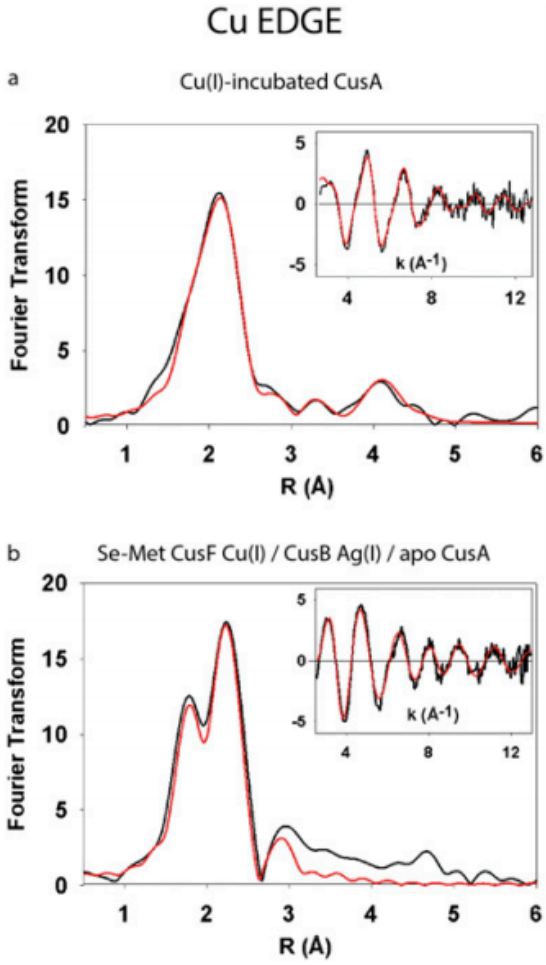

Fig. 5.10 The "active" CusA pump binds Cu(I) in a motif not observed previously. (A) Cu K-edge of apo CusA incubated with tetrakis(acetonitrile)-copper(I). (B) Cu K edge FT of putative Cu(I)-CusA, which appeared upon incubation of Se-Met Cu(I) CusF, Ag(I) CusB, and apo CusA proteins. The spectra produced in each of these cases differ considerably. The spectrum in A has a multiple scattering contribution from a single histidine and two short sulfur bonds and is thought to be a Cu(I) binding site on the outer surface of CusA rather than a site in the interior of the pump. In contrast, the spectrum in B has no imidazole ring-induced multiple scattering and is dominated by signals arising from two methionines and one oxygen/nitrogen ligand.

through the CusA pore and into the large and highly solvated CusC channel.

Mixed Met + O/N ligation is not expected to be a stable ligand set for Cu(I) since the harder (more electronegative) O-donors of amide carbonyls, carboxylates, or –OH groups of serine, threonine or tyrosine will decrease the reduction potential via stabilization of the cupric state and thus promote oxidation. The preference of Cu(I) for soft bases (His, Cys and Met) is manifest in the coordination environments of cytoplasmic metallochaperones that display the Atx1-like CXXC bis-thiolate binding motif (Boal and Rosenzweig 2009; Robinson and Winge 2010) and the Met-rich sites found in periplasmic copper binding proteins (Arnesano *et al.* 2003; Chong *et al.* 2009; Fu *et al.* 2013; Zhang *et al.* 2006). However, in the context of Cu(I) transport through membrane channels, kinetic lability may be more important than thermodynamic stability, and indeed high binding affinity is likely to inhibit transport, unless accompanied by energy input that can toggle high- and low-affinity states via conformational change, as has been proposed as a mechanism for intra-membrane transport in P1B-type ATPases (Sarret *et al.* 2010). Of significance to the present study, the two intra-membrane Cu(I) binding sites of CopA from *Archaeoglobus fulgidus* were identified as being comprised of sulfur + oxygen-coordination, with Cys2-Tyr and Met-Asn-Ser ligand sets (Gourdon *et al.* 2011). Further, an "entry" site comprised of Met-Asp-Glu triad was identified close to the locus where the N-terminal (Atx-like) metal binding domain docks onto the trans-membrane domain of *Legionella pneumoniae* CopA, and later shown to be important for ATP driven trans-membrane transport from the chaperone CopZ in the *A. fulgidus* protein (Gonzalez-Guerrero *et al.* 2008).

The preponderance of these mixed sulfur/oxygen ligand environments is an emerging theme in intra-membrane metal transport which may function to ensure that copper is progressively oxidized to the less toxic cupric state as it transits from CusF through the pump and eventually into the large diameter, negatively charged outer membrane channel CusC (Padilla-Benavides *et al.* 2013). Indeed it is possible that the CusC channel also contains dioxygen molecules which would oxidize the Cu(I), and extrude it as the non-toxic Cu(II) species. It has been similarly proposed for the CopA Cu^{+}-ATPase in *Archaeoglobus fulgidus* that the change in architecture of its two trans-membrane sites toward increasing oxygen ligands aids in vectorial copper (I) transport from the cytoplasm and likely prohibits backwards movement into the cytoplasm (Gourdon *et al.* 2011). Further experiments are planned to test these concepts.

The complexity of the Cus Ag(I)/Cu(I) efflux pump, as well as the prevalence of copper detoxification systems in Gram-negative bacteria, emphasizes our need to fully explore the underlying bioinorganic chemistry. Studying metal transfer spectroscopically and combining this knowledge with the study of the microbiology of the organism should reveal valuable antimicrobial targets. Our future work entails the extensive kinetic profiling of metal transfer between the three key Cus components and will enrich the structural information provided in the current work.

CHAPTER 6

FUTURE DIRECTIONS AND GENERAL CONCLUSIONS

6.1 Ongoing studies of *E. coli* CusB NT and CusF –Fluorescence and Rapid Freeze Quench XAS studies

In the previous chapter, we tracked metal ion movement in the periplasmic CusF(CBA) Cu/Ag efflux pump in *E. coli* using a series of experiments that tracked SeM-labeled proteins sequentially in the presence of Cu(I) and Ag(I) ions. In that work (Chacón *et al.* 2014), we determined that the periplasmic adaptor protein CusB likely plays the role of a "sensor-switch", which when loaded with Cu or Ag ions, could allow the metallochaperone CusF access to the CusA pump entry site in order to efflux metal ions. However, it has sustained our interest greatly that the interaction between CusF and CusB is highly specific. Not only will CusF and N-terminal CusB transfer metal ions to one another (Mealman *et al.* 2012b), but they will *only* do so if one of the proteins is in the apo form, as shown in the previous chapter. This behavior is what prompted the assignment of a *sensing* role to CusB, and suggests an in vivo scenario in which the metallation state of CusF or CusB could act as a means of communicating Cu(I) or Ag(I) ion levels in the periplasm between the two proteins.

Our goals going forward from the previous work have therefore been to investigate the kinetics of metal ion transfer between CusF and CusB. This is not a trivial task, because both proteins bind the same spectroscopically "quiet" metals, and their active sites are in fact nearly identical in metal binding affinity (Bagai *et al.*

2007). To accurately track the kinetics of metal ion transfer between CusF and CusB, we have turned to fluorescence spectroscopy. As mentioned in chapter 2, fluorescence in proteins is largely due to tryptophan (Trp) (Burstein *et al.* 1973). Trp residues, are sensitive to their local environment, and therefore are an extremely sensitive chemical probe. Most Trp residues will be exited by a photon at an energy of approximately ~280 nm, and emit the photon at ~ 350 nm.

Work by Xue and coworkers had determined that the single, active-site Trp in CusF (Trp 44) was fluorescence-active and could be quenched by the addition of Cu(I) (Xue *et al.* 2007). We attempted to replicate the Trp quenching experiment from that work, using a Horiba-Yvon Fluoromax spectrophotometer (Horiba Scientific, Inc.) to monitor the fluorescence emission of the Trp 44 in Cu(I)-loaded CusF that had been excited at 295 nm. We immediately noticed that as the 350nm peak was quenched by Cu(I), a broad, low-intensity peak appeared at ~487 nm that was not present in the Xue *et al.* work. We performed a series of controls to confirm that the 487 nm peak was not due to chemical or spectroscopic artifact, which included a spectrum of a Cu(I)-loaded CusF W44A mutant that showed no fluorescence in any region (**Figure 6.1**). Additionally, we performed an excitation scan by parking at 485 nm and observing an atypically sharp emission peak at ~304 nm, which correlates reasonably well with the Trp excitation energy (**Figure 6.2**). The 487 nm peak is stoichiometric to the amount of Cu(I) added to CusF (**Figure 6.3**), and is isosbestic to the disappearance of the 350 nm Trp peak. Furthermore, the 487 nm feature is highly sensitive to oxygen, and disappears rapidly upon exposure to air. We posit that this sensitivity lead to a Trp fluorescence spectra by Xue *et al.* that does

not exhibit the same feature at 487 nm. Interestingly, we found that Cu(II) appears to also quench Trp fluorescence stoichiometrically, yet does not produce the putative charge transfer peak (**Figure 6.3**). More work will be needed to determine why Cu(II) has a quenching effect, since it has been shown previously not to bind to CusF.

We next used the fluorescence signal at 350 nm and 487 nm to track metal ion transfer from CusB to CusF, which was successful (**Figure 6.4**), and finally, performed a series of cold temperature (~5 °C) kinetic experiments, wherein anaerobic, apo CusF was rapidly stirred just before the point of vortex, and a concentrated solution of Cu(I)-loaded CusB was injected into the septa-sealed cuvette.

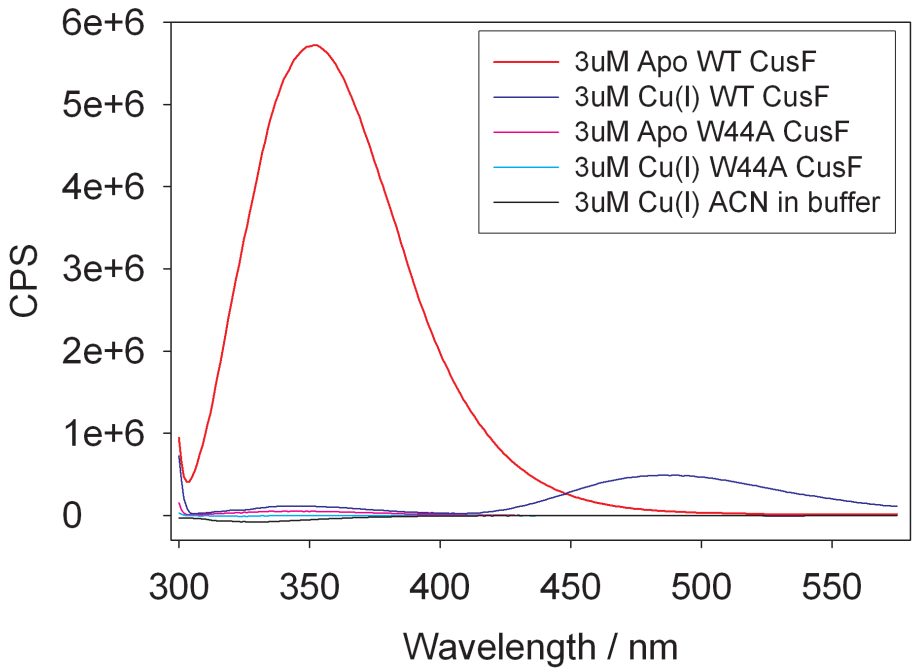

Fig 6.1 The metallochaperone CusF exhibits a novel fluorescence peak at 487 nm when Cu(I) is bound.

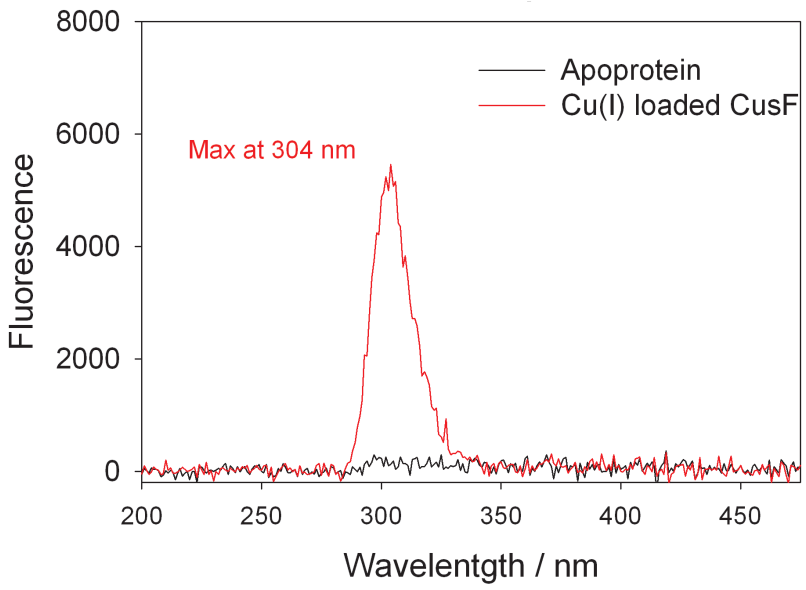

Fig 6.2 Excitation fluorescence spectrum of Cu(I)-CusF when energy is parked at 487 nm. The novel fluorescence peak at 487 nm of Cu(I)-CusF is attributed to excitation of Trp 44 as evidence by an emission at 304 nm.

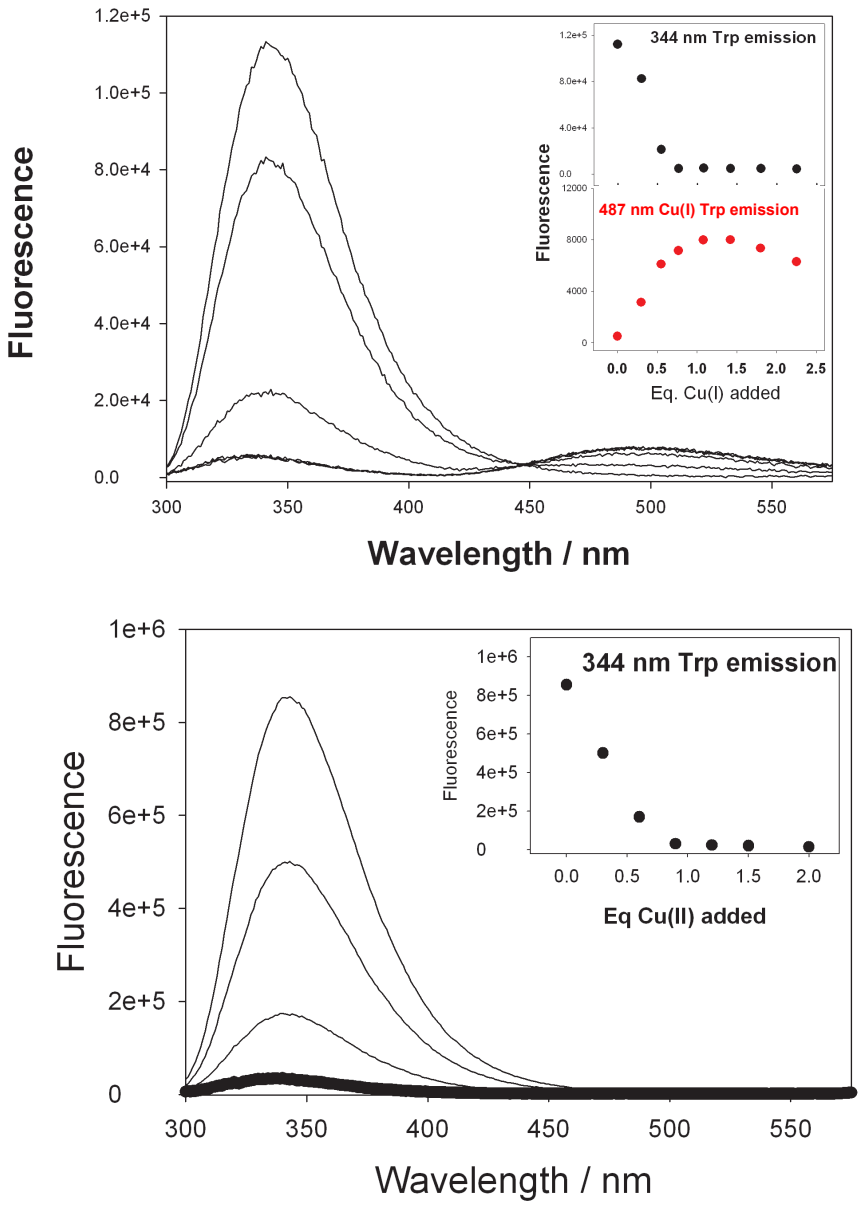

Fig 6.3 Fluorescence spectra of the Cu(I) and Cu(II) titration of CusF, with excitation at 295 nm. Top panel, Cu(I) titration, with insets of signal versus equivalents of Cu(I) added for both the 350 nm peak and the 487 nm peak. Bottom panel, Cu(II) titration, with inset of signal versus equivalents of Cu(II) added for the 350 nm Trp 44 peak.

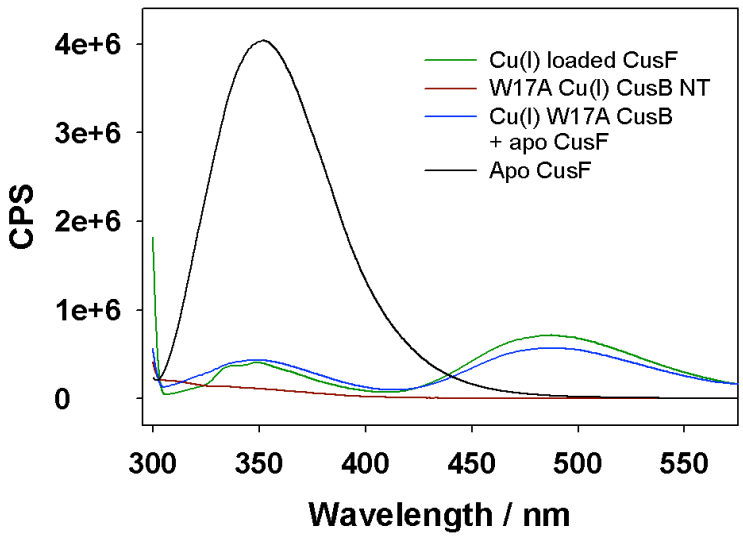

Fig 6.4 Fluorescence spectra of the incubation of W17A Cu(I)-loaded CusB NT with apo CusF, as compared to apo and Cu(I) loaded CusF.

The resulting increase in fluorescence at 487 nm was monitored in real time, but we believe that the limited time resolution of the fluorescence spectrometer was only able to capture an initial time-of-mixing curve; Nevertheless, the data do provide a relative time frame for metal-transfer (~5 seconds, with the initial reaction occurring within a second) that was used to design a rapid freeze quench XAS experiment. At room temperature, Cu(I)-loaded, CusB NT (at two equivalents of CusB in order to ensure full final Cu(I) transfer to CusF) was rapidly mixed with one equivalent of anaerobic, apo Se-Met labeled CusF in 50mM HEPES and 5% ethylene glycol as a glassing agent. Samples were sprayed into liquid ethane and packed into adapted XAS cuvettes, as described in Chapter 2.4. Time points were taken at arbitrary intervals with the earliest point at 15.2 ms and the latest point (aside from the endpoint) at 5 sec. Samples were analyzed by Se EXAFS by the methods previously described in

this dissertation.

While preliminary the results are extremely promising, and appear to indicate a biphasic mechanism, with an extremely fast phase of initial Cu(I)-CusB to apo CusF transfer, followed by a slower transfer phase (**Figure 6.5**). These experiments will be replicated at cold temperatures in order to better resolve the early transfer rate, as well as conducted with various glassing agents to improve the freezing time.

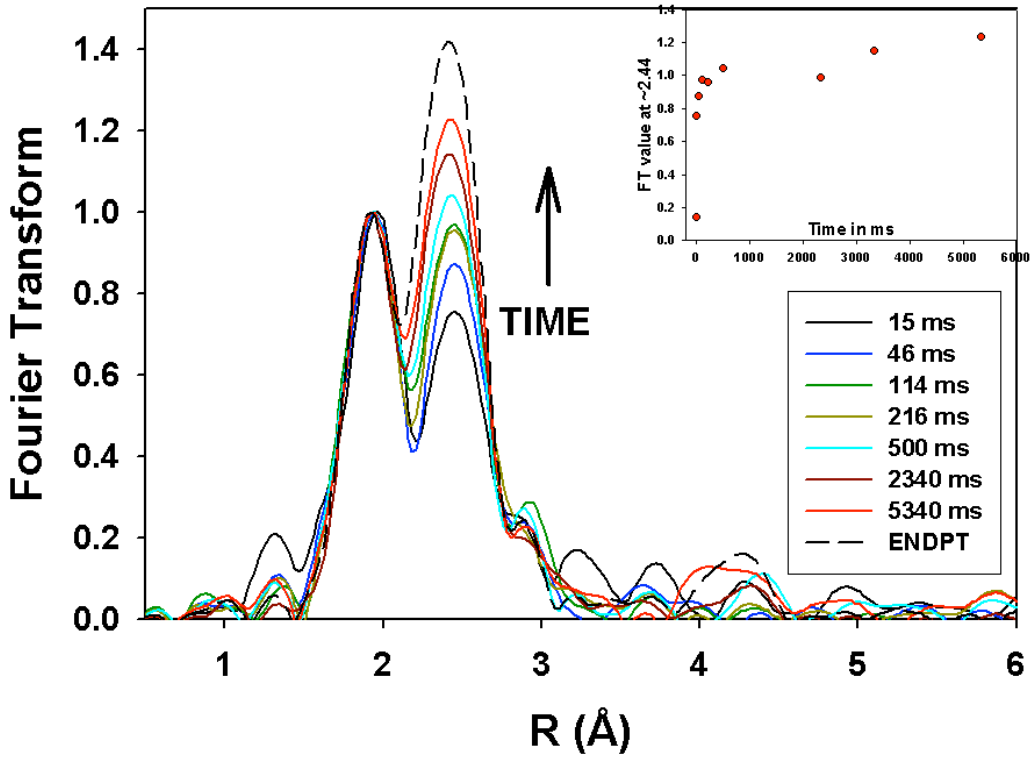

Fig 6.5. Se edge FT of the metal transfer reactions between Cu(I) loaded CusB NT and apo CusF via freeze quench preparation. Time points are indicated in the inset figure legend.

6.3 Future Research and General Conclusions

The nature of the pathway to maturity of CuA is still under investigation, particularly with regards to the possible metallochaperones involved. While PCuAC has been implicated, the work described in this dissertation indicates that PCuAC is only responsible for metallation of a single site of CuA with CuA. More work is needed to understand the mechanism of PCuAC to CuA metal transfer, in the form of RFQ XAS experiments in which the Se edge of Se-Met labeled CuA is monitored for changes. In the case of the Sco metallochaperone, we have begun the design of a streptavidin tagged construct of Sco, which will be incubated with CuA in a series of experiments designed to react the two proteins to form the dead end complex. We then will separate the reacted proteins by the use of a streptavidin column for further analysis by UV-vis, and XAS. Further, the overall mechanism of detoxification by the CusC(F)BA Cu/Ag efflux system has been described in this dissertation, yet the nature of the relationship between CusF and CusB is still unclear. The RFQ-XAS and fluorescence experiments described in section 6.1 are well underway and indicate a complex communication between the two proteins.

Metal ions as used in living systems can act as a double-edged sword –they are vital bionutrients and act in a plethora of biochemical processes, yet in even slight excess, are harmful, if not fatal. We have come to understand that in Nature, by limiting the locations where each metal ion is permitted in the cell, tuning metal affinities in metalloproteins to exert thermodynamic and kinetic control, and using quick-responding gene regulation to respond to times of metal ion dearth and excess,

homeostasis can be successfully maintained. However, there remains much work to be done in order to understand the intricacies of the bioinorganic chemistry of the cell.

The work in this dissertation is a combination of protein biochemistry and spectroscopy, and attempts to further illuminate our understanding of how a metal is loaded into the correct protein and what mechanisms underlie protein-to-protein metal transfer. The use of SeM labeling in tandem with x-ray absorption spectroscopy, as well as stopped flow UV-Vis techniques and EPR, have proven instrumental to determining the mechanism of assembly of CuA, the initial electron transporting subunit of cytochrome c oxidase. The same tandem SeM labeling XAS technique, combined with the use of multiple types of metal ions have illuminated the pathway of metal ion travel in a highly complex bacterial efflux pump, where ambiguity has hitherto frustrated our efforts to understand.

The future investigation of metalloprotein systems by the use of metal binding competition, rapid freeze quench XAS, and steady state or stopped flow fluorescence spectroscopy will further aid our goals, and our hope remains that these continued findings may have human health implications, as well as lead to basic discoveries of our incredible, natural world.

LITERATURE CITED

Abriata LA, Banci L, Bertini I, Ciofi-Baffoni S, Gkazonis P, Spyroulias GA, Vila AJ, Wang S (2008) Mechanism of CuA assembly. *Nature Chemical Biology* 4(10):599-601.

Adman ET (1991) Copper protein structures. *Adv Protein Chem* 42:145-97.

Andrew CR, Lappalainen P, Saraste M, Hay MT, Lu Y, Dennison C, Canters GW, Fee JA, Nakamura N, Sanders-Loehr J (1995) Engineered Cupredoxins and Bacterial Cytochrome c Oxidases Have Similar CuA Sites: Evidence from Resonance Raman Spectroscopy. *Journal of the American Chemical Society* 117(43):10759-10760.

Andruzzi L, Nakano M, Nilges MJ, Blackburn NJ (2005) Spectroscopic Studies of Metal Binding and Metal Selectivity in *Bacillus subtilis* BSco, a Homologue of the Yeast Mitochondrial Protein Sco1p. *Journal of the American Chemical Society* 127(47):16548-16558.

Arciero DM, Pierce BS, Hendrich MP, Hooper AB (2002) Nitrosocyanin, a red cupredoxin-like protein from *Nitrosomonas europaea*. *Biochemistry* 41(6):1703-9.

Arguello JM, Raimunda D, Padilla-Benavides T (2013) Mechanisms of copper homeostasis in bacteria. *Front Cell Infect Microbiol* 3:73.

Arnesano F, Banci L, Bertini I, Cantini F, Ciofi-Baffoni S, Huffman DL, O'Halloran TV (2001a) Characterization of the Binding Interface between the Copper Chaperone Atx1 and the First Cytosolic Domain of Ccc2 ATPase. *Journal of Biological Chemistry* 276(44):41365-41376.

Arnesano F, Banci L, Bertini I, Huffman DL, O'Halloran TV (2001b) Solution structure of the Cu(I) and apo forms of the yeast metallochaperone, Atx1. *Biochemistry* 40(6):1528-39.

Arnesano F, Banci L, Bertini I, Mangani S, Thompsett AR (2003) A redox switch in CopC: An intriguing copper trafficking protein that binds copper(I) and copper(II) at different sites. *Proceedings of the National Academy of Sciences* 100(7):3814-3819.

Bagai I, Liu W, Rensing C, Blackburn NJ, McEvoy MM (2007) Substrate-linked Conformational Change in the Periplasmic Component of a Cu(I)/Ag(I) Efflux System. *Journal of Biological Chemistry* 282(49):35695-35702.

Bagai I, Rensing C, Blackburn NJ, McEvoy MM (2008) Direct Metal Transfer between Periplasmic Proteins Identifies a Bacterial Copper Chaperone. *Biochemistry* 47(44):11408-11414.

Balatri E, Banci L, Bertini I, Cantini F, Ciofi-Baffoni S (2003) Solution structure of Sco1: a thioredoxin-like protein Involved in cytochrome c oxidase assembly. *Structure* 11(11):1431-43.

Banci L (2005) A copper(I) protein possibly involved in the assembly of CuA center of bacterial cytochrome c oxidase. *Proceedings of the National Academy of Sciences* 102(11):3994-3999.

Banci L, Bertini I, Cantini F, Felli IC, Gonnelli L, Hadjiliadis N, Pierattelli R, Rosato A, Voulgaris P (2006) The Atx1-Ccc2 complex is a metal-mediated protein-protein interaction. *Nat Chem Biol* 2(7):367-368.

Banci L, Bertini I, Ciofi-Baffoni S, Huffman DL, O'Halloran TV (2001) Solution structure of the yeast copper transporter domain Ccc2a in the apo and Cu(I)-loaded states. *J Biol Chem* 276(11):8415-26.

Banci L, Bertini I, Ciofi-Baffoni S, Kozyreva T, Zovo K, Palumaa P (2010) Affinity gradients drive copper to cellular destinations. *Nature* 465(7298):645-8.

Barry AN, Blackburn NJ (2008) A Selenocysteine Variant of the Human Copper Chaperone for Superoxide Dismutase. A Se-XAS Probe of Cluster Composition at the Domain 3−Domain 3 Dimer Interface. *Biochemistry* 47(17):4916-4928.

Barry AN, Clark KM, Otoikhian A, van der Donk WA, Blackburn NJ (2008) Selenocysteine Positional Variants Reveal Contributions to Copper Binding from Cysteine Residues in Domains 2 and 3 of Human Copper Chaperone for Superoxide Dismutase. *Biochemistry* 47(49):13074-13083.

Basumallick L, Sarangi R, DeBeer George S, Elmore B, Hooper AB, Hedman B, Hodgson KO, Solomon EI (2005) Spectroscopic and density functional studies of the red copper site in nitrosocyanin: role of the protein in determining active site geometric and electronic structure. *J Am Chem Soc* 127(10):3531-44.

Basumallick L, Szilagyi RK, Zhao Y, Shapleigh JP, Scholes CP, Solomon EI (2003) Spectroscopic studies of the Met182Thr mutant of nitrite reductase: role of the axial ligand in the geometric and electronic structure of blue and green copper sites. *J Am Chem Soc* 125(48):14784-92.

Berry SM, Ralle M, Low DW, Blackburn NJ, Lu Y (2003) Probing the Role of Axial Methionine in the Blue Copper Center of Azurin with Unnatural Amino Acids. *Journal of the American Chemical Society* 125(29):8760-8768.

Binsted N, Hasnain SS (1996) State of the art analysis of whole X-ray absorption spectra. *Journal of Synchrotron Radiation* 3(Part 4):185–196.

Blackburn NJ, Barr ME, Woodruff WH, van der Oost J, de Vries S (1994) Metal-metal bonding in biology: EXAFS evidence for a 2.5 A copper-copper bond in the CuA center of cytochrome oxidase. *Biochemistry* 33(34):10401-7.

Blackburn NJ, de Vries S, Barr ME, Houser RP, Tolman WB, Sanders D, Fee JA (1997) X-ray Absorption Studies on the Mixed-Valence and Fully Reduced Forms of the Soluble CuA Domains of Cytochrome c Oxidase. *Journal of the American Chemical Society* 119(26):6135-6143.

Blackburn NJ, Ralle M, Gomez E, Hill MG, Pastuszyn A, Sanders D, Fee JA (1999) Selenomethionine-Substituted Thermus thermophilus Cytochrome ba3: Characterization of the CuA Site by Se and Cu K-EXAFS. *Biochemistry* 38(22):7075-7084.

Boal AK, Rosenzweig AC (2009) Structural Biology of Copper Trafficking. *Chemical Reviews* 109(10):4760-4779.

Botella H, Stadthagen G, Lugo-Villarino G, de Chastellier C, Neyrolles O (2012) Metallobiology of host-pathogen interactions: an intoxicating new insight. *Trends in Microbiology* 20(3):106-112.

Bray RC (1961) Sudden freezing as a technique for the study of rapid reactions. *Biochem J* 81:189-93.

Braymer JJ, Giedroc DP (2014) Recent developments in copper and zinc homeostasis in bacterial pathogens. *Curr Opin Chem Biol* 19:59-66.

Burstein EA, Vedenkina NS, Ivkova MN (1973) Fluorescence and the location of tryptophan residues in protein molecules. *Photochemistry and Photobiology* 18(4):263-279.

Chacón KN, Blackburn NJ (2012a) Stable Cu(II) and Cu(I) Mononuclear Intermediates in the Assembly of the CuA center of *Thermus thermophilus* Cytochrome Oxidase. *Journal of the American Chemical Society*:120904161326001.

Chacón KN, Blackburn NJ (2012b) Stable Cu(II) and Cu(I) Mononuclear Intermediates in the Assembly of the CuA center of *Thermus thermophilus* Cytochrome Oxidase. *Journal of the American Chemical Society*:16401-16412.

Chacón KN, Mealman TD, McEvoy MM, Blackburn NJ (2014) Tracking metal ions through a Cu/Ag efflux pump assigns the functional roles of the periplasmic proteins. *Proceedings of the National Academy of Sciences* 111(43):15373-15378.

Chaturvedi KS, Henderson JP (2014) Pathogenic adaptations to host-derived antibacterial copper. *Frontiers in Cellular and Infection Microbiology* 4:3.

Chong LX, Ash MR, Maher MJ, Hinds MG, Xiao Z, Wedd AG (2009) Unprecedented binding cooperativity between Cu(I) and Cu(II) in the copper resistance protein CopK from *Cupriavidus metallidurans* CH34: implications from structural studies by NMR spectroscopy and X-ray crystallography. *J Am Chem Soc* 131(10):3549-64.

Clark KM, Yu Y, Marshall NM, Sieracki NA, Nilges MJ, Blackburn NJ, van der Donk WA, Lu Y (2010) Transforming a blue copper into a red copper protein: engineering cysteine and homocysteine into the axial position of azurin using site-directed mutagenesis and expressed protein ligation. *J Am Chem Soc* 132(29):10093-101.

Conroy O, Kim E-H, McEvoy MM, Rensing C (2010) Differing ability to transport nonmetal substrates by two RND-type metal exporters. *FEMS Microbiology Letters* 308(2):115-122.

DeBeer George S, Metz M, Szilagyi RK, Wang H, Cramer SP, Lu Y, Tolman WB, Hedman B, Hodgson KO, Solomon EI (2001) A quantitative description of the ground-state wave function of Cu(A) by X-ray absorption spectroscopy: comparison to plastocyanin and relevance to electron transfer. *J Am Chem Soc* 123(24):5757-67.

Franke S, Grass G, Rensing C, Nies DH (2003) Molecular Analysis of the Copper-Transporting Efflux System CusCFBA of *Escherichia coli*. *Journal of Bacteriology* 185(13):3804-3812.

Fu Y, Tsui HC, Bruce KE, Sham LT, Higgins KA, Lisher JP, Kazmierczak KM, Maroney MJ, Dann CE, 3rd, Winkler ME et al. (2013) A new structural paradigm in copper resistance in *Streptococcus pneumoniae*. *Nat Chem Biol* 9(3):177-83.

Gamelin DR, Randall DW, Hay MT, Houser RP, Mulder TC, Canters GW, de Vries S, Tolman WB, Lu Y, Solomon EI (1998) Spectroscopy of Mixed-Valence CuA-Type Centers: a Ligand-Field Control of Ground-State Properties Related to Electron Transfer. *Journal of the American Chemical Society* 120(21):5246-5263.

George GN. 1995. EXAFSPAK. Menlo Park, CA: Stanford Synchrotron Radiation Laboratory.

George GN, Bray RC, Cramer SP (1986) Extended X-ray absorption fine structure studies of transient species during xanthine oxidase turnover by using rapid freezing *Biochemical Society Transactions* 14:651-652.

Gonzalez-Guerrero M, Eren E, Rawat S, Stemmler TL, Arguello JM (2008) Structure of the two transmembrane Cu+ transport sites of the Cu+ -ATPases. *J Biol Chem* 283(44):29753-9.

Gourdon P, Liu XY, Skjorringe T, Morth JP, Moller LB, Pedersen BP, Nissen P (2011) Crystal structure of a copper-transporting PIB-type ATPase. *Nature* 475(7354):59-64.

Gudipaty SA, Larsen AS, Rensing C, McEvoy MM (2012) Regulation of Cu(I)/Ag(I) efflux genes in *Escherichia coli* by the sensor kinase CusS. *FEMS Microbiology Letters* 330(1):30-37.

Gudipaty SA, McEvoy MM (2014) The histidine kinase CusS senses silver ions through direct binding by its sensor domain. *Biochim Biophys Acta* 1844(9):1656-61.

Gurman S, Binsted N, Ross I (1984) A rapid, exact, curved-wave theory for EXAFS calculations. *Journal of Physics C: Solid State Physics* 17:143–151.

Gurman S, Binsted N, Ross I (1986) A rapid, exact, curved-wave theory for EXAFS calculations. II. The multiple-scattering contributions. . *Journal of Physics C: Solid State Physics* 19:1845–1861.

Hay MT, Lu Y (2000) Metal-binding properties of an engineered purple CuA center in azurin. *J Biol Inorg Chem* 5(6):699-712.

Hernandez-Montes G, Arguello JM, Valderrama B (2012) Evolution and diversity of periplasmic proteins involved in copper homeostasis in gamma proteobacteria. *BMC Microbiol* 12:249.

Hirooka K, Edahiro T, Kimura K, Fujita Y (2012) Direct and indirect regulation of the ycnKJI operon involved in copper uptake through two transcriptional repressors, YcnK and CsoR, in Bacillus subtilis. *J Bacteriol* 194(20):5675-87.

Hood MI, Skaar EP (2012) Nutritional immunity: transition metals at the pathogen-host interface. *Nat Rev Microbiol* 10(8):525-37.

Horng YC, Cobine PA, Maxfield AB, Carr HS, Winge DR (2004) Specific copper transfer from the Cox17 metallochaperone to both Sco1 and Cox11 in the assembly of yeast cytochrome C oxidase. *J Biol Chem* 279(34):35334-40.

Horng YC, Leary SC, Cobine PA, Young FB, George GN, Shoubridge EA, Winge DR (2005) Human Sco1 and Sco2 function as copper-binding proteins. *J Biol Chem* 280(40):34113-22.

Kim E-H, Nies DH, McEvoy MM, Rensing C (2011) Switch or Funnel: How RND-Type Transport Systems Control Periplasmic Metal Homeostasis. *Journal of Bacteriology* 193(10):2381-2387.

Klomp LWJ, Lin S-J, S.Yuan D, Klausner RD, Culotta VC, Gitlin JD (1997) Identification and Functional Expression of HAH1, a Novel Human Gene Involved in Copper Homeostasis. *Journal of Biological Chemistry* 272(14):9221-9226.

Kulathila R, Kulathila R, Indic M, van den Berg B (2011) Crystal Structure of *Escherichia coli* CusC, the Outer Membrane Component of a Heavy Metal Efflux Pump. *PLoS One* 6(1):e15610.

Leary SC (2004) Human SCO1 and SCO2 have independent, cooperative functions in copper delivery to cytochrome c oxidase. *Human Molecular Genetics* 13(17):1839-1848.

Leary SC, Cobine PA, Kaufman BA, Guercin G-H, Mattman A, Palaty J, Lockitch G, Winge DR, Rustin P, Horvath R (2007) The Human Cytochrome c Oxidase Assembly Factors SCO1 and SCO2 Have Regulatory Roles in the Maintenance of Cellular Copper Homeostasis. *Cell Metabolism* 5(1):9-20.

Leary SC, Sasarman F, Nishimura T, Shoubridge EA (2009) Human SCO2 is required for the synthesis of CO II and as a thiol-disulphide oxidoreductase for SCO1. *Human Molecular Genetics* 18(12):2230-2240.

Lieberman RL, Arciero DM, Hooper AB, Rosenzweig AC (2001) Crystal structure of a novel red copper protein from *Nitrosomonas europaea*. *Biochemistry* 40(19):5674-81.

Liu B, Chen Y, Doukov T, Soltis SM, Stout CD, Fee JA (2009) Combined microspectrophotometric and crystallographic examination of chemically reduced and X-ray radiation-reduced forms of cytochrome ba3 oxidase from *Thermus thermophilus*: structure of the reduced form of the enzyme. *Biochemistry* 48(5):820-6.

Loftin IR, Franke S, Blackburn NJ, McEvoy MM (2007) Unusual Cu(I)/Ag(I) coordination of *Escherichia coli* CusF as revealed by atomic resolution crystallography and X-ray absorption spectroscopy. *Protein Science* 16(10):2287-2293.

Lok C-N, Ho C-M, Chen R, Tam PK-H, Chiu J-F, Che C-M (2008) Proteomic Identification of the Cus System as a Major Determinant of Constitutive *Escherichia coli* Silver Resistance of Chromosomal Origin. *Journal of Proteome Research* 7(6):2351-2356.

Long F, Su CC, Lei HT, Bolla JR, Do SV, Yu EW (2012) Structure and mechanism of the tripartite CusCBA heavy-metal efflux complex. *Philosophical Transactions of the Royal Society B: Biological Sciences* 367(1592):1047-1058.

Long F, Su CC, Zimmermann MT, Boyken SE, Rajashankar KR, Jernigan RL, Yu EW (2010) Crystal structures of the CusA efflux pump suggest methionine-mediated metal transport. *Nature* 467(7314):484-8.

Matsumura H, Moenne-Loccoz P (2014) Characterizing millisecond intermediates in hemoproteins using rapid-freeze-quench resonance Raman spectroscopy. *Methods Mol Biol* 1122:107-23.

Mattatall NR (2000) Characterization of YpmQ, an Accessory Protein Required for the Expression of Cytochrome c Oxidase in *Bacillus subtilis*. *Journal of Biological Chemistry* 275(37):28802-28809.

Mealman TD, Bagai I, Singh P, Goodlett DR, Rensing C, Zhou H, Wysocki VH, McEvoy MM (2011) Interactions between CusF and CusB Identified by NMR Spectroscopy and Chemical Cross-Linking Coupled to Mass Spectrometry. *Biochemistry* 50(13):2559-2566.

Mealman TD, Blackburn NJ, McEvoy MM (2012a) Metal Export by CusCFBA, the Periplasmic Cu(I)/Ag(I) Transport System of *Escherichia coli*. *Curr Top Membr* 69(23046651):163-196.

Mealman TD, Zhou M, Affandi T, Chacón KN, Aranguren ME, Blackburn NJ, Wysocki VH, McEvoy MM (2012b) N-Terminal Region of CusB Is Sufficient for Metal Binding and Metal Transfer with the Metallochaperone CusF. *Biochemistry* 51(34):6767-6775.

Nilges MJ. 1979. SIMPIP. Illinois EPR Research Center.

Nittis T, George GN, Winge DR (2001) Yeast Sco1, a protein essential for cytochrome c oxidase function is a Cu(I)-binding protein. *J Biol Chem* 276(45):42520-6.

Olesen K, Veselov A, Zhao Y, Wang Y, Danner B, Scholes CP, Shapleigh JP (1998) Spectroscopic, kinetic, and electrochemical characterization of heterologously expressed wild-type and mutant forms of copper-containing nitrite reductase from *Rhodobacter sphaeroides* 2.4.3. *Biochemistry* 37(17):6086-94.

Ostermeier C, Harrenga A, Ermler U, Michel H (1997) Structure at 2.7 A resolution of the *Paracoccus denitrificans* two-subunit cytochrome c oxidase complexed with an antibody FV fragment. *Proc Natl Acad Sci U S A* 94(20):10547-53.

Outten FW, Huffman DL, Hale JA, O'Halloran TV (2001) The Independent cue and cusSystems Confer Copper Tolerance during Aerobic and Anaerobic Growth in *Escherichia coli*. *Journal of Biological Chemistry* 276(33):30670-30677.

Padilla-Benavides T, McCann CJ, Arguello JM (2013) The Mechanism of Cu+ Transport ATPases: Interaction with Cu+ Chaperones and the role of transient metal-binding sites. *Journal of Biological Chemistry* 288(1):69-78.

Penfield KW, Gewirth AA, Solomon EI (1985) Electronic structure and bonding of the blue copper site in plastocyanin. *Journal of the American Chemical Society* 107(15):4519-4529.

Rae TD, Schmidt PJ, Pufahl RA, Culotta VC, O'Halloran TV (1999) Undetectable intracellular free copper: the requirement of a copper chaperone for superoxide dismutase. *Science* 284(5415):805-8.

Ralle M, Lutsenko S, Blackburn NJ (2003) X-ray Absorption Spectroscopy of the Copper Chaperone HAH1 Reveals a Linear Two-coordinate Cu(I) Center Capable of Adduct Formation with Exogenous Thiols and Phosphines. *Journal of Biological Chemistry* 278(25):23163-23170.

Rensing C, Pribyl T, Nies DH (1997) New functions for the three subunits of the CzcCBA cation-proton antiporter. *J Bacteriol* 179(22):6871-9.

Robinson NJ, Winge DR (2010) Copper Metallochaperones. *Annual Review of Biochemistry* 79(1):537-562.

Rodrigue A, Effantin G, Mandrand-Berthelot MA (2005) Identification of rcnA (yohM), a nickel and cobalt resistance gene in *Escherichia coli*. *J Bacteriol* 187(8):2912-6.

Rubino JT, Franz KJ (2012) Coordination chemistry of copper proteins: how nature handles a toxic cargo for essential function. *J Inorg Biochem* 107(1):129-43.

Rutherford JC, Bird AJ (2004) Metal-Responsive Transcription Factors That Regulate Iron, Zinc, and Copper Homeostasis in Eukaryotic Cells. *Eukaryotic Cell* 3(1):1-13.

Saier MH, Tam R, Reizer A, Reizer J (1994) Two novel families of bacterial membrane proteins concerned with nodulation, cell division and transport. *Molecular Microbiology* 11(5):841-847.

Samanovic MI, Ding C, Thiele DJ, Darwin KH (2012) Copper in microbial pathogenesis: meddling with the metal. *Cell Host & Microbe* 11(2):106-115.

Sarret Gr, Favier A, Coves J, Hazemann J-L, Mergeay M, Bersch B (2010) CopK from *Cupriavidus metallidurans* CH34 Binds Cu(I) in a Tetrathioether Site: Characterization by X-ray Absorption and NMR Spectroscopy. *Journal of the American Chemical Society* 132(11):3770-3777.

Savelieff MG, Lu Y (2010) Cu(A) centers and their biosynthetic models in azurin. *J Biol Inorg Chem* 15(4):461-83.

Savelieff MG, Wilson TD, Elias Y, Nilges MJ, Garner DK, Lu Y (2008) Experimental evidence for a link among cupredoxins: red, blue, and purple copper transformations in nitrous oxide reductase. *Proc Natl Acad Sci U S A* 105(23):7919-24.

Shadle SE, Penner-Hahn JE, Schugar HJ, Hedman B, Hodgson KO, Solomon EI (1993) X-ray absorption spectroscopic studies of the blue copper site: metal and ligand K-edge studies to probe the origin of the EPR hyperfine splitting in plastocyanin. *Journal of the American Chemical Society* 115(2):767-776.

Siluvai GS, Mayfield M, Nilges MJ, Debeer George S, Blackburn NJ (2010) Anatomy of a red copper center: spectroscopic identification and reactivity of the copper centers of *Bacillus subtilis* Sco and its Cys-to-Ala variants. *J Am Chem Soc* 132(14):5215-26.

Siluvai GS, Nakano M, Mayfield M, Blackburn NJ (2011) The essential role of the Cu(II) state of Sco in the maturation of the Cu(A) center of cytochrome oxidase: evidence from H135Met and H135SeM variants of the *Bacillus subtilis* Sco. *J Biol Inorg Chem* 16(2):285-97.

Siluvai GS, Nakano MM, Mayfield M, Nilges MJ, Blackburn NJ (2009) H135A controls the redox activity of the Sco copper center. Kinetic and spectroscopic studies of the His135Ala variant of *Bacillus subtilis* Sco. *Biochemistry* 48(51):12133-44.

Slutter CE, Sanders D, Wittung P, Malmström BG, Aasa R, Richards JH, Gray HB, Fee JA (1996) Water-Soluble, Recombinant CuA-Domain of the Cytochrome ba3 Subunit II from *Thermus thermophilus*. *Biochemistry* 35(11):3387-3395.

Solomon EI (2006) Spectroscopic methods in bioinorganic chemistry: blue to green to red copper sites. *Inorg Chem* 45(20):8012-25.

Solomon EI, Baldwin MJ, Lowery MD (1992) Electronic structures of active sites in copper proteins: contributions to reactivity. *Chemical Reviews* 92(4):521-542.

Soulimane T, Buse G, Bourenkov GP, Bartunik HD, Huber R, Than ME (2000) Structure and mechanism of the aberrant ba(3)-cytochrome c oxidase from *Thermus thermophilus*. *EMBO J* 19(8):1766-76.

Su C-C, Long F, Lei H-T, Bolla JR, Do SV, Rajashankar KR, Yu EW (2012) Charged Amino Acids (R83, E567, D617, E625, R669, and K678) of CusA Are Required for Metal Ion Transport in the Cus Efflux System. *Journal of Molecular Biology* 422(3):429-441.

Su C-C, Yang F, Long F, Reyon D, Routh MD, Kuo DW, Mokhtari AK, Van Ornam JD, Rabe KL, Hoy JA et al. (2009) Crystal Structure of the Membrane Fusion Protein CusB from *Escherichia coli*. *Journal of Molecular Biology* 393(2):342-355.

Svensson-Ek M, Abramson J, Larsson G, Tornroth S, Brzezinski P, Iwata S (2002) The X-ray crystal structures of wild-type and EQ(I-286) mutant cytochrome c oxidases from *Rhodobacter sphaeroides*. *J Mol Biol* 321(2):329-39.

Thompson AK, Gray J, Liu A, Hosler JP (2012) The roles of *Rhodobacter sphaeroides* copper chaperones PCu(A)C and Sco (PrrC) in the assembly of the copper centers of the aa(3)-type and the cbb(3)-type cytochrome c oxidases. *Biochim Biophys Acta* 1817(6):955-64.

Tseng TT, Gratwick KS, Kollman J, Park D, Nies DH, Goffeau A, Saier MH, Jr. (1999) The RND permease superfamily: an ancient, ubiquitous and diverse family that includes human disease and development proteins. *J Mol Microbiol Biotechnol* 1(1):107-25.

Tsukihara T, Aoyama H, Yamashita E, Tomizaki T, Yamaguchi H, Shinzawa-Itoh K, Nakashima R, Yaono R, Yoshikawa S (1995) Structures of metal sites of oxidized bovine heart cytochrome c oxidase at 2.8 A. *Science* 269(5227):1069-74.

Ucisik MN, Chakravorty DK, Merz KM, Jr. (2013) Structure and dynamics of the N-terminal domain of the Cu(I) binding protein CusB. *Biochemistry* 52(39):6911-23.

Valencia E, Braz V, Guzzo C, Marques M (2013) Two RND proteins involved in heavy metal efflux in *Caulobacter crescentus* belong to separate clusters within proteobacteria. *BMC Microbiology* 13(1):79.

Vivian JT, Callis PR (2001) Mechanisms of Tryptophan Fluorescence Shifts in Proteins. *Biophysical Journal* 80(5):2093-2109.

Walker JM, Huster D, Ralle M, Morgan CT, Blackburn NJ, Lutsenko S (2004) The N-terminal Metal-binding Site 2 of the Wilson's Disease Protein Plays a Key Role in the Transfer of Copper from Atox1. *Journal of Biological Chemistry* 279(15):15376-15384.

White C, Lee J, Kambe T, Fritsche K, Petris MJ (2009) A Role for the ATP7A Copper-transporting ATPase in Macrophage Bactericidal Activity. *Journal of Biological Chemistry* 284(49):33949-33956.

Williams JC, Sue C, Banting GS, Yang H, Glerum DM, Hendrickson WA, Schon EA (2005) Crystal structure of human SCO1: implications for redox signaling by a mitochondrial cytochrome c oxidase "assembly" protein. *J Biol Chem* 280(15):15202-11.

Williams PA, Blackburn NJ, Sanders D, Bellamy H, Stura EA, Fee JA, McRee DE (1999) The CuA domain of *Thermus thermophilus* ba3-type cytochrome c oxidase at 1.6 A resolution. *Nat Struct Mol Biol* 6(6):509-516.

Wilmanns M, Lappalainen P, Kelly M, Sauer-Eriksson E, Saraste M (1995) Crystal structure of the membrane-exposed domain from a respiratory quinol oxidase complex with an engineered dinuclear copper center. *Proc Natl Acad Sci U S A* 92(26):11955-9.

Wilson TD, Savelieff MG, Nilges MJ, Marshall NM, Lu Y (2011) Kinetics of Copper Incorporation into a Biosynthetic Purple CuA Azurin: Characterization of Red, Blue, and a New Intermediate Species. *J Am Chem Soc*.

Wolschendorf F, Ackart D, Shrestha TB, Hascall-Dove L, Nolan S, Lamichhane G, Wang Y, Bossmann SH, Basaraba RJ, Niederweis M (2011) Copper resistance is

essential for virulence of *Mycobacterium tuberculosis*. *Proceedings of the National Academy of Sciences of the United States of America* 108(4):1621-1626.

Xiao Z, Brose J, Schimo S, Ackland SM, La Fontaine S, Wedd AG (2011) Unification of the Copper(I) Binding Affinities of the Metallo-chaperones Atx1, Atox1, and Related Proteins: Dectection Probes and Affinity Standards. *Journal of Biological Chemistry* 286(13):11047-11055.

Xiao Z, Wedd AG (2010) The challenges of determining metal-protein affinities. *Nat Prod Rep* 27(5):768-89.

Xue Y, Davis AV, Balakrishnan G, Stasser JP, Staehlin BM, Focia P, Spiro TG, Penner-Hahn JE, O'Halloran TV (2007) Cu(I) recognition via cation-π and methionine interactions in CusF. *Nature Chemical Biology* 4(2):107-109.

Zhang L, Koay M, Maher MJ, Xiao Z, Wedd AG (2006) Intermolecular transfer of copper ions from the CopC protein of *Pseudomonas syringae*. Crystal structures of fully loaded Cu(I)Cu(II) forms. *J Am Chem Soc* 128(17):5834-50.

BIOGRAPHICAL SKETCH

Kelly N. Chacón was born on August 5th, 1981, in Auburn, WA. In 2009 she received a B.S. degree with Latin and departmental honors in Chemistry with an emphasis on Biochemistry from Portland State University. In the Fall of 2010, she began her graduate studies at the Institute of Environmental Health, in the Biochemistry and Molecular Biology program, within the School of Medicine at Oregon Health and Science University. She is a McNair Scholar, an NSF Graduate Research Fellow, a Vertex Scholar, and an OHSU Research Roadmap Scholar. In the Fall of 2015, she will join the Reed College faculty as an assistant professor of Biochemistry, in Portland, Oregon.

Publications as of 2015:

Chacón KN, Blackburn NJ (2012) Stable Cu(II) and Cu(I) Mononuclear Intermediates in the Assembly of the CuA center of *Thermus thermophilus* Cytochrome Oxidase. *Journal of the American Chemical Society* 134:16401-16412.

Mealman TD, Zhou M, Affandi T, Chacón KN, Aranguren ME, Blackburn NJ, Wysocki VH, McEvoy MM (2012) N-Terminal Region of CusB Is Sufficient for Metal Binding and Metal Transfer with the Metallochaperone CusF. *Biochemistry* 51(34):6767-6775.

Chacón KN, Mealman TD, McEvoy MM, Blackburn NJ (2014) Tracking metal ions through a Cu/Ag efflux pump assigns the functional roles of the periplasmic proteins. *Proceedings of the National Academy of Sciences USA* 111(43):15373-15378.